Effect of Ternary Additives on the Evolution of Structure Formation in Aqueous PEO-PPO-PEO Micelles

by

Andre Lamont Thompson

A dissertation submitted in partial fulfillment
of the requirements for the degree of
Doctor of Philosophy
(Materials Science and Engineering)
in the University of Michigan
2018

Doctoral Committee:

Professor Brian J. Love, Chair
Assistant Professor Geeta Mehta
Professor Michael J. Solomon
Associate Professor Anish Tuteja

Andre Lamont Thompson

andrelt@umich.edu

ORCID iD: 0000-0001-5717-6902

ACKNOWLEDGMENTS

I sincerely thank my advisor, Brian Love, for his friendship and mentorship throughout my graduate schooling. His guidance and support have been essential in my academic development and success. I also like to thank my advisors at DuPont, Portia Yarborough, and at NIST, Rick Davis, for their advice and mentorship throughout this challenging process.

I acknowledge the Rackham Graduate School at UM for support. I also like to thank the GEM Fellowship funded through DuPont and the National Physical Science Consortium (NPSC) Fellowship funded through the National Institute of Standards and Technology (NIST) for their financial support. I also thank the numerous teachers, colleagues, and lab mates with whom I have had the pleasure of interacting with and learning from throughout the research projects outlined in this dissertation.

Lastly, I thank friends, family, loved ones, my friends in SMES-G and AGEP, and my community at Oak Grove A.M.E. Church for being in my corner and cheering me on and providing motivation and words of encouragement along this academic journey. As well as all of my teammates on my UM intramural teams, that provided me with fun times and great memories along this journey. I am grateful to have so many people in my life that have helped develop me into the research scientist, engineer, and person I am today.

TABLE OF CONTENTS

LIST OF FIGURES

Figure

LIST OF TABLES

Table

ABSTRACT

Amphiphilic solutions and dispersions represent a key way that low solubility additives can be mixed within aqueous systems. While the phase behavior and gel structure of neat micelle solutions have been well studied, less is known about the effects of ternary constituents like a low solubility additive on micelle structure. In this dissertation, we probe the link between amphiphile micelle gels housing other hydrophilic or hydrophobic molecules and the effect on permeability and flame retardancy.

Differential scanning calorimetry was performed on solutions of poly(ethylene oxide)-poly(propylene oxide)-poly(ethylene oxide) (PEO-PPO-PEO) (L101, 10% PEO; P104, 40% PEO; P105, 50% PEO; and F108, 80% PEO) amphiphiles (0-2% mass/v) to resolve their critical micelle concentrations (0.4-3.0% mass/v). Work was done from 2-10% mass/v copolymer concentrations and co-formulated methylparaben and cisplatin (0-0.1% mass/v) to resolve any deviation in the enthalpy of micelle formation (250-360 kJ/mol). Enthalpy-entropy compensation plots revealed combinations of both drug influenced and drug invariant interaction with forming micelle structures. P104 was most sensitive with cisplatin over all other amphiphiles, noted as a decrease from 302K to 289K when containing up to 0.1% cisplatin. The statistical significance of this cisplatin-induced perturbation was a linear regression from the ΔH-ΔS plots and it was significant at a 95% confidence interval. Other cisplatin-amphiphile combinations were more statistically insignificant.

Small-angle x-ray scattering determined temperature dependent colloidal crystal formation in 31% amphiphile solutions both neat and co-formulated with cisplatin (up to 0.1% mass/v). Focusing on P104, we noted a ~4.0% rise in crystal expansion over the 25°C temperature sweep. Adding cisplatin results in a 4-5% reduction in the unit cell dimensions, which is attributed to decreased water content in the hydrophilic corona by adding cisplatin. Upon heating, added drug changed the nucleation behavior within the sample from a homogenous process to a more heterogeneous distribution of nucleated species.

Dynamic diffusion experiments were performed on 20% mass/v micelle gels (F127, 70% PEO) mixed with indicator dyes and cisplatin (0.1% mass/v) by UV-visible spectroscopy. Each additive was tested neat at room temperature and 40°C, and formulated with F127 at room temperature and 40°C. The behavior of the added drug was complicated as the first 5 hours of permeation resulted in a burst delivery (6% total release with cisplatin-F127-RT compared to 4% cisplatin-RT). The higher fluence at elevated temperature is attributed to coalescing the amphiphiles that blocked transport on the tube walls as they formed colloidal gels. There is likely a separate factor at higher temperature and higher permeability if the membrane pores also expand with temperature.

Lastly, micelle gels (F127) were used for fire retardants for cotton. Vertical flame tests, thermogravimetric analysis (TGA), micro-scale combustion calorimetry (MCC), and microscopy were used to assess flammability and coating quality of fire retardant-encapsulated micelle gels. After coating, the cotton fabrics were more ignition resistant and, if ignition occurred, the coatings self-extinguished. Coated cotton was found to decompose at higher temperatures (150°C vs 75°C cotton control). Coating thicknesses resulted in a >200% mass gain which still requires further optimization. But the combination of flame-retardants packaged in an amphiphilic matrix

retarded cotton flame ignition. Overall, polyether based amphiphiles have shown as schemes for both cisplatin and combinations of flame retardants both of which either have low solubility with flame retardants or high systemic toxicity in vivo like cisplatin.

CHAPTER I

Background and Motivation

1.1 Amphiphilic Triblock Copolymers

Polyethylene oxide-polypropylene oxide-polyethylene oxide (PEO-PPO-PEO) triblock copolymers are amphiphilic block copolymers known commercially as Pluronic surfactants. A variety of surfactants are commercially available, with differing hydrophobic block cores (PPO) and hydrophilic arm (PEO) lengths ratios. Commercial preparations of Pluronic surfactants often contain impurities of the PPO homopolymer, and di- and triblock copolymers with different molecular weights and PEO/PPO mass ratio than the desired product [1, 2]. These impurities can be removed using gel permeation chromatography (GPC) to selectively filter for polymer chains of the desired molecular weight [1, 3].

1.2 Micellization Process

Dispersed solutions of Pluronic surfactants will undergo self-assembly, known as micellization. Micellization can be achieved by varying concentration at a given temperature, or by varying temperature for a given concentration. A schematic of this process is shown in Figure 1.1 [4].

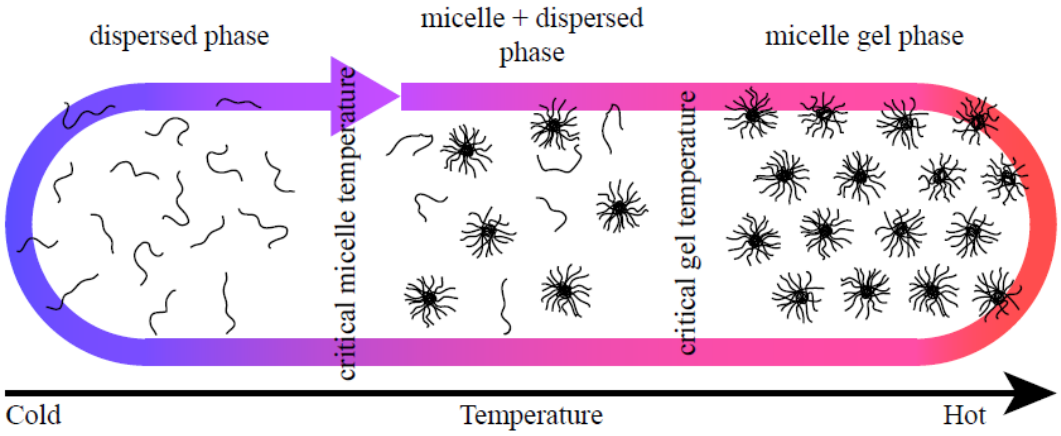

Figure 1.1: Temperature-dependent micellization and gelation of Pluronic surfactants [4].

As the solution crosses the critical micelle temperature (cmt), micelle gels will form and an equilibrium balance of micelle gels and dispersed polymer chains will coexist [5, 6]. The driving force for micellization is entropic in nature, due to the hydrophobic effect [7], where hydrophobic molecules associate with one another in order to dissipate the "water cages" of order water molecules that form around each hydrophobic molecule.

Scientists have previously researched temperature-dependent micellization and ordering of PEO-PPO-PEO triblock copolymers in aqueous solutions [8-18]. As the temperature of these solutions is increased, the decreasing aqueous solubility of the PPO segments often causes micelle formation of hydrophobic (PPO) cores with hydrophilic (PEO) normally forming the shells pointed out into aqueous solvent [15]. Lam et al. [17] suggested micelles grow via Ostwald ripening and Barba et al. [18] suggested that the volume fraction occupied by the micelles in solution rises with increasing temperature. The micelles experience repulsive interactions and order into quasicrystalline cubic lattices which give these structures their gel-like properties [15]. Conventional polymer hydrogels are typically formed via covalent bonding formation between adjacent polymer chains (crosslinking), or physical entanglement of multiple chains, resulting in a mechanically robust tangled network [19]. In a micelle gel, the lattice

ordering of individual micelles offer mechanical stability [20] because there is no covalent bonding in micelle gel formation, and the micellization behavior is driven by temperature or concentration; thus making the gelation process reversible.

1.3 Applications of Micelle Gels

Micelle gels have found multiple industrial applications as emulsifiers, stabilizers lubricators, and detergents [21, 22]. Our group has even experimented with micelle gels as a potential use in fire retardant applications, which is outlined in Chapter V [23]. However, micelle gels are particularly attractive for use in biomedical applications because of the gels reversible temperature-dependent gelation behavior. Biomedical researchers are interested in this reversible temperature-dependent gelation behavior because one can use ambient metabolic heating to trigger gelation if the gel temperatures of these amphiphiles is sufficiently low [24-28]. These solutions can be injected as a liquid at low temperatures, which then form gels *in situ* as the solution warms to body temperature [15]. The rigidity of the gel formation allows one to inject drug infused copolymers and after gelation the gel regulates the localized permeation of added pharmaceuticals, which might lead to a more sustained delivery and longer local residence time [28]. Micelle gels are also biocompatible as they can interact with host tissues with minimum concern for cytotoxicity [29]. This delivery strategy is more favorable compared to more conventional gels that are liquid at high temperatures and gels at low temperatures because the heated fluid from conventional gels (which would gel upon cooling to body temperature) may be damaging to surrounding tissues or skin [4].

1.4 Micelles Gels for Chemotherapeutic Applications

One of the main treatments for both localized and metastatic cancer is chemotherapy, which is used in conjunction with surgery and radiotherapy [30]. It is ideal to deliver a sufficient quantity of drug to tumorous cells, while minimizing systemic side effects and toxicity. However, the drug effectiveness is retarded due to the complications with administering them such as inefficient distribution, limited chemotherapeutic solubility, an inability to permeate cell membranes, rapid clearance, and the lack of selectivity between normal cells and cancer cells [30]. Cis-dichlorodiammineplatinum(II) (cisplatin) is one of the most potent and widely-used anticancer drugs for treating testicular, ovarian, bladder, cervical, head, neck, oesophageal, and small-cell lung cancers [31, 32]. Cisplatin interacts with DNA and interferes with the normal cell transcription and replication processes, resulting in apoptosis [31, 33]. Despite its effectiveness, the clinical use of cisplatin and its derivatives is limited due to severe systemic side effects including nephrotoxicity, neurotoxicity, ototoxicity, nausea, and vomiting [34]. Therefore, developing efficient drug delivery systems that selectively increase the concentration of chemotherapeutics in diseased cells and tumors are of great significance and value.

To increase the therapeutic efficacy, chemotherapeutic drugs are often coupled with polymeric micelles and surfactants [35-37]. Blocky amphiphilic copolymers with a large solubility difference between hydrophilic and hydrophobic segments are known to assemble in an aqueous environment into polymeric micelles with a 10-100 nm size range [38-41]. These micelles have a narrow size distribution and are characterized by their core-shell architecture, where hydrophobic segments are segregated from the aqueous exterior to form a hydrophobic inner core surrounded by hydrophilic segments [35]. Interests in applying block copolymer micelles as drug delivery systems have increased because of the high drug-loading capacity of

the inner core as well as some level of increased tolerance of the drug loaded micelles compared to neat drugs [42-46]. The aggregation and surface properties of polymeric micelles in solution depend on external factors such as pH, temperature, pressure, and the presence of additives [47]. Thus, the properties of polymeric micelles in solution can be effectively tuned to a desired range and application by altering these external factors. Mandal et al. [48-50] has conducted various physicochemical studies on PEO-PPO-PEO micelles in sodium dodecyl sulfate (SDS) in the absence and presence of various micellized drugs, peptides, and additives as a function of various molar compositions using various techniques. Moulik et al. [51] have also recently reported about the effect of various additives on aqueous normal and reverse pluronic micelles. Therefore, even though there are a variety of structures including microspheres [52, 53], dendrimers [54], liposomes [55-58], carbon nanohorns [59-61], carbon nanotubes [30], and nanoparticles; gold [62], silver [63], Fe_3O_4 [64, 65], pH-responsive compounds [66, 67] and silica [68, 69]; that can be used as drug delivery agents, polymeric micelles' high drug-loading ability and toxicity shield effect [42-46] suggests they are sufficient drug delivery platforms to compliment other used drug delivery materials.

1.5 Previous Research of Micelle Gels for Drug Delivery

Research on drug-loaded micelles has included rheology [70, 16], DSC [12, 14, 71, 72], SAXS [70, 12, 15], SANS [73, 13], and cloud point determinations [10]. From these, assessments of how each perturbant affects the micelle formation temperature are related to the drug content and interactions of the drug component within the amphiphile matrix. Functional evaluations of drug loaded micelles have focused on drug release and cell culture studies [74]. Sharma et al. [12] studied how adding organics affected the evolution of ordered structures forming from PEO–PPO–PEO based solutions as resolved by SAXS.

Solutes of greater pharmaceutical significance have also been studied including the aggregation of neat forms of commercial PEO-PPO-PEO amphiphilic copolymers produced by a range of suppliers including Pluronic F127 (~12,000 g mol^{-1} molecular mass, 70/% PEO content) [75], mixed F127 dispersions formulated with naproxen and indomethacin [11], vancomycin [76], lecithin [77], pilocarpine [78], methotrexate [79], and separately lidocaine and prilocaine formulated into eutectic mixed micelle solutions of F68 and F127 [80]. Sharma et al. [12] has previously studied the effects of two anti-inflammatory agents, naproxen and indomethacin, on the lower and upper gelation temperature of F127 solutions. They concluded that the drugs shifted both the liquid-to-gel and gel-to-liquid boundaries to lower temperatures and the presence of the drug molecules promotes self-assembly of F127 [11], suggesting that different drugs were influencing the thermodynamic driving to form the micelle. In their later work they examined the gelation of F127 in the presence of a series of hydrophobic pharmaceuticals, to identify any correlation between gelation and physicochemical parameters of drug solutes [12].

1.6 Motivation

Thermodynamics of micelle and gel formation is relatively well known for a variety Pluronic surfacnts. Kinetic or transient effects, however, are less known for specific combinations of amphiphilic copolymers with varying hydrophilicity and chemotherapeutic drugs. There is a large potential to encounter non-equilibrium transition conditions in real-world applications, and more work needs to be done under these conditions. There may be transient factors in the formation or properties of micelle gels, and these factors need to be studied in order to achieve maximum optimization of micelle formation for a given application. Little is known about how the presence of a ternary additive affects the gel properties of amphiphilic micelles

with varying hydrophilicity or the mechanism by which enhanced release or delivery profiles are achieved.

The aim of this dissertation work was to provide a more comprehensive study of the effects, both microscopically and macroscopically, on the gel formation and properties of micelles with varying hydrophilicity. The rationale for understanding how ternary additives perturb the micelle formation energetics and where within the micelle ternary additives are partitioned is key to resolving how formulated micelles perform as drug delivery vehicles. In this dissertation, we attempt to better understand the linkage between forming structures of amphiphiles housing other molecules and the effect on availability and performance. Four main methods were used to complete this study: differential scanning calorimetry (DSC), small-angle x-ray scattering (SAXS), ultraviolet-visible (UV-Vis) spectroscopy, and flammability testing methods. The energetics of micellization and gel formation was probed using DSC. Structural studies on the micelle lattices were carried out using SAXS. Diffusion studies and release characteristics of the micelle gels were measured using UV-Vis. Vertical flame tests (VFT), thermogravimetric analysis (TGA), micro-scale combustion calorimetry (MCC), and scanning electron microscopy (SEM) were all used to test for flammability and coating quality of fire retardant-encapsulated micelle gels. Efforts were made to explore kinetic effects such as increasing heating rates, in order to determine if transient effects play a significant role in gel formation. By thoroughly studying the effects of ternary additives on micelle gel formation, a more complete picture of the molecular interactions taking place will be developed which will lead to a better understanding of ternary additives and their interactions with amphiphilic copolymer micelles and gels. This understanding may prove useful in the optimization of polymer formulations used in pharmaceutical, biomedical, or other applications.

CHAPTER II

Thermodynamic Characterization of Micelle Formation

2.1 Introduction

The rationale for understanding how ternary additives affect micelle formation energetics is key to resolving how formulated micelles perform as drug delivery vehicles. The thermodynamic analysis of solubility within a micelle has been presented in the form of an enthalpy-entropy compensation, first described by Lumry and Rajender [81]. $\Delta G_{micellization}$ is the free energy to take one mole of amphiphile dispersed in solution into the micelle phase and is given by [82, 83]

$$\Delta G_{micelliation} = RT_{micelle}\ln(cmc) \tag{2.1}$$

Where $T_{micelle}$ is the micelle formation temperature, and cmc is the critical micelle concentration. The enthalpy is the integral of each micelle formation endotherm. The entropy of micelle formation is extracted from rearranging the Gibbs Helmholtz Equation to yield [82, 83]

$$\Delta S_{micelle} = \frac{(\Delta H_{micelle} - \Delta G_{micellization})}{T_{micelle}} \tag{2.2}$$

resolved at the micelle formation temperature at each concentration of amphiphile used. From the determinations of $\Delta S_{micelle}$ and $\Delta H_{micelle}$, a direct plot can resolve both the slope, identified as the compensation temperature, $T_{compensation}$, and the intercept (identified as ΔH_0). Cornish-Bowden [84] explained that the name enthalpy-entropy compensation refers to the idea that variations in ΔH that accompany variations in the temperature at which each molecule is

normally active are “compensated for” by variations in ΔS. The compensation temperature represents the driving force for solute-solute and solute-solvent interactions [14, 81-83, 85-96] and has been identified for neat amphiphiles in solution [71, 97] and ionic liquids such as the Gemini surfactants [98]. According to Jolicoeur et al. [99, 100], since hydrophobic interactions contribute largely to micelle stability, a general enthalpy-entropy correlation yields a compensation value characteristic of such interactions [90]. Chen et al. [101, 81] explained for a compensation phenomenon, the micellization could be described as consisting of a two-part process: (a) the “desolvation” part, i.e., the dehydration of the hydrocarbon tail of surfactant molecules, and (b) the “chemical” part, i.e., aggregation of the hydrocarbon tails of surfactant molecules to form a micelle.

In terms of probing the origins of what is meant by solute-solute and solute-solvent interactions, it might also be worth resolving how micelle formation and subsequent ordering of them regulate the solution thermodynamics. Consider the driving force for forming spherical micelles in solution from neat amphiphilic copolymers. Goldstein has suggested that the driving force for forming micelles suggests that it can be idealized as a spherical core (with a volume of a sphere) with the hydrophobic sections binding together to form an agglomerate of constant density [102]. That suggests that there is an enthalpy for forming this organized structure as $\Delta H_{\text{micelle core.}}$ Goldstein also points to the co-location of the hydrophilic sections that are bonded to the center blocks and are conveyed to an interface contributing to a core-shell interfacial energy [102]. Like Goldstein’s analysis, a more detailed analysis would include contributions linked with the lengths of the different blocks [102]. In addition, if the phase separation to cluster the hydrophobic sections is the main driving force for micellization, there may be small contributions to the free energy associated with the energetics of forming the shell and the

interface between the shell and the surrounding aqueous solution. This would lead to four terms contributing to the free energy of micelle formation, as shown in Equation 2.3.

$$\Delta G_{micelliation} = V_{core}\,\Delta H_{micelle\,core} + SA_{c-s}\sigma_{c-s} + V_{shell}\Delta H_{shell} + SA_{shell}\,\sigma_{shell} \quad (2.3)$$

For an amphiphile that forms a sphere, V_{core} is the volume of the hydrophobic core and the first interface encountered from the micelle center is the core-shell (c-s) interface where the hydrophilic ends are pointed out into the aqueous phase. The interface region between the hydrophobic and hydrophilic regions will create a surface energy term; called $\sigma_{c\text{-}s}$ with the total energy of this term linked with the surface area (SA) of the interaction, in this instance a sphere. The larger the enthalpic payoff for driving these block copolymers together into forming micelles, the hydrophobic blocks take their hydrophilic ends with them and there is a need to situate the hydrophilic chain ends in the most entropically favorable arrangement, which is much more constrained than when dispersed in solution. At the boundary where the shell interacts with the aqueous medium, there is a separate interfacial energy, σ_{shell} term, also linked with the surface area of that interaction, SA_{shell}.

As a function of radial dimensions, Equation (2.3) can be rearranged in the dilute micelle region (no micelle-micelle interactions, just discrete micelles in solution) as

$$\Delta G_{micelliation} = \frac{4}{3}\pi r^3\,\Delta H_{micelle\,core} + 4\pi r^2\sigma_{c-s@r} + \frac{4}{3}\pi(R^3 - r^3)\Delta H_{shell} + 4\pi R^2\sigma_{shell} \quad (2.4)$$

where *r* is the radius of the hydrophobic core, *R* is the radius of the entire micelle including the swollen shell, $\sigma_{c\text{-}s}$ corresponds to the surface energy between the core and shell, and σ_{shell} is the surface energy between the micelle and the aqueous medium from which the micelles formed. For block copolymers, there is the discrete linkage between the driving force to cluster hydrophobic blocks together and the corresponding entropic penalty that arises since the hydrophilic ends are constrained by the covalent bonding to the core.

Any drug that is absorbed into the micelle core or shell could migrate within the core-shell structure and probably has its largest effect in regulating the surface energy between the core and the shell. Small molecules that are substantially more hydrophobic might swell the micelle core, but large-scale swelling of micelles has not been observed. If the small molecules were substantially more hydrophilic, they would be influencing the ΔH_{shcll} term, which is small, or they could swell the shell. The suggestion that there is interplay between the enthalpic driving forces to form well-defined structures in solution is offset by the constraint of what volumes the tail sections of the block copolymer is the origin of the compensation temperature. That small molecules can regulate the compensation temperature is an acknowledgment that their distribution controls the contributions to the free energy found in Equation (2.4).

It is also thought that a deviation in the compensation temperature from neat solutions is a useful indicator of drug loading interactions with an amphiphile if the ternary constituent is strongly interacting with it. Ravi et al. [103] proposed at the compensation temperature the enthalpy and entropy changes fully compensate one another, and there is no change in ΔG upon changing the reactant [103]. Similar compensation temperatures for systems may mean that the processes occurring in the different systems are the same, but the mechanisms of the processes may still be different [103]. Therefore, if the two processes are have identical compensation temperatures, then the fraction of the total free energy arising from the enthalpy contribution is the same in both processes [103]. If the compensation temperatures are different, then the mechanisms of the two processes must be different [103]. Mechanisms meaning the ways in which solutes are retained i.e. location of retention or driving force of retention and intermolecular forces [103]. Resolving how a drug mimic also affected the compensation temperature has been done in our study [72] outlined in this chapter with methylparaben and

Pluronic P105. This chapter also outlines our evaluation of the thermodynamics of micelle formation using Pluronics L101, P104, P105, and F108 solutions and cisplatin as a ternary additive [104].

Our group has previously evaluated the enthalpy and structural changes in F127 micelles by several methods [16, 15] . We showed that neat F127 solutions formed micelles more abruptly suggesting a nucleation-based mechanism. Methylparaben, co-formulated as an anti-fungal constituent in topical creams, was found to soften the transition such that ordered micelle formation occurred at lower temperatures and the size of the enthalpy grew more systematically with changes in temperature [16, 15]. In an attempt to span a wider range in sequestration behavior between strongly hydrophobic and strongly hydrophilic amphiphiles, we report on research results on the enthalpy and structural changes that occur in the amphiphiles L101 (~3,800 g mol^{-1} molecular mass, 10/% PEO content), P104 (~5,900 g mol^{-1} molecular mass, 40% PEO content), P105 (~6,500 g mol^{-1} molecular mass, 50% PEO content), and F108 (~14,600 g mol^{-1} molecular mass, 80% PEO content) both in the neat state and when mixed with the hydrophilic drug cisplatin [cis-dichlorodiammine-platinum (II)].

There has been common interest in resolving how adding other, more potent drugs like chemotherapeutics affected micelle structure and formation characteristics. Among them were platinum-based chemotherapeutics such as cisplatin, carboplatin (cis-diammine (1,1-cyclobutanedicarboxylato)) platinum, and oxaliplatin (cis-[1R,2R-cyclohexanediamine-N,NV] [oxalato(2-)-O,OV]) platinum that are often used in treating bladder, cervix, lung, ovarian and colorectal cancers [105, 106]. Prior clinical work characterizing the effects of three Pluronic triblock copolymers (from hydrophilic F127, through P85, and to the more hydrophobic L61) has examined on the cytotoxicity of carboplatin to a rat colorectal carcinoma cell line [107]. Other

efforts to package chemotherapeutics directly as drug-infused micelles for vascular delivery have also been using cisplatin in F127 [108].

Other efforts have explored how mixing aqueous polymeric micelles with different drugs helps in nanoscale drug delivery [109], polymeric micelles for cancer chemotherapy [110], PC-14 cells treated with cisplatin-incorporated polymeric micelles [111], drugs in block copolymer micelles [112], multidrug-resistant human ovarian carcinoma cells by P85 [113], micelles in anticancer drug delivery [114], cisplatin-incorporated polymeric micelles treated on tumors in mice [37], polymeric micelles for delivery of poorly water-soluble compounds [115], targeting, imaging, and triggered release of micelles in anticancer therapy [116], sized controlled polymeric micelles containing cisplatin [117], and hydrogels from cisplatin-loaded block copolymers in drug delivery [118]. These studies show the importance of exploring chemotherapeutic drugs like cisplatin when mixed with PEO-PPO-PEO copolymers. In this chapter, we look to study how cisplatin is partitioned into PEO-PPO-PEO copolymers from the thermodynamic side.

If the presence of a chemotherapeutic alters the driving force for micelle formation, one would naturally conclude that solute-solvent interactions are controlling features in regulating micelle formation. As a result, it seems reasonable to probe the impact on the compensation temperature by perturbing the thermodynamics through the addition of small molecule chemotherapeutics in these structures. We report in this chapter on our efforts to use the hydrophilic perturbant cisplatin into a range of PEO-PPO-PEO copolymers of varying hydrophilicity, as determined by a calorimetric assessment of both the critical micelle formation composition and the size of endotherms measured as temperatures are varied.

The experiments, results, and discussion covered in this chapter were submitted and published in the *Journal of Colloid and Interface Science [72]* and *Journal of Thermal Analysis and Calorimetry [104]*.

2.2 Materials and Methods

PEO-PPO-PEO (Pluronic P105, Pluronic P104, Pluronic L101, Pluronic F108: BASF Wyandotte MI) were obtained and used as received. Aqueous solutions of L101, P104, P105, and F108 were each prepared according to "cold" processing methods [29] and formulated in varying concentrations to probe the enthalpy of micellization. Methylparaben (Sigma-Aldrich) was added to aqueous solutions of varying P105. Two types of formulation protocols were created for P105 and methylparaben. One fixed the P105 content and varied the amount of methylparaben. The other scheme used a fixed amount of methylparaben and varied the P105 content. Cisplatin (Sigma-Aldrich) was added to aqueous solutions of varying Pluronics (L101, P104, P105, F108).

The structures of methylparaben, cisplatin, and the polymers are shown in Figure 2.1 [72, 104]. Two types of formulation protocols were followed for cisplatin and the copolymers. One varied each copolymer (L101, P104, P105, and F108) content in solution from 2% mass v^{-1} to 10% mass v^{-1} in 2% mass v^{-1} increments. The other scheme fixed each Pluronic (L101, P104, P105, and F108) content at 10% mass v^{-1} and varied the amount of cisplatin in solution from 0% mass v^{-1} to 0.1% mass v^{-1} in 0.02% mass v^{-1} increments.

As dispersions were produced, aliquots were extracted by syringe, deposited into DSC pans, and tested using a TA Instruments Q-2000 DSC. Tests were conducted under nitrogen purge while the temperature was ramped from 0-40°C at 10°C min^{-1}, typical of other heating rates measures for other amphiphilic copolymers since the micelle forms between the 20°C and 30°C range. At least three replicates were evaluated per formulation.

The onset and peak temperatures and the size of the endotherm were determined from the heat flow curve. As the contents of each Pluronic were lowered (L101, P104, P105, and F108), the micellization endotherm shrunk and at some concentration, no endotherm was observed indicating the concentration was below the critical micellization concentration (cmc).

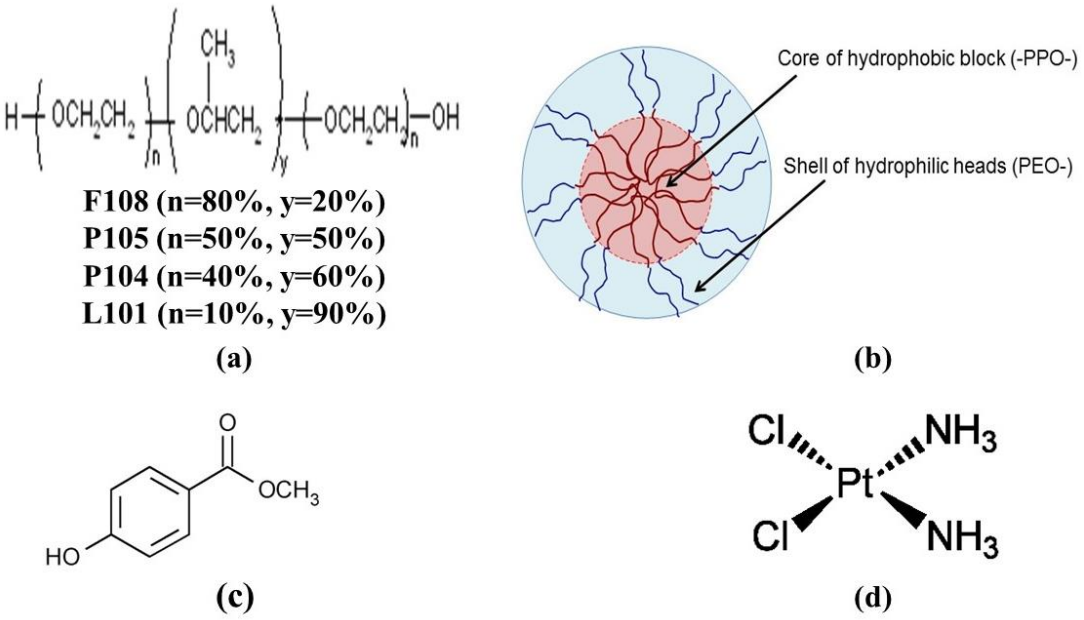

Figure 2.1: (a) Examples of Pluronics F108, P105, P104, and L101 (b) example of PEO-PPO-PEO micelle structure (c) methylparaben (d) cisplatin [72, 104].

2.3 Results and Discussion

2.3.1 DSC Results for Neat Micelles in Aqueous Solution

The influence of amphiphilic copolymer P105 content by DSC is noted in Table 2.1 and Figure 2.2 [72]. The temperature of the peak in the micelle formation is shifted slightly to lower temperatures (~2^{o}C) by adding more copolymer to solution. The enthalpy is also reduced with less P105 in solution since there are fewer micelles that can form in more diluted mixtures of amphiphile in solution above the cmc.

Table 2.1: DSC results for 4-10% P105 in H_2O. Larger P105 concentrations show both a lower $T_{micelle}$ and a larger ΔH on a per gram basis [72].

P105 concentrations (%mass v^{-1})	ΔH (J/g)	Micelle Formation Temperature (ºC)
2.0	0.81 ± 0.06	23.5 ± 0.07
4.0	1.96 ± 0.05	21.2 ± 0.11
6.0	3.27 ± 0.29	19.2 ± 0.08
8.0	3.68 ± 0.14	18.5 ± 0.04
10.0	4.09 ± 0.18	18.3 ± 0.2

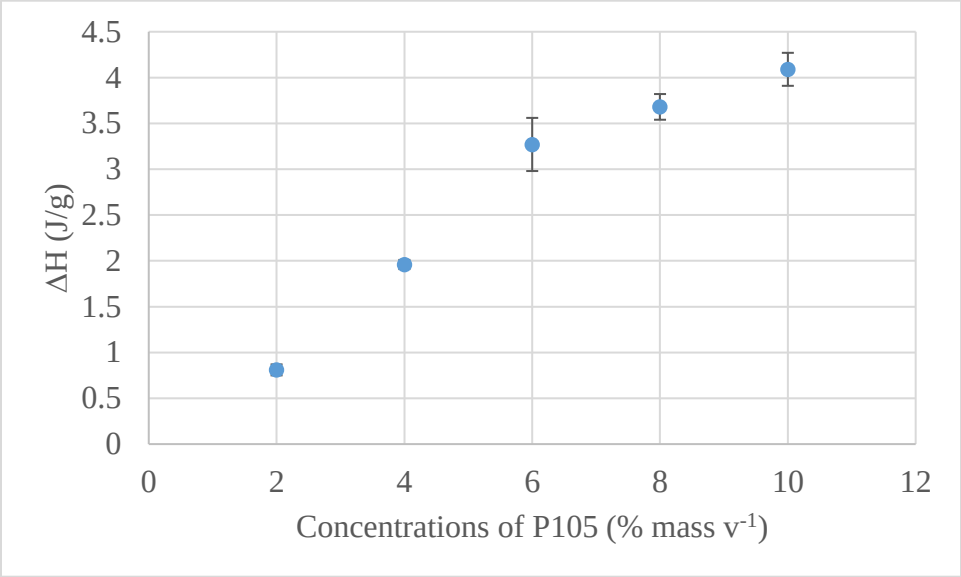

Figure 2.2: Increasing the concentrations of P105 in water also increased the enthalpy (ΔH) [72].

2.3.2 Critical Micelle Concentrations

As the concentration of amphiphilic copolymer is diluted, there are some minor distortions in the ΔH peak shape. At a low enough concentration, the micelle endotherm is not observed, as shown in Figures 2.3-2.6. The driving force is insufficient to form micelles below some threshold and that demarcation we note here as the cmc.

Figure 2.3 shows the concentration dependence of P105; the endotherm is suppressed at 0.4% mass v^{-1} [72]. The P105 cmc we resolved by DSC is slightly higher than that observed by Alexandridis et al. [119, 120] (0.3% mass v^{-1}) using UV-visible absorption spectroscopy at 25ºC

[119, 120]. For the larger thermodynamic analysis we used the cmc determinations from Alexandridis et al. [119, 120] for determining ΔS and ΔG although similar trends arise using the cmc resolved by DSC.

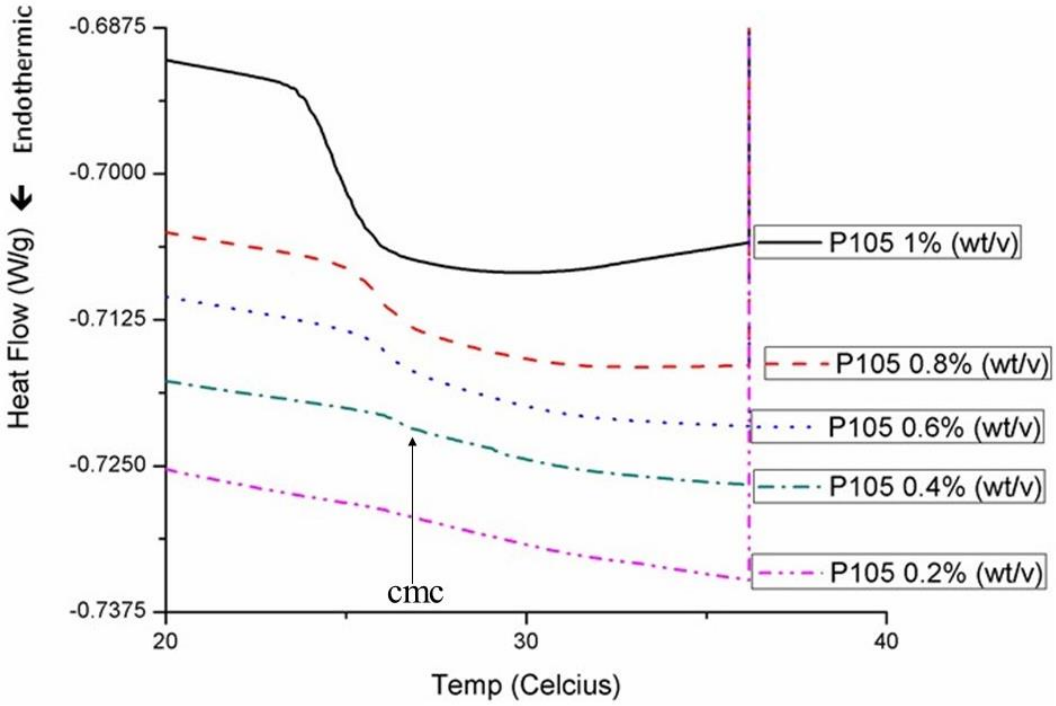

Figure 2.3: DSC results at P105 content: the critical micelle concentration (cmc) of neat Pluronic P105 was noted between 0.2% and 0.4% mass v^{-1} [72].

Figure 2.4 shows the concentration dependence of P104; the endotherm is suppressed at ~0.5% mass v^{-1} at ~24.5^{o}C [104]. The P104 cmc we resolved by DSC is slightly higher than that observed by Alexandridis et al. [10, 9] (0.3% mass v^{-1}) using UV-visible absorption spectroscopy at 25^{o}C.

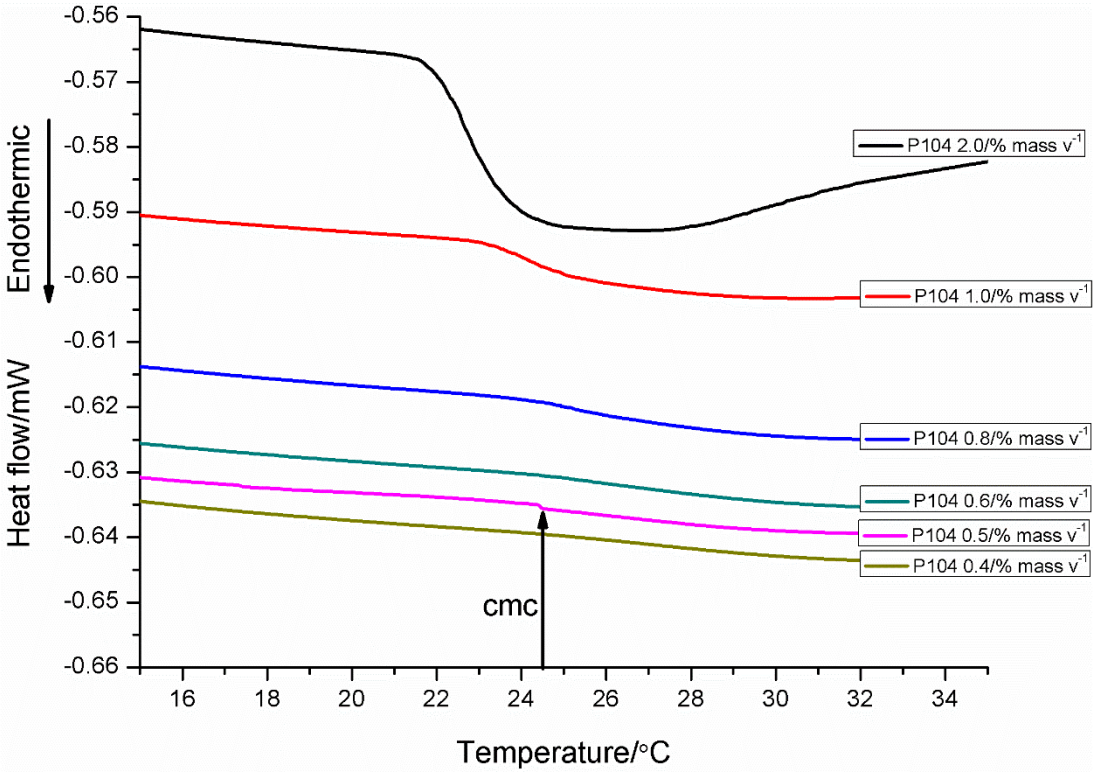

Figure 2.4: DSC results at low P104 content: the critical micelle concentration (cmc) of neat Pluronic P104 was noted at ~0.5% mass v^{-1} at ~24.5°C by DSC [104].

It makes sense that the cmc for P104 is similar to that of P105 because the ratio of hydrophilic (40% PEO) to hydrophobic (60% PPO) molecules is similar to that of P105's ratio (50% hydrophobic to 50% hydrophilic).

Figure 2.5 shows the concentration for L101; the endotherm is suppressed at ~3.0% mass v^{-1} at ~12.5°C [104].

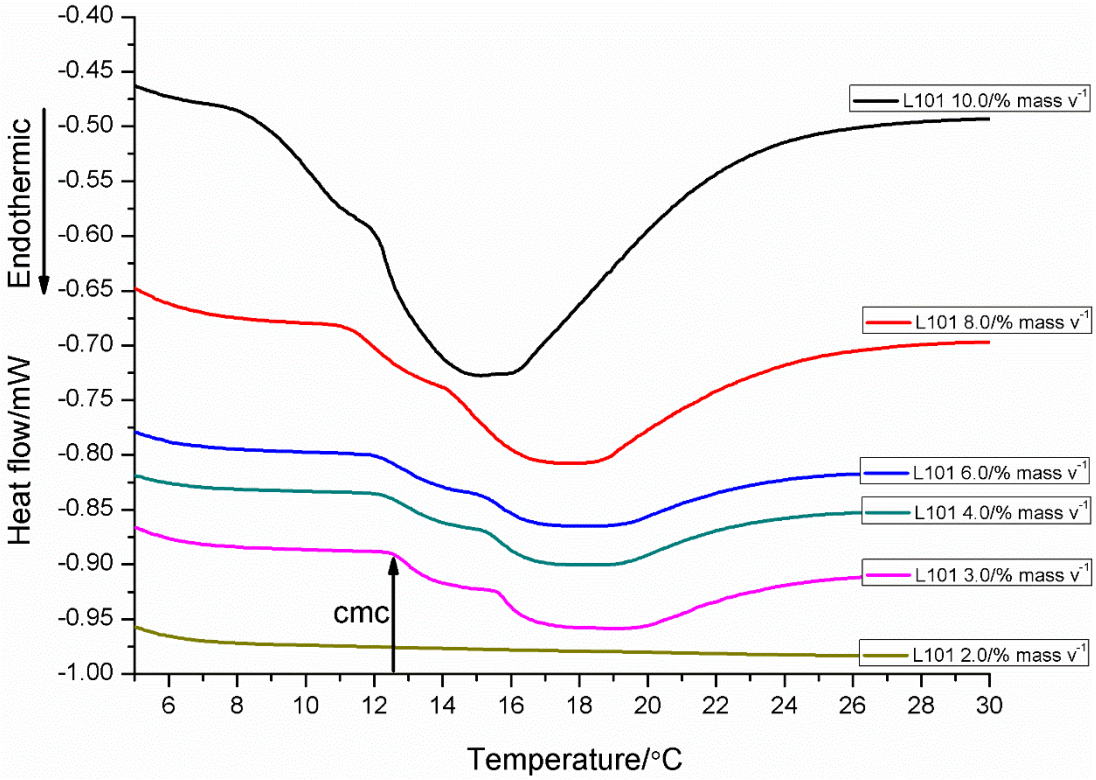

Figure 2.5: DSC results at low L101 content: the critical micelle concentration (cmc) of neat Pluronic L101 was noted at ~3.0% mass v^{-1} at ~12.5°C by DSC [104].

It makes sense that the cmc for L101 is at a higher concentration than the cmcs of both P104 and P105 because there is a larger hydrophobic region (40% PPO) compared to the hydrophilic region (10% PEO) that forces the micelle to form at higher concentrations.

Figure 2.6 shows the concentration dependence for F108; the endotherm is suppressed at ~4.0% mass v^{-1} at ~29.4°C [104]. The F108 cmc we resolved by DSC is slightly lower than that observed by Alexandridis et al. [10, 9] (4.5% mass v^{-1}) using UV-visible absorption spectroscopy at 25°C.

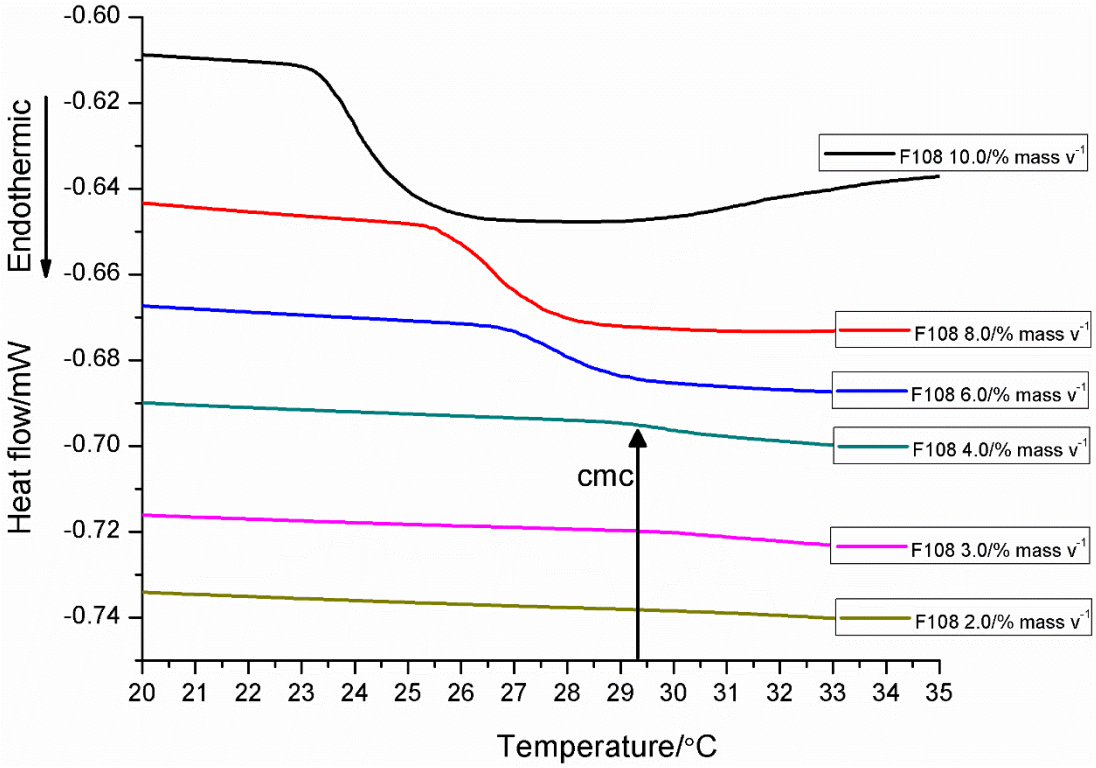

Figure 2.6: DSC results at low F108 content: the critical micelle concentration (cmc) of neat Pluronic F108 was noted at ~4.0% mass v^{-1} at ~29.4°C by DSC [104].

It makes sense that the cmc for F108 occurs at a higher concentration than the cmc's of both P105 and P104 because the ratio of hydrophilic (80/% PEO) to hydrophobic (20/% PPO) molecules is so far apart that the micelle is unable to form at lower concentrations. This would help explain why the cmc for L101 also occurs at a high concentration of 3.0% mass v^{-1} because the ratio of hydrophilic to hydrophobic is so far apart. We would expect the cmc for the more hydrophilic polymer, F108, to have a higher cmc than the more hydrophobic polymer, L101, because the aqueous solution in which it is suspended helps create a favorable environment where the micelle can form much easier at a higher concentration.

For the larger thermodynamic analysis, we used our cmc values of each copolymer for determining ΔS and ΔG. To address the question of how ternary additives affect the

thermodynamics of micelle formation, extractions from the low to high concentration regimes allow the determination of ΔG and direct measurements of the enthalpy of micellization. From these measurements, thermodynamic plots of ΔH-ΔS can be produced both in a neat state and in the presence of methylparaben or cisplatin. Figures 2.8-2.10 show the enthalpy-entropy compensation plots for P105 and P104, for their neat states and are compared to each amphiphile solution mixed with methylparaben or cisplatin. Two types of behaviors were observed with, a cisplatin-influenced compensation temperature profile (P104) and a cisplatin-insensitive compensation temperature profile (L101, P105, and F108).

2.3.3 Effect of Methylparaben on Micelle Formation Energetics

Figure 2.7 shows how adding methylparaben (MP) to 10% P105 solutions with increasing amounts of MP affected ΔH, which changed from 350.8 to 318.2 kJ mol^{-1} when increasing amounts of MP was added up to 1% mass v^{-1} [72]. The presence of MP modulates the interaction energy of the mixtures and reduces the size of both the micelle formation endotherm and its peak temperature. A similar suppression was noted by Bouchemal et al. [121] who characterized 1,2 propanediol in F127 and noted a ~20% smaller endotherm when added as much as 2.3 w/v%. Kelarakis noted the near athermal micellization in other diblocks [122, 123]. If ternary compounds raise structural disorder, the enthalpy contribution to micelle formation should be reduced.

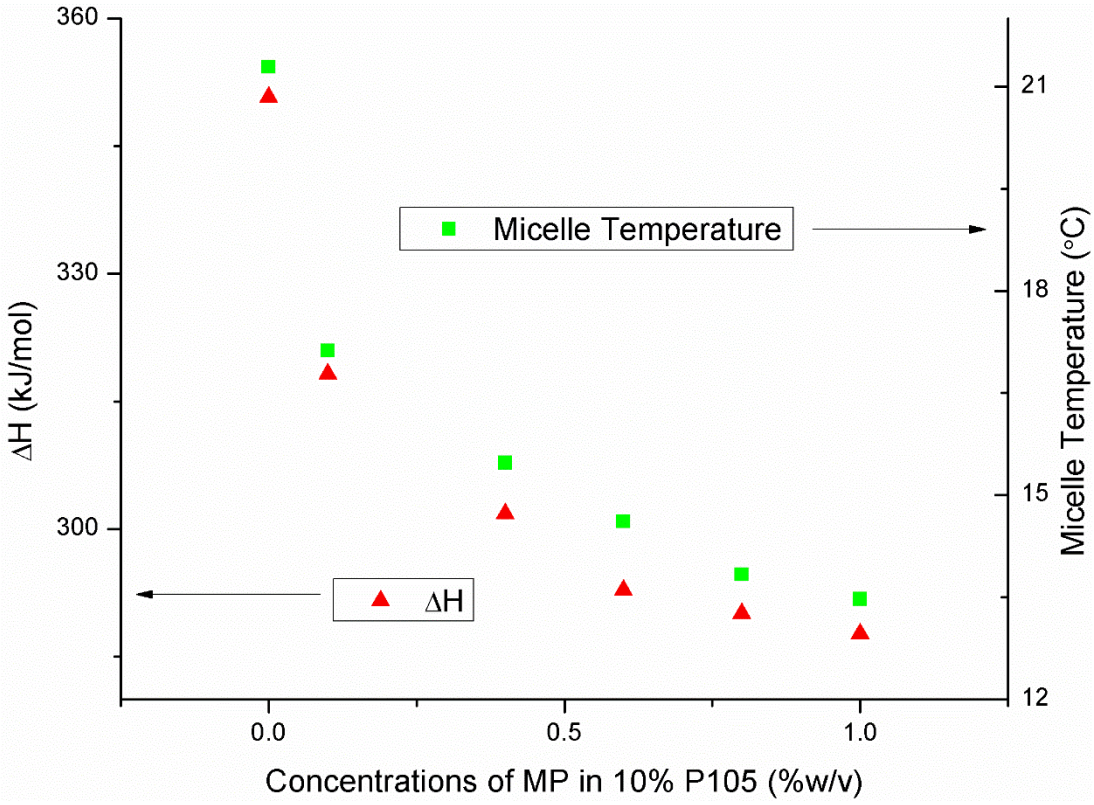

Figure 2.7: Increasing concentrations of MP in 10% P105 reduces both the $T_{micelle}$ and ΔH [72]. Standard deviation less than 0.05 for all points, therefor error bars are too small to be shown given the scale of the y-axis.

At higher concentrations relative to the P105 solution concentration, the presence of MP cannot suppress micelle formation. 80% of the original endotherm is still observable in 10% P105 with 1% MP.

The larger question overall is how the relative impact of the ternary additive affects the thermodynamics. To address this question, extractions from the low concentration regime allow the determination of ΔG and direct measurements of the enthalpy of micellization. From these measurements, thermodynamic plots of ΔH-ΔS can be produced both in a neat state and in the presence of MP.

Figure 2.8 is the enthalpy-entropy compensation plot for neat P105 (grey squares) that yields a compensation temperature of 294 K [72]. The compensation temperature determined for

neat P105 is very similar to that resolved for the 8-series of Pluronic (e.g. F68, F98) of 291.2 K [124]. Adding MP to the mixture triggers a rise in the compensation temperature from 294 K to 328 K (blue circles) treated as a separate dataset.

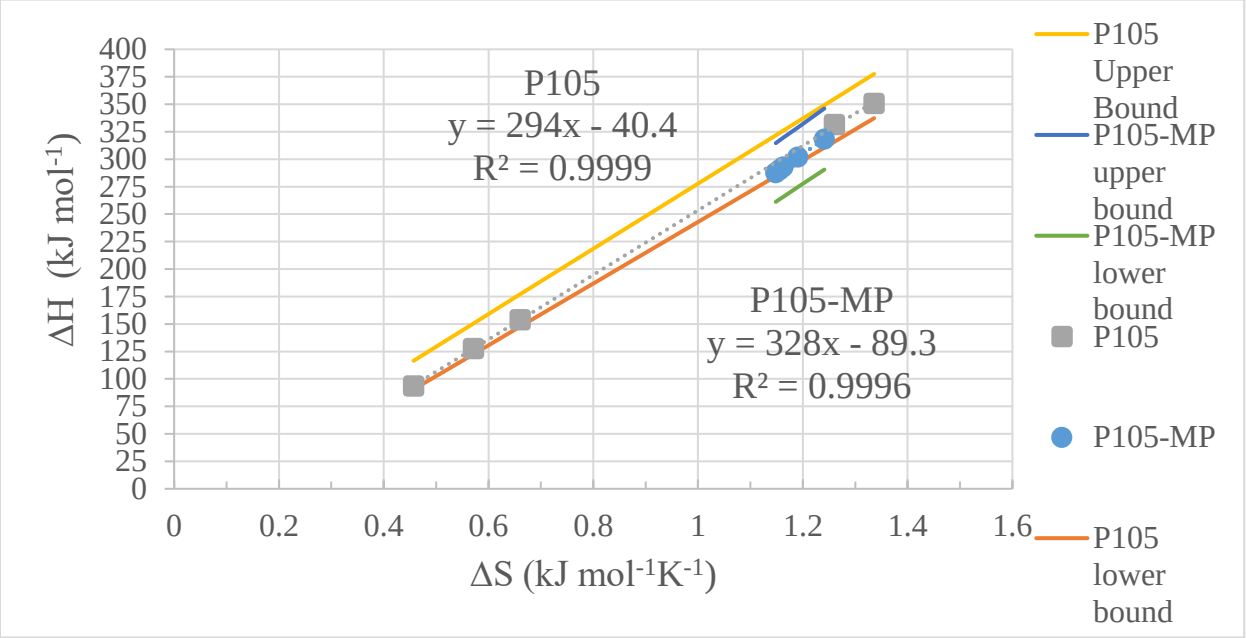

Figure 2.8: The enthalpy-entropy (ΔH-ΔS) compensation plot for P105, solutions both neat (grey squares) and co-formulated with MP (blue circles) [72]. Upper and lower bounds for neat P105 (yellow line slope = 297 K, and red line slope = 281 K respectively) and co-formulated with MP (blue line slope = 340 K, and green line slope = 317 K) represent 95% confidence intervals.

If the compensation temperature represents solute-solvent interactions, then the slopes of the ΔH-ΔS curves with and without ternary additives should be different. It seems appropriate that adding a ternary species might influence the energetics of micelle formation. We compared our results to published work by Bouchemal et al. [14] who using 1,2-propanediol with F127 using Isothermal Titraction Microcalorimetry. Interestingly, by using separate temperature compensation slope determinations, we observe from their results a similar rise in the compensation temperature from 293.3 to 316.5 K when co-formulated with 1,2-propanediol [14]. Their original analysis reported a mean $T_{compensation}$ of 298.1 K [14].

2.3.4 Effect of Cisplatin on Micelle Formation Energetics

Figure 2.9 is the enthalpy-entropy compensation plot for neat P105 that yields a compensation temperature of 289 K [104]. This determination is similar to that resolved for other PEO-PPO-PEO micelle structures (F108, F98, F88, F68, F38, and P65) of 291.03 K [71], 294.9 K for F88 and F68 [92], 293.3 K for F127 [14], 281 K for 12 Pluronics [91], between 280-298 K for a range of copolymers [93], 285 K for series of hydrocarbons [81], 293.9 K for neat P105 determined by an averaging algorithm [72], and 287 K through 319 K on 23 amphiphile systems [94]. Here we found that adding cisplatin to P105 was within range of the compensation temperature for neat P105. If there is an interaction between P105 and cisplatin, the energetics of the new interactions are not influencing the structure. This observation makes sense if the cisplatin is more bound in the aqueous solution and not interacting strongly within then micelle. We observed similar behavior for other PEO-PPO-PEO copolymers that were both more (F108) and less (L101) hydrophilic and found similar statistical insignificance of cisplatin on the modified compensation temperature.

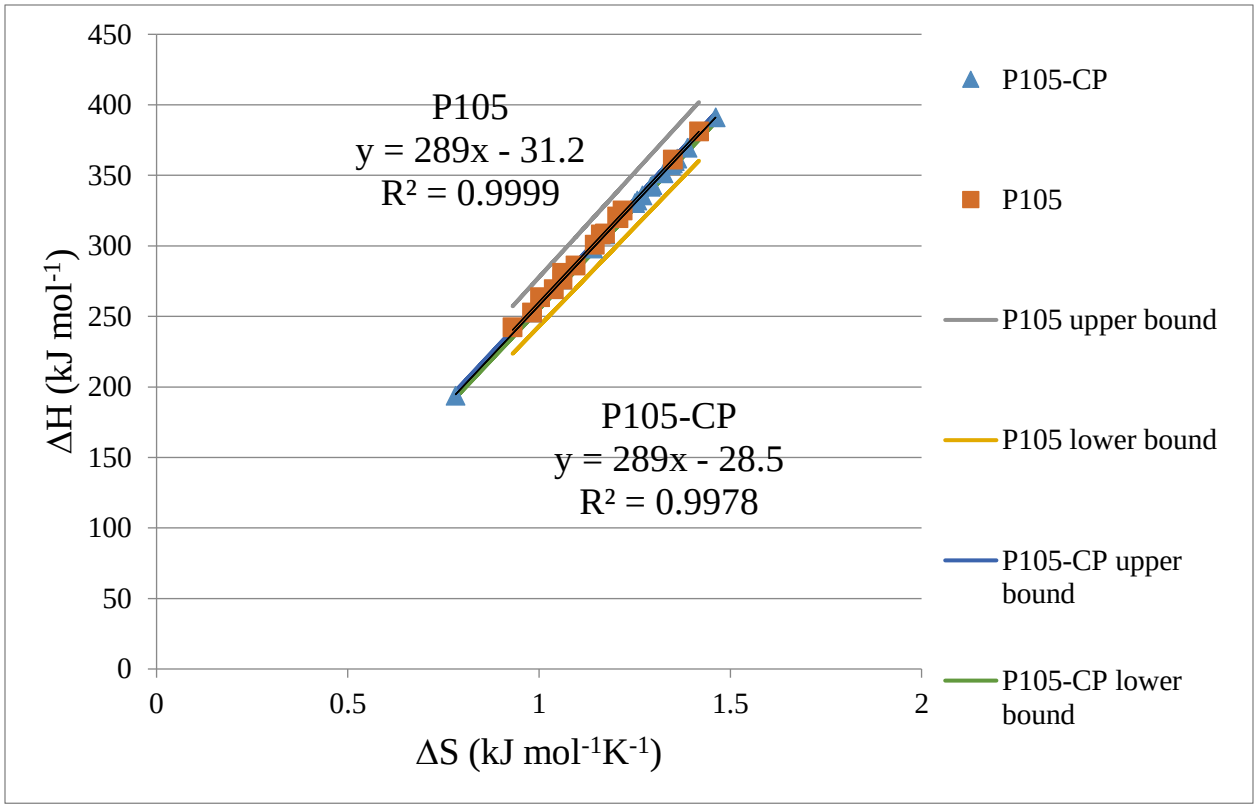

Figure 2.9: The enthalpy-entropy (ΔH-ΔS) compensation plot for P105, both neat (blue triangle) and co-formulated with cisplatin (orange squares) [104]. Upper and lower bounds for neat P105 (grey line slope = 297 K, and yellow line slope = 281 K respectively) and co-formulated with cisplatin (blue line slope = 290 K, and green line slope = 288 K) represent 95% confidence intervals.

Figure 2.10 is the enthalpy-entropy compensation plot for neat P104 that yields a compensation temperature of 302 K [104]. The P104 compensation temperature is higher compared to the other copolymers investigated as part of this study, but similar to that resolved for ionic surfactants of 319 K [90], Tetronic T904 in Na_2SO_4 (317.9 K) [93], 328.43 K for P105 co-formulated with methylparaben [72], and 287 K through 319 K on 23 amphiphile systems [94]. Adding cisplatin to the mixture reduces the compensation temperature from 302 K to 289 K, typical of the other PEO-PPO-PEO mixtures [14, 71, 72, 81, 91, 93, 94]. We attribute the compensation temperatures decrease in drug-loaded P104 condition to a larger interaction between cisplatin and the copolymer structure. Lee et al. [85] indicated that when the addition of a solute decreases both the enthalpy and entropy, this indicates a lowering of solution

hydrophobicity and is a characteristic of solute-solute and solute-solvent interactions. It is conceivable that cisplatin is more situated at the core/shell interface which would likely lead to a larger thermodynamic effect. If the cisplatin was less effective at changing the compensation of the other mixtures, then we assume that the drug is more fully engulfed in the corona or in solution, thus not affecting the hydrophobicity of the overall solution.

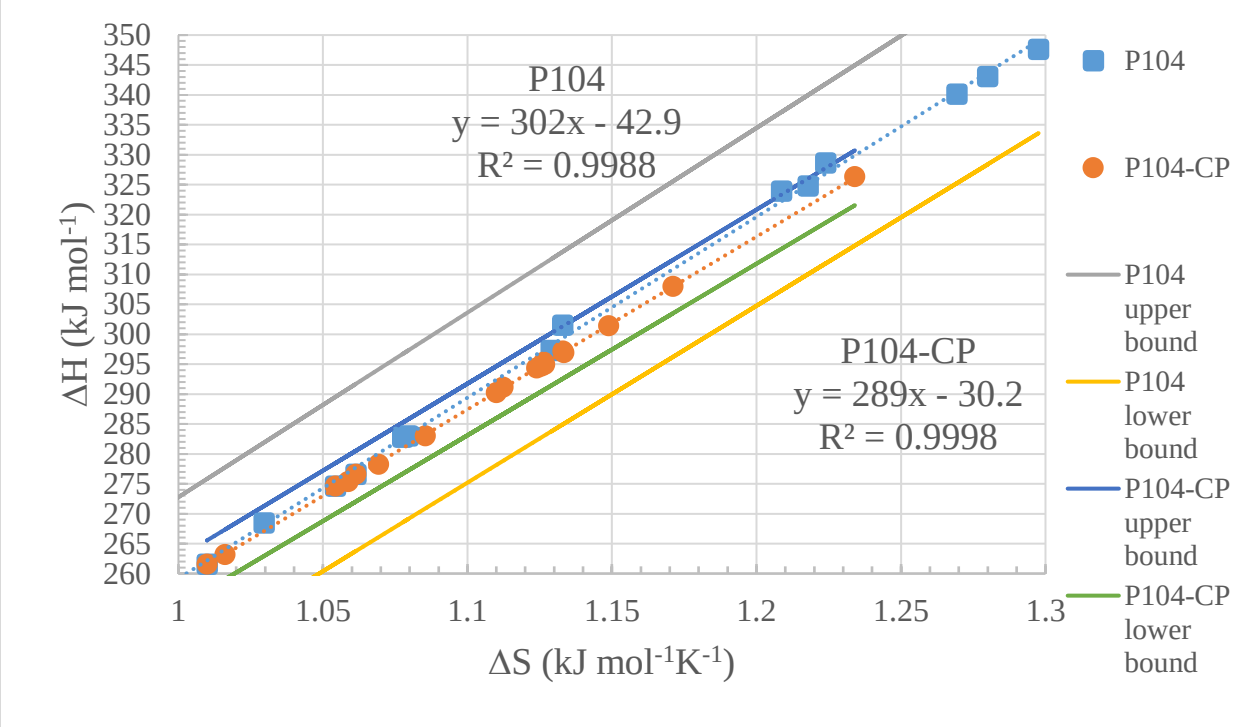

Figure 2.10: The enthalpy-entropy (ΔH-ΔS) compensation plot for P104, both neat (blue squares) and co-formulated with cisplatin (orange circles) [104]. Upper and lower bounds for neat P104 (grey line slope = 308 K, and yellow line slope = 296 K respectively) and co-formulated with cisplatin upper and lower bounds (blue line slope = 291 K, and green line slope = 287 K respectively) represent 95% confidence intervals.

A summary of the enthalpy-entropy compensation temperatures for all the PEO-PPO-PEO copolymers we have studied (P105, P104, F108, L101) in both the neat states and co-formulated with cisplatin, along with corresponding correlation values (R^2), are presented in Table 2.2 [104]. A summary of our cmc values compared with others are also included.

Table 2.2 Copolymer cmc values, compensation values, and correlation values of neat and co-formulated with cisplatin [104]. Each compensation temperature was tested to determine whether the slopes were statistically significantly different from one another with a 95% confidence interval.

PEO-PPO-PEO Copolymer type	cmc/% mass v^{-1} by DSC	cmc/% mass v^{-1} by Cloud Point	Neat compensation temperature (K)	R^2	Cisplatin-modulated compensation temperature (K)	R^2
P105	0.4%	0.3% [10]	289 CI [281, 297]	0.9978	289 CI [288, 290]	0.9999
P104	0.5%	0.3% [10]	302 CI [296, 308]	0.9988	289 CI [287, 291]	0.9998
F108	4.0%	4.5% [10]	297 CI [292, 298]	0.9998	296 CI [294, 297]	0.9998
L101	~3.0%		283 CI [281, 285]	0.9999	284 CI [281, 287]	0.9996

Along with P105, the compensation temperatures for L101 and F108 also showed very little changes from the neat states to the cisplatin-loaded states, which suggests that cisplatin does not seem to affect the energetics of micelle formation in the copolymers. Cisplatin is likely fully contained in the hydrophilic regions of each dispersion.

Since the compensation temperature represents solute-solvent interactions [14, 81-83, 85-96], then the slopes of ΔH-ΔS curves with and without ternary additives should be different if the ternary constituent interferes with energetics of micelle formation. As observed in our previous study with methylparaben [72], adding a ternary species influenced the energetics of micelle formation. Here, we observe a compensation temperature invariance adding cisplatin to P105, F108, and L101. The invariance suggests that the energetics of micelle formation are not being influenced by the presence of cisplatin. Instead, we only observed a change in the energetics of micelle formation adding cisplatin to P104, which is more similar to our observations with methylparaben and F127 [16, 15].

A schematic of cisplatin sequestration within micelles is provided in Figure 2.11 [104]. Cisplatin is considered to be hydrophilic due to its polarity, but Ng et al. [125] has referred to it as being moderately hydrophilic. As such, it is postulated that cisplatin is found both distributed within the corona and at the core-shell interface. There have been other efforts to conjugate and

alter the cisplatin binding within the micelle, following work by Desale et al. [126], who used an anionic glutamic acid block to coerce cisplatin more comprehensively to the core-shell interphase separating the hydrophilic and hydrophilic blocks. The moderate hydrophilicity of cisplatin might help explain why in the DSC we only observed a variation in the compensation temperature with and without cisplatin for P104. There is something about the ratio of hydrophilic to hydrophobic segments for P104 that interacts with cisplatin and affects the energetics. The key experiment is to perform controlled scattering studies to identify exactly where within micelles the platinum beacons are situated on average. The presence of cisplatin is essentially a perturbant in the micelle and if it disrupts the organization of the micelle, it seems plausible that the energetics of micelle formation might be suppressed if the payoff for forming a micelle comes with the penalty of distributing the cisplatin within the formed micelle.

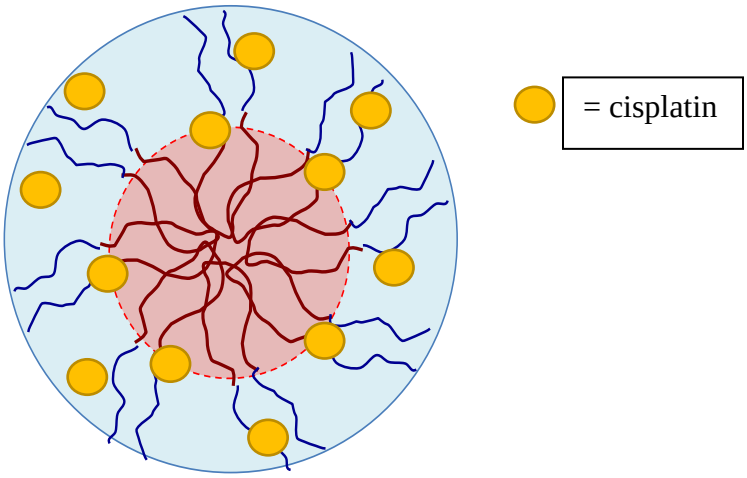

Figure 2.11: Schematic showing how cisplatin is distributed within micelles portioning between the PEO corona and the core-shell interface with PEO-PPO-PEO Pluronic P104 [104].

2.4 Conclusions

We have probed how MP and cisplatin affects PEO-PPO-PEO micelle formation in the low concentration regime to identify a critical micelle concentration and at higher concentrations co-formulated with MP and cisplatin. The critical micelle concentrations found for the copolymers we tested were similar to those from previous work [72, 10, 9]. Increasing P105 from 4% to 10% reduced $T_{micelle}$ and raised the endotherm. We propose that the enthalpy-entropy compensation plot for neat and MP or cisplatin-loaded solutions of amphiphilic copolymers can resolve the perturbation in the micelle formation energetics due to the additive. The $T_{compensation}$ values found here have also been compared to measurements from previous works [14, 71, 72, 81, 90-94]. The use of temperature compensation plots is an indicator of surfactant quality in formulated dispersions coerced into directed assembly. $T_{compensation}$ was essentially invariant adding cisplatin to the highly hydrophobic copolymer (L101), the hydrophilic copolymer (F108) and had a profound effect on the more amphiphilic P104. These results might help explain where within amphiphilic copolymer micelles various drugs of a certain hydrophilicity are situated if cisplatin is partitioned to the core-shell interface of the micelle. The large difference in the behavior of $T_{compensation}$ between P104 and P105 belied their subtle difference in the structure, which was not anticipated as the $T_{compensation}$ for P105 was also invariant by adding cisplatin. Our findings present a rationale for explaining how the presence of ternary additives, like MP and cisplatin, interacts thermodynamically with forming micelles and the potency of the interaction between drug and micelle might regulate drug bioavailability.

2.5 Acknowledgments

We acknowledge the Rackham Summer Institute at UM for support and discussions with KA Juggernauth, NAK Meznarich, and KM Batzli during the project. We would also like to thank the GEM Fellowship funded through DuPont and the National Physical Science Consortium (NPSC) fellowship funded through the National Institute of Standards and Technology (NIST) for their financial support.

CHAPTER III

Structural Analysis of Micelle Formation

3.1 Introduction

It is known that ternary additives can influence the aqueous micellization and gelation behavior of PEO-PPO-PEO amphiphiles [15, 16, 72, 104]. Methylparaben, for example, lowers the gelation temperature of the amphiphile F127 solution by as much as 10-15^{o}C [12, 16]. A structural evaluation is important to understand the structure-property relationship that exists in these pharmaceutical loaded amphiphile formulations.

In the previous chapter, we probed how cisplatin affects the PEO-PPO-PEO micelle formation in the low concentration regime to identify a critical micelle concentration and at higher concentrations co-formulated with cisplatin [104]. We proposed that the enthalpy-entropy compensation plots for neat and cisplatin-loaded solutions of amphiphilic copolymers can resolve the perturbation in the micelle formation energetics due to the additive [104]. The use of temperature compensation plots is an indicator of surfactant quality in formulated dispersions coerced into directed assembly [104]. $T_{compensation}$ was essentially invariant adding cisplatin to the highly hydrophobic copolymer L101, the hydrophilic copolymer F108, and the more amphiphilic copolymer P105, but cisplatin had a profound effect on the more amphiphilic P104 [104].

Our group has previously investigated the effect of heating rate on the gelation of both F127 and F127-methylparaben solutions and found that not only does the presence of methylparaben lower the gelation temperature; it also accelerates the gel transition [16]. We also

previously used small-angle X-ray scattering (SAXS) to investigate the crystalline structure of F127 solutions as they are heated through their gelation temperatures both neat and co-formulated with methylparaben and dexamethasone [15]. We found that the presence of methylparaben and dexamethasone facilitates or enhances the structural ordering, allowing ordered phases to emerge at lower temperatures and remain at higher temperatures as compared to the neat F127 solutions [15]. However, the gelation kinetics of amphiphiles P104, P105, and F108 as they interact with a ternary additive like cisplatin is less well known. A more direct evaluation of structural evolution is needed to better understand the transition from the disordered to the ordered state for P104, P105, and F108.

SAXS and SANS scattering have been used previously to study the structure and organization of micellar systems [1, 5, 127, 128, 15], including P104 [129-141], P105 [142-147], and F108 [148-156]. These techniques allow insight into both the structures within the micelles and the lattice structures into which they arrange. Svensson et al. [135] noticed SAXS diffraction patterns for P104 in the normal micellar liquid crystalline phase, I1, composition 31% mass v^{-1} at 25^{o}C. Using DSC, we also noticed P104 was profoundly influenced by the presence of cisplatin that must influence the core-shell interface between the hydrophobic and hydrophilic regions of the micelle [104]. In this chapter, we use SAXS to investigate the crystalline structure of P104, P105, and F108 solutions as they are heated through their gelation temperatures. Our aim is to identify changes in quasicrystalline lattice formation as an effect of added pharmaceuticals, and resolve whether cisplatin is located within the micelles' core, shell, core-shell interface, or randomly dispersed in solution. We also observe structural changes associated with the presence of cisplatin on P104, P105, and F108 and examine the different kinetics of gel formation with varying core-shell dimension. With the complications for therapeutic delivery linked with the

limited solubility of hydrophobic drugs, key features in bioavailability could be linked to the thermodynamic mixing drug and amphiphile combinations.

The experiments, results, and discussion covered in this chapter are in final preparations to be submitted for review [157].

3.2 Materials and Methods

3.2.1 Solution Preparation

Pluronics P104, P105, and F108 were obtained from BASF (Wyandotte, MI) and used as received. Aqueous solutions of 31% mass v^{-1} P104, P105, and F108 were each prepared according to the "cold" processing method of Schmolka [29] by dissolving weighed amounts of each amphiphile into distilled water, which were then left to solubilize quiescently at 4^{o}C. At this high concentration, repeated cool/mix cycles were needed to fully solubilize the polymers. Cisplatin (Sigma-Aldrich) was used as received and added to aqueous solutions of these varying Pluronics (P104, P105, F108).

Two types of formulation protocols were followed. One fixed each Pluronic (P104, P105, and F108) content and cisplatin content at 31% mass v^{-1} and 0.1% mass v^{-1} respectively, to investigate the structures formed in both neat and co-formulated with cisplatin to study both the progressive evolution and breakdown of these structures as the temperature is increased from 10^{o}C to 35^{o}C. To see if cisplatin affects the kinetics of micelle and gel formation temperatures as a function of concentration, we also fixed P104 (31% mass v^{-1}) and varied the cisplatin concentrations from 0.02% to 0.1% mass v^{-1} in 0.02% increments through 10^{o}C to 35^{o}C.

3.2.2 Small-Angle X-Ray Scattering (SAXS)

SAXS experiments were conducted at Argonne National Laboratory (Argonne, IL) at the Advanced Photon Source (APS) on beamline 12-BM-B operating at 12 keV. Static heating tests were used to probe the structure at a series of discrete temperatures between 10^{o}C and 35^{o}C. Each sample was aliquoted into thin-walled capillary tubes (0.01 mm wall thickness) and simultaneously placed into the heating stage illumination. Each sample was subjected to a 1-minute equilibration time at 10^{o}C to ensure the sample temperature was uniform and steady. Scattering data was collected for each sample for 1 minute. After measuring each sample at the corresponding temperature, the heating stage ramped up 2^{o}C, followed by a subsequent 1-minute equilibration, then re-exposed again for 1 minute. This process was repeated until 34^{o}C was reached. During the heating and equilibration phases, the X-ray shutters were closed to avoid unnecessary exposure to the beam. The starting and final temperatures were chosen to be well below and above the gelation temperature of the sample, respectively from prior determinations of the critical micelle concentrations of P104, P105, and F108 using DSC [72, 104].

3.2.3 Data Collection and Analysis

2D SAXS data were collected. The data was integrated around the azimuthal axis to generate 1D plots of the measured intensity as a function of the scattering vector q using SASView. Peak positions in the generated I (q) plots were quantified using OriginLab's peak analyzer function. These peaks were then compared to the expected reflections for the various known crystal structures in order to identify the structures present in the solution. Table 3.1 [157] presents a summary of the first five peaks and their positions relative to the fundamental scattering peak for the fcc and bcc crystal systems [15].

Table 3.1: Summary of expected peaks and relative peak positions for the bcc and fcc crystal systems

Crystal	q_0	q_1	q_2	q_3	q_4
bcc	(110)	(200)	(211)	(220)	(310)
position	q_0	$2^{1/2}\, q_0$	$3^{1/2}\, q_0$	$4^{1/2}\, q_0$	$5^{1/2}\, q_0$
fcc	(111)	(200)	(220)	(311)	(222)
Position	q_0	$(4/3)^{1/2} q_0$	$(8/3)^{1/2}\, q_0$	$(11/3)^{1/2} q_0$	$(12/3)^{1/2} q_0$

The size of a cubic unit cell a, can be obtained by plotting $(q/2\pi)^2$, where q is the scattering vector, versus the Miller indices $(h^2 + k^2 + l^2)$ of the cubic structures, according to Equation (3.1) [140].

$$(q/2\pi)^2 = (1/a)^2(h^2 + k^2 + l^2) \tag{3.1}$$

At the APS beamline 12-BM-B, 12 keV of beam energy was used allowing us to solve for frequency, ν, in Equation (3.2).

$$E = h\nu \tag{3.2}$$

Where E is energy of the beam and h is Planck's constant. Using frequency, ν, and speed of light, c, Equation (3.3) can be used to solve for the wavelength, λ, of the X-rays.

$$\lambda = \frac{c}{\nu} \tag{3.3}$$

The relationship between q and theta for SAXS is identified in Equation (3.4) where 2θ is the angle between the incident X-ray beam and the detector measuring the scattering intensity.

$$q = \frac{4\pi \sin(\theta)}{\lambda} \tag{3.4}$$

Using Bragg's law, Equation (3.5) can be used to solve for the spacing, d, between adjacent (hkl) lattice planes.

$$d = \frac{\lambda}{2\sin(\theta)} \tag{3.5}$$

Finally, using the spacing, d, for cubic crystals as length, L, and the change in temperature, ΔT, assuming negligible effect of pressure, the linear thermal expansion coefficient, α_L, can be calculated with Equation (3.6).

$$\alpha_L = \frac{\Delta L}{L \Delta T} \tag{3.6}$$

where L is the original length, and ΔL/ΔT is the rate of change of the linear dimension per unit change in temperature.

3.3 Results and Discussion

3.3.1 Phase Structure Identification

Figure 3.1 [157] compares the presence of ordered phases for neat P104 (31% mass v^{-1}) and P104 mixed cisplatin (0.1% mass v^{-1}) at 28^{o}C with peak identifications. Crystal structures were determined based on their ratio to the fundamental peak. A full list of peak positions and phase structure for neat P104 (31% mass v^{-1}) and cisplatin mixed P104 (0.02%-0.1% mass v^{-1}) at 28^{o}C is listed in Table 3.2 [157].

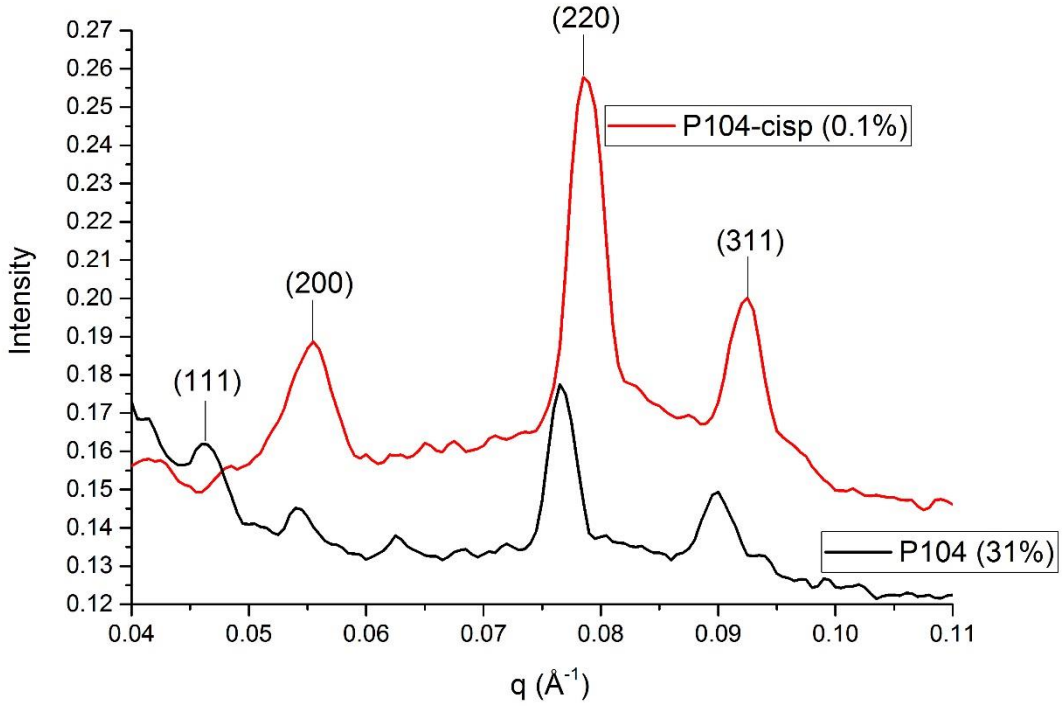

Figure 3.1: Comparison of peak identifications of neat P104 (31% mass v^{-1}) and P104 mixed cisplatin (0.1% mass v^{-1}) at 28°C [157].

Upon analyzing neat P104 at 28°C, it appears the primary peak, (111) at q_0, is suppressed with added cisplatin, while preserving the higher order peaks. The higher order peaks are also enhanced with added cisplatin, evidenced by a sharp rise in the signal to noise ratio. For example, for the fcc peak (220) at $(4/3)^{1/2}q_0$ for neat P104, the intensity increased from 0.13:0.18, while with added cisplatin, the intensity for the same peak increased from 0.16:0.26. This suggests cisplatin either enhances the structural ordering of the fcc phase of micelle formation in P104 or the platinum atom, itself a strong scatterer, and its colocation in organized arrays within the micelles enhances the coherence of the scattering when its partitioned within the colloidal crystals. Since the higher order peaks are enhanced and no broad scattering is observed once cisplatin is added, it is reasonable to consider that cisplatin is situated within the micelle structure and not randomly distributed in solution. This adds further evidence to our previous claim (using

DSC) that the moderately hydrophilic cisplatin is found both distributed within the corona and at the core-shell interface of the micelle structure [104]. There are also slight shifts to higher q values with added cisplatin (Table 3.2), which the presence of cisplatin reduces the lattice plane spacing [157]. This observation compares to work we have previously discovered using DLS to determine micelle size [16]. We concluded the presence of methylparaben increased the micelle monodispersity, which led to tighter packing with fewer defects in the lattice, thus producing small observed shifts in the lattice parameter [16]. Further studies are needed to better characterize the size of P104, P105, and F108 micelles with added cisplatin. The additives may play a role in facilitating transitions between regions within the micelle.

Not shown here, adding cisplatin had little effect on the temperature where ordering occurred relative to neat P104 samples. For example, an ordered phase was first seen in the 20^{o}C measurement for neat P104, as compared to 17^{o}C-20^{o}C measurement for the cisplatin mixed P104 samples. The breakdown of the neat P104 ordered phases were, however, evident at higher temperatures. As shown in Figure 3.1 [157], the fcc phase is present at 28^{o}C, but a breakdown of the fcc phase occurs between 30^{o}C -34^{o}C. As the concentration of cisplatin increased, however, the presence of ordered phases was preserved at slight higher temperatures (29^{o}C-30^{o}C). This indicates a cisplatin induced stabilization of the quasicrystalline lattice in P104 gels at slightly higher temperatures. Preserving ordered phases with the addition of a ternary additive was previously observed with the addition of methylparaben and dexamethasone in F127 gels [15].

Figure 3.2 [157] compares the presence of ordered phases for neat P105 (31% mass v^{-1}) and P105 mixed cisplatin (0.1% mass v^{-1}) at 28^{o}C with peak identifications. A full list of peak positions and phase structure for neat P105 (31% mass v^{-1}) and cisplatin mixed P105 (0.1% mass v^{-1}) at 28^{o}C is listed in Table 3.2 [157].

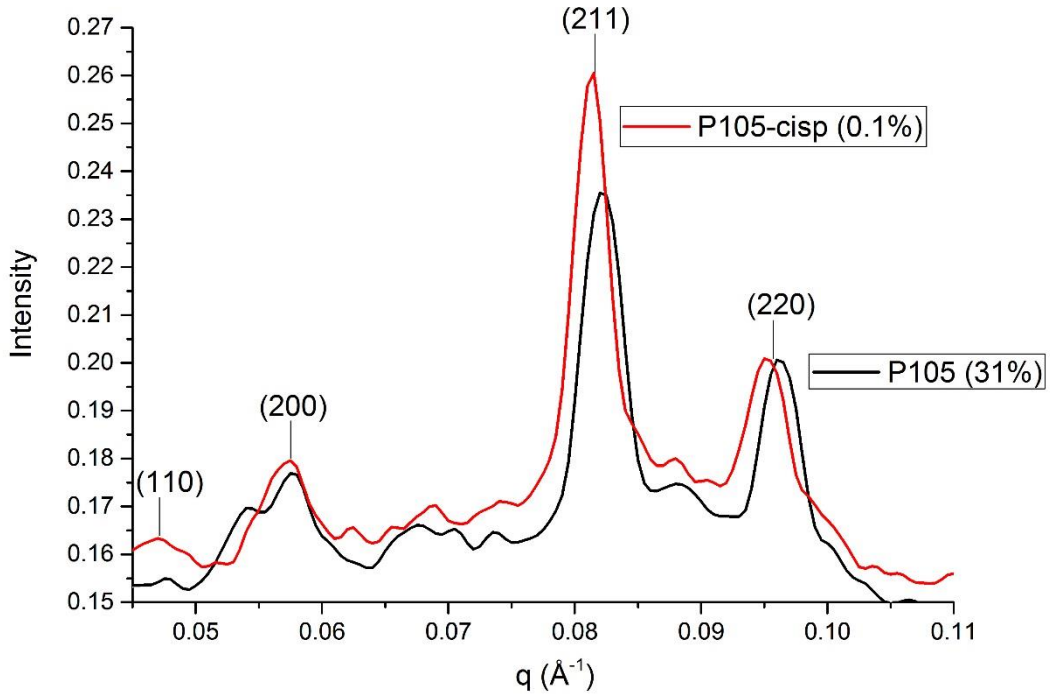

Figure 3.2: Comparison of peak identifications of neat P105 (31% mass v^{-1}) and P105 mixed cisplatin (0.1% mass v^{-1}) at 28°C [157].

In this case, for cisplatin mixed P105 at 28°C, it appears the primary peak, (110) at q_0, was not suppressed, but only the bcc peak (211) at $3^{1/2}q_0$ was enhanced (increase from 0.16:0.23 to 0.17:0.26). The bcc peak (200) at $2^{1/2}q_0$ is also more defined with added cisplatin which suggests cisplatin enhances the structural ordering of the bcc phases of micelle formation in P105 and the phases are stable. Since the higher order peaks are enhanced and no random scattering is observed once cisplatin is added, this also indicates cisplatin is situated within the micelle structure and not randomly distributed in solution. There is a slight shift to lower q values with added cisplatin (Table 3.2), which indicates cisplatin is increasing the lattice plane spacing by a small amount [157].

Similar to P104, the presence of cisplatin had little effect on the temperature where ordering occurred relative to neat P105 samples. For example, an ordered phase was first seen in

the 18°C measurement for neat P105 as compared to 20°C measurement for the cisplatin mixed P105 samples. Breakdown of the ordered phases was also evident at higher temperatures for neat P105 as the bcc phase with the highest intensity was at 28°C, with decreasing intensity at 30°C, and random scattering at 34°C. For cisplatin mixed P105, however, the highest intensity was preserved at 30°C, with random scattering at 34°C. Cisplatin helped to stabilize the quasicrystalline lattice in P105 gels as well.

Figure 3.3 [157] compares the presence of ordered phases for neat F108 (31% mass v^{-1}) and F108 mixed cisplatin (0.1% mass v^{-1}) at 28°C with peak identifications. A full list of peak positions and phase structure for neat F108 (31% mass v^{-1}) and cisplatin mixed F108 (0.1% mass v^{-1}) at 28°C is listed in Table 3.2 [157].

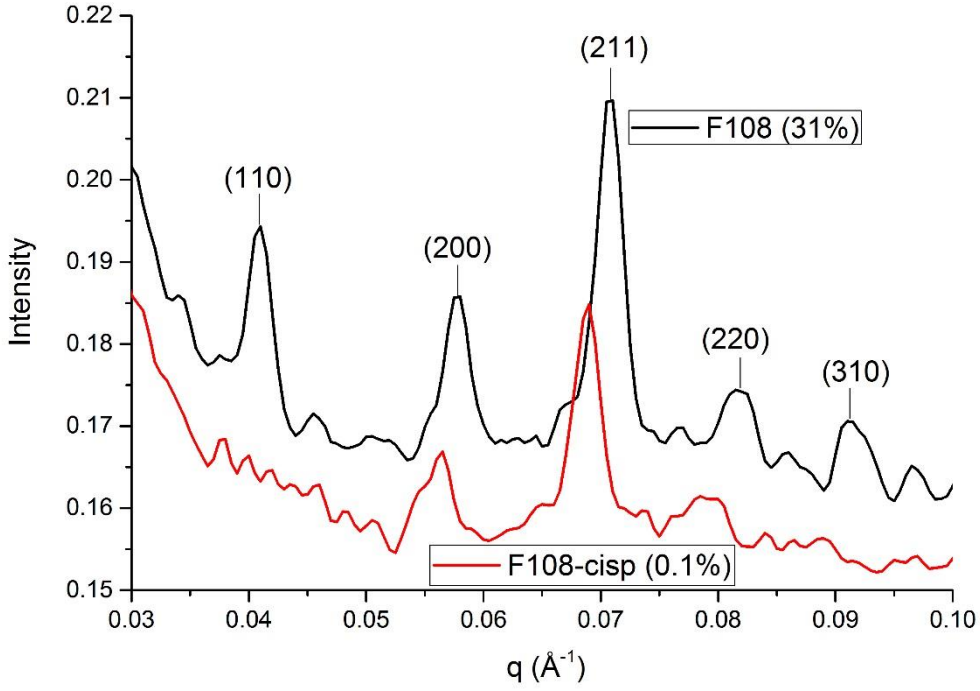

Figure 3.3: Comparison of peak identifications of neat F108 (31% mass v^{-1}) and F108 mixed cisplatin (0.1% mass v^{-1}) at 28°C [157].

Similar to cisplatin mixed P104 at 28°C, cisplatin mixed F108 has the primary peak, (110) at q_0, suppressed significantly. This primary peak suppression was observed previously with dexamethasone and F127 [15] and thin films of poly(alkoxyphenylenevinylene-b-isoprene) rod-coil copolymers arranged into lamellar structures [158]. In this case, cisplatin reduces the higher order peaks (from 0.17:0.21 to 0.16:0.18), which suggests cisplatin destabilizes the structural ordering of the bcc phase of micelle formation in F108. Since the higher order peaks are compressed and there is evidence of random scattering observed once cisplatin is added, this would suggest cisplatin is not fully situated within the micelle structure and it is randomly distributed in solution. This would make sense, since cisplatin is moderately hydrophilic and F108 is 80% hydrophilic, so the platinum particles are randomly distributed throughout the corona and aqueous solution. Similar to P105, there are also slight shifts to lower q values with added cisplatin for F108 (Table 3.2), which indicates cisplatin is expanding the lattice plane spacing [157].

Similar to P104 and P105, the presence of cisplatin also had little effect on the temperature where ordering occurred relative to the neat F108 samples. An ordered phase was first seen in the 22°C measurement for neat F108, as compared to 23°C measurement for the cisplatin mixed F108 sample. Breakdown of the ordered phases was evident at higher temperatures for neat F108 as the phases with the highest intensity was present at 30°C, and random scattering at 34°C. For cisplatin mixed F108, the same trend was observed. This indicates cisplatin has no effect on the stabilization of the quasicrystalline lattice in F108 gels.

Studies have been carried out to measure the localization or interaction of ternary additives with PEO-PPO-PEO micelles [159-163]. Desale et al. [164] used an anionic glutamic acid block to coerce cisplatin more comprehensively to the core-shell interphase separating the

hydrophilic and hydrophobic blocks to conjugate and alter the cisplatin binding within the micelle. Based on prior work [104], we believe that the added cisplatin is also localized in the core-shell interphase of the micelles for P104, and P105. The moderate hydrophilicity of cisplatin might help explain why the enhanced intensity of structural ordering in P104 and P105, but not in F108. There is something about the ratio of hydrophilic to hydrophobic segments for P104 and P105 that interacts with cisplatin and affects the energetics.

Table 3.2 [157] shows the identified peak positions for each sample in Figures 3.1, 3.2, and 3.3 [157], and the associated crystal structure identified from peaks present at 28ºC. Table 3.2 [157] also shows the calculated size of each cubic unit cell, a (Å), using Equation (3.1), and the calculated linear thermal expansion coefficient, α_L ($^oC^{-1}$), using Equation (3.6) [157].

Table 3.2: Fundamental (q_0) and higher order (q_n) peaks (in units of $Å^{-1}$), identified phase structure, fcc ([a]), bcc ([b]), unit cell size, a (Å), and linear thermal expansion coefficient, α_L ($^oC^{-1}$), at 28ºC for neat P104, P105, and F108 (31% mass v^{-1}) and mixed cisplatin (0.02% - 0.1% mass v^{-1}) [157].

Sample	**q_0** ($Å^{-1}$)	**q_1**	**q_2**	**q_3**	**q_4**	**Phase**	**a**(Å)	**α_L** ($^oC^{-1}$)
Neat P104	.0462	.0541[a]	.0765[a]	.0900[a]	-	FCC	**232**	**$9.7x10^{-3}$**
P104-cisp 0.02%	.0463	.0537[a]	.0761[a]	.0891[a]	-	FCC	**234**	**$8.1x10^{-3}$**
P104-cisp 0.04%	.0493	.0555[a]	.0785[a]	.0918[a]	-	FCC	**226**	**$8.6x10^{-3}$**
P104-cisp 0.06%	.0509	.0535[a]	.0781[a]	.0910[a]	-	FCC	**227**	**$9.0x10^{-3}$**
P104-cisp 0.08%	.0492	.0546[a]	.0776[a]	.0909[a]	-	FCC	**229**	**$9.0x10^{-3}$**
P104-cisp 0.1%	.0483	.0556[a]	.0787[a]	.0925[a]	-	FCC	**226**	**$8.8x10^{-3}$**
Neat P105	.0478	.0577[b]	.0822[b]	.0962[b]	-	BCC	**187**	**$3.8x10^{-3}$**
P105-cisp 0.1%	.0470	.0573[b]	.0813[b]	.0953[b]	-	BCC	**189**	**$4.4x10^{-3}$**
Neat F108	.0410	.0578[b]	.0709[b]	.0820[b]	.0913[b]	BCC	**217**	**$1.8x10^{-4}$**

F108-cisp 0.1%	.0399	.0565[b]	.0691[b]	.0790[b]	.0890[b]	BCC	**223**	**1.6×10^{-3}**

It is interesting to note that the most hydrophobic copolymer, P104, is fcc, while the most amphiphilic, P105, and most hydrophilic, F108, is bcc. This may indicate that hydrophilicity plays a role in the phase of the micelle structures at these temperatures.

For P104, the neat copolymer and cisplatin mixed copolymer were all fcc phases with identifying peaks (111), (200), (220), and (311) (at q_0, $(4/3)^{1/2}q_0$, $(8/3)^{1/2}q_0$, $(11/3)^{1/2}q_0$, respectively). Santos et al [140] also reported fcc phase structure in the Fm3m space group for 30%, 40%, and 34% P104 in 70% H_2O, 60% H_2O, and 63.4% H_2O/2.4% poly(acrylic acid) respectively at 25°C. For P105, the neat copolymer and cisplatin mixed copolymer were all bcc phases with identifying peaks (110), (200), (211), and (220) (at q_0, $2^{1/2}q_0$, $3^{1/2}q_0$ and $2q_0$ respectively). Hossain et al. [145] also reported bcc phase structure in the Im3m space group for 39% P105 in 61% water at 25°C. Alexandridis et al. [147], however, observed a primitive phase structure in the Pm3n crystallographic space group for 40%/60% P105/formamide at 30°C. For F108, the neat copolymer and cisplatin mixed copolymer were both bcc phases with identifying peaks (110), (200), (211), (220), and (310) (at q_0, $2^{1/2}q_0$, $3^{1/2}q_0$, $2q_0$, and $5^{1/2}q_0$ respectively). Quinn et al. [152], however, reported a reversed "double diamond-type" cubic phase, with a Pn3m space group for 0.5 g L^{-1} F108-graphene dispersions at 25°C.

3.3.2 Unit Cell Size

Figure 3.4 [157] shows the effect cisplatin concentration has on the unit cell size of P104 micelles using Equation (3.1) for neat P104 (31% mass v^{-1}) and cisplatin (0.02%-0.1% mass v^{-1}) mixed P104 at 28°C. The calculated unit cell size for each sample is listed in Table 3.2.

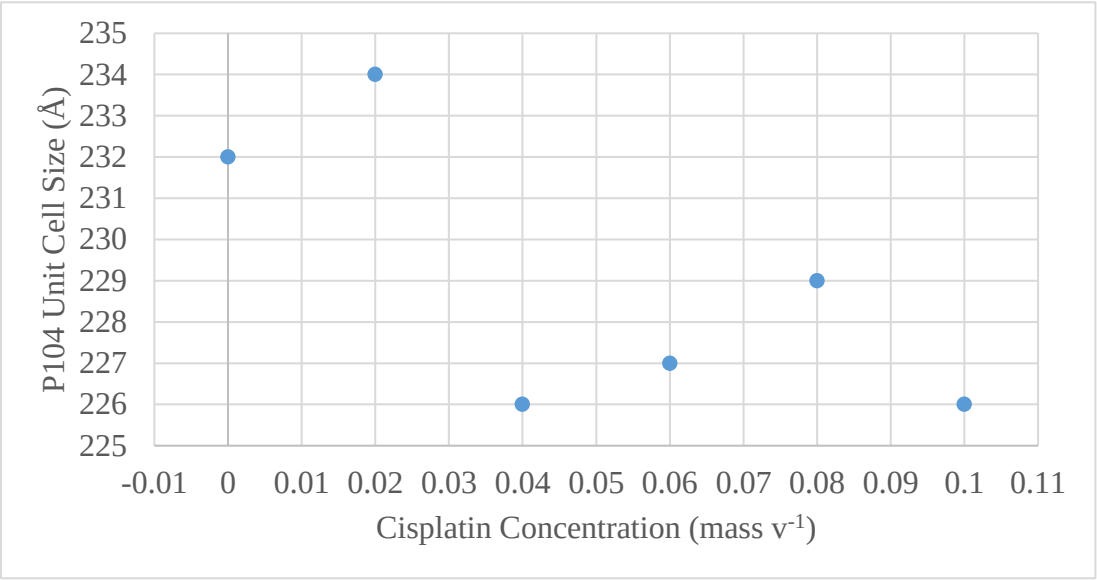

Figure 3.4: Neat P104 (31% mass v^{-1}) and cisplatin (0.02-0.1% mass v^{-1}) mixed P104 unit cell determination $(q/2\pi)^2$ versus $(h^2 + k^2 + l^2)$ from Equation (3.1) [157].

As shown in Figure 3.4 [157] and calculated unit cell size values in Table 3.2 [157], cisplatin has a slight effect on the size of the unit cell for P104. As the concentration of cisplatin increases, the size of the unit cell decreases. For example, neat P104 has a unit cell size of 232 Å, while 0.02%, 0.04%, 0.06%, 0.08%, and 0.1% each have unit cell sizes of 234 Å, 226 Å, 227 Å, 229 Å, and 226 Å respectively. This suggests that the volume of the unit cell is decreasing with increasing cisplatin concentration. This also suggests there is a decrease in water swelling of the PEO block. Kayali et al. [136] observed a similar trend of decreasing interfacial area per PEO block with increasing copolymer content in P104. Our neat P104 unit cell size is larger than those by Santos et al. [140] who calcuated 207 Å for 30% P104/70% H_2O. When Santos et al. [140] increased P104 to 36%, and mixed with 54% H_2O and 10% poly(acrylic acid)$_{25}$, they saw a more dramatic decrease in unit cell size from 207 Å to 154 Å.

Figure 3.5 [157] shows the plot of determining the size of the unit cell using Equation (3.1) for neat P105 (31% mass v^{-1}) and cisplatin (0.1% mass v^{-1}) mixed P105 at 28°C. The calculated unit cell size for each sample is listed in Table 3.2 [157].

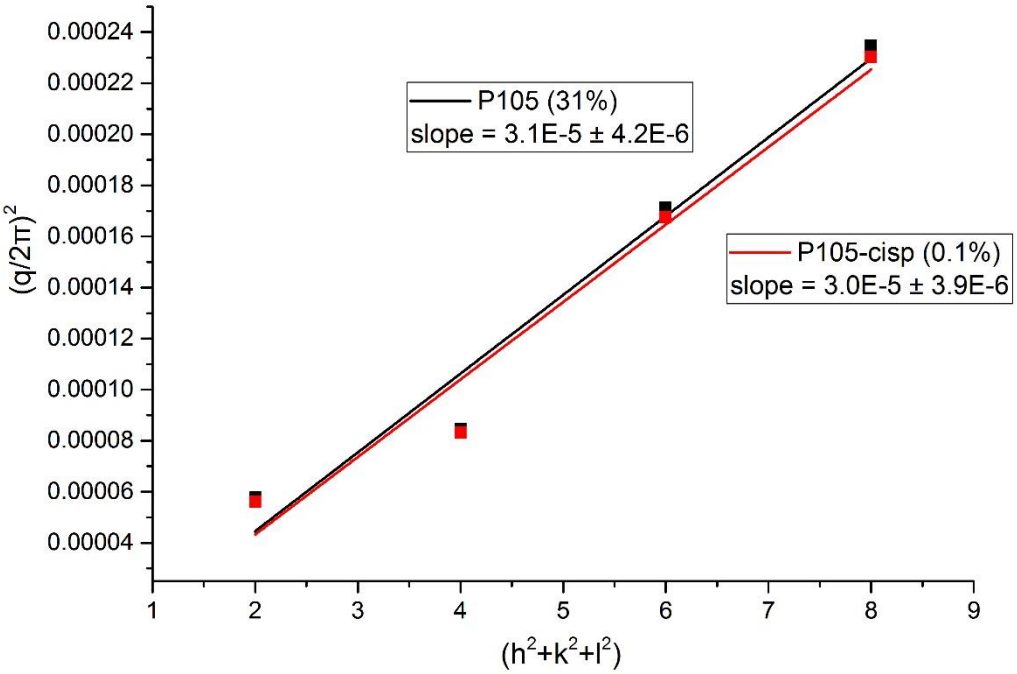

Figure 3.5: Neat P105 (31% mass v^{-1}) and cisplatin (0.1% mass v^{-1}) mixed P105 unit cell determination $(q/2\pi)^2$ versus $(h^2 + k^2 + l^2)$ from Equation (3.1) [157].

Evidenced by the similar slopes and calculated unit cell size values in Table 3.2 [157], cisplatin has no significant effect on the size of the unit cell for P105. Neat P105 has a unit cell size of 187 Å, while 0.1% cisplatin mixed P105 slightly increased to 189 Å. The no effect on unit cell size with the addition of a ternary additive was previously observed by our group using DLS for neat F127 (110 Å) and methylparaben mixed F127 (110 Å) at 90° scattering angle [16]. Alexandridis et al. [146] also observed only a slight increase in micelle radius as the volume

fraction of P105 was increased at 25°C, but in this case, it was attributed to the increased amount of PPO in the system which caused a decrease in the area of the PEO block.

Figure 3.6 [157] shows the plot of determining the size of the unit cell using Equation (3.1) for neat F108 (31% mass v^{-1}) and cisplatin (0.1% mass v^{-1}) mixed F108 at 28°C. The calculated unit cell size for each sample is listed in Table 3.2 [157].

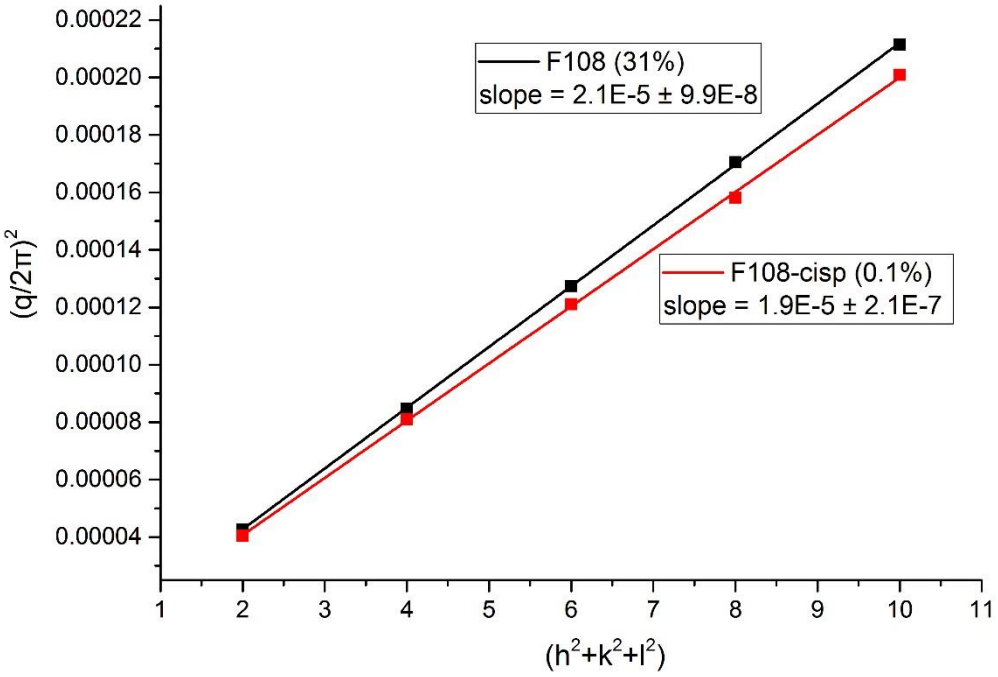

Figure 3.6: Neat F108 (31% mass v^{-1}) and cisplatin (0.1% mass v^{-1}) mixed F108 unit cell determination $(q/2\pi)^2$ versus $(h^2 + k^2 + l^2)$ from Equation (3.1) [157].

In this case, the addition of cisplatin has a slighly higher effect on the size of the unit cell for F108 compared to P105, as shown in Table 3.2 and Figure 3.6 [157]. Neat F108 has a unit cell size of 217 Å, while 0.1% cisplatin mixed F108 increased to 223 Å. This suggests that the addition of cisplatin causes a slight swelling of the micelle structure. Santos et al. [140] also observed an increase in the unit cell size from 207 Å for 30% P104/70 H_2O, to 214 Å for 34.1% P104/63.4% H_2O/2.4% poly(acrylic acid)$_{6000}$.

It is interesting to note that with the addition of cisplatin, the more hydrophobic P104 saw a slight decrease in unit cell size, the more amphiphilic P105 saw no change, and the more hydrophilic F108 saw a slight increase in unit cell size. This may suggest that hydrophobicity plays a role in the size of the unit cell when a slightly hydrophilic ternary additive is introduced.

3.3.3 d-spacing and Thermal Expansion

Figure 3.7 [157] shows the length distance, d (Å), between adjacent (hkl) lattice planes for the fcc crystal structure of neat P104 (31% mass v^{-1}) and cisplatin (0.02%-0.1% mass v^{-1}) mixed P104 with increasing temperature.

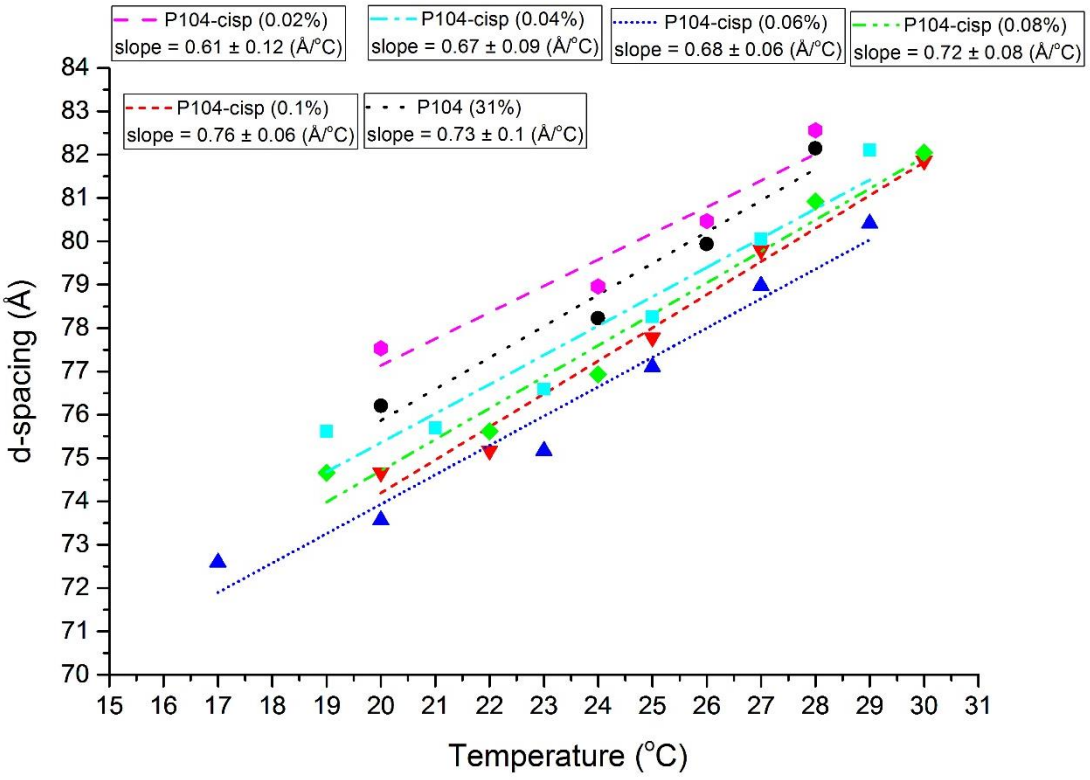

Figure 3.7: d-spacing (Å) of neat P104 (31% mass v^{-1}) and cisplatin (0.02%-0.1% mass v^{-1}) mixed P104 with increasing temperature [157].

As shown in Figure 3.7 [157], as the concentration of cisplatin is decreased, the spacing between adjacent lattice planes for P104 is decreasing with increasing temperature. For example,

the distance per unit temperature for neat P104 is 0.73 Å/ºC. The distance per unit temperature for decreasing cisplatin concentration is 0.76 Å/ºC, 0.72 Å/ºC, 0.68 Å/ºC, 0.67 Å/ºC, and 0.61 Å/ºC for 0.1%, 0.08%, 0.06%, 0.04%, and 0.02% respectively. This suggests that the distance between lattice planes for P104 and cisplatin is concentration dependent. This also suggest that without the presence of cisplatin, water has a swelling effect of the PEO block causing the distance between adjacent lattice planes to decrease. Santos et al. [140] also observed a similar trend as the calculated length of 45.3% P104/54.7% H_2O was 129 Å, and with the formulation of 49% P10/31% H2O/20% PAA_{6000} and 54.4% P104/20.7% H2O/24.9% PAA_{25}, the distance decreased to 119 Å and 109 Å respectively.

Using the data in Figure 3.7 [157] and Equation (3.6), the linear thermal expansion coefficient, α_L, was calculated for neat P104 (31% mass v^{-1}) and cisplatin (0.02%-0.1% mass v^{-1}) mixed P104. Results are shown in Table 3.2 [157]. As expected, the linear thermal expansion coefficient is decreasing as the concentration of cisplatin is decreasing. For example, the coefficient at neat P104 is $9.7x10^{-3}$ $^oC^{-1}$, while with added cisplatin, the coefficient decreases to $8.8x10^{-3}$ $^oC^{-1}$, $9.0x10^{-3}$ $^oC^{-1}$, $9.0x10^{-3}$ $^oC^{-1}$, $8.6x10^{-3}$, and $8.1x10^{-3}$ $^oC^{-1}$, for 0.1%, 0.08%, 0.06%, 0.04%, and 0.02% cisplatin respectively. This further indicates that water has a swelling effect without the presence of cisplatin which decreases the distance between adjacent lattice planes of the fcc P104 crystal structure as the temperature is increased.

Figure 3.8 [157] shows the length distance, d (Å), between adjacent (hkl) lattice planes for the bcc crystal structure of neat P105 (31% mass v^{-1}) and cisplatin (0.1% mass v^{-1}) mixed P105 with increasing temperature.

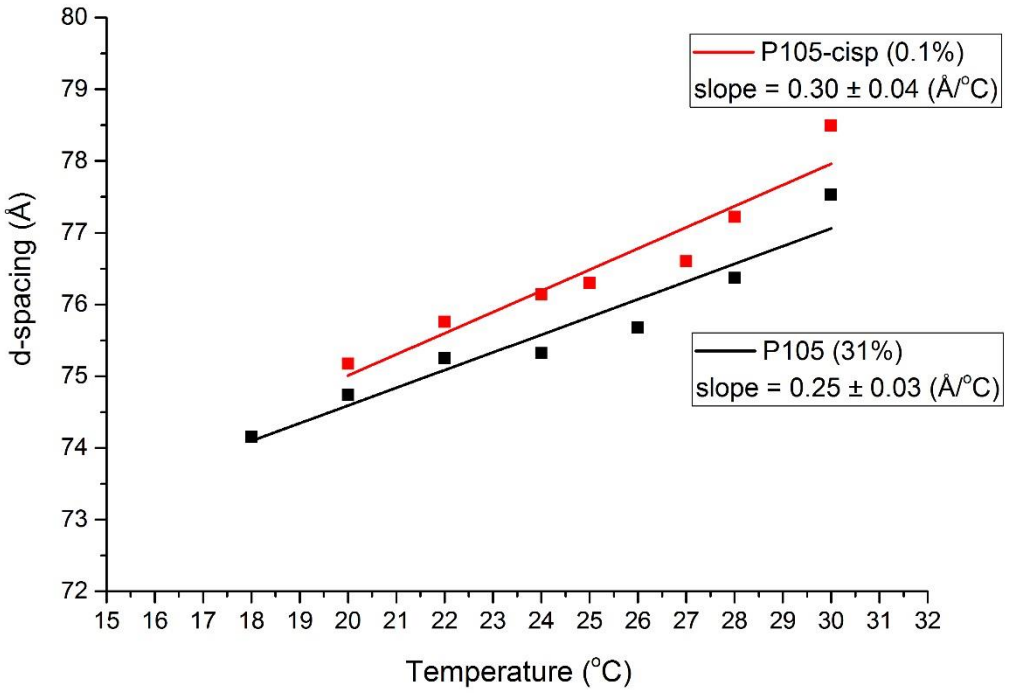

Figure 3.8: d-spacing (Å) of neat P105 (31% mass v^{-1}) and cisplatin (0.1% mass v^{-1}) mixed P105 with increasing temperature [157].

For P105, it seems cisplatin has the opposite effect compared to P104 for the spacing between adjacent lattice planes. As shown in Figure 3.8 [157], the spacing per unit temperature in neat P105 is 0.25 Å/°C, while with added cisplatin this length slightly increases to 0.30 Å/°C. This suggests that cisplatin has no swelling effect of the PEO block, and overall the structural parameter is only slightly influenced by temperature or the addition of cisplatin. Alexandridis et al. [146] also reported a slight increase in the lattice paramenters, d (Å), for 60%/40% P105/water, but overall the phases are not much influenced by the increase in temperature (from 20°C to 70°C). Our d-spacing length values for adjacent P105 lattice planes are comparable to Hossain et al. [145] that reported between 50 Å and 100 Å for 39:61 P105-water at 25°C.

Using the data in Figure 3.8 and Equation (3.6) [157], the linear thermal expansion coefficient, α_L, was calculated for neat P105 (31% mass v^{-1}) and cisplatin (0.1% mass v^{-1}) mixed

P104. Results are shown in Table 3.2 [157]. As expected, the linear thermal expansion coefficient slightly increased with the addition of cisplatin from $3.8x10^{-3}\ ^{o}C^{-1}$ for neat P105, to $4.4x10^{-3}\ ^{o}C^{-1}$ for cisplatin mixed P105. This further indicates that cisplatin has no swelling effect of the PEO block, and the overall structure is slightly influenced by temperature.

Figure 3.9 [157] shows the length distance, d (Å), between adjacent (hkl) lattice planes for the bcc crystal structure of neat F108 (31% mass v^{-1}) and cisplatin (0.1% mass v^{-1}) mixed F108 with increasing temperature.

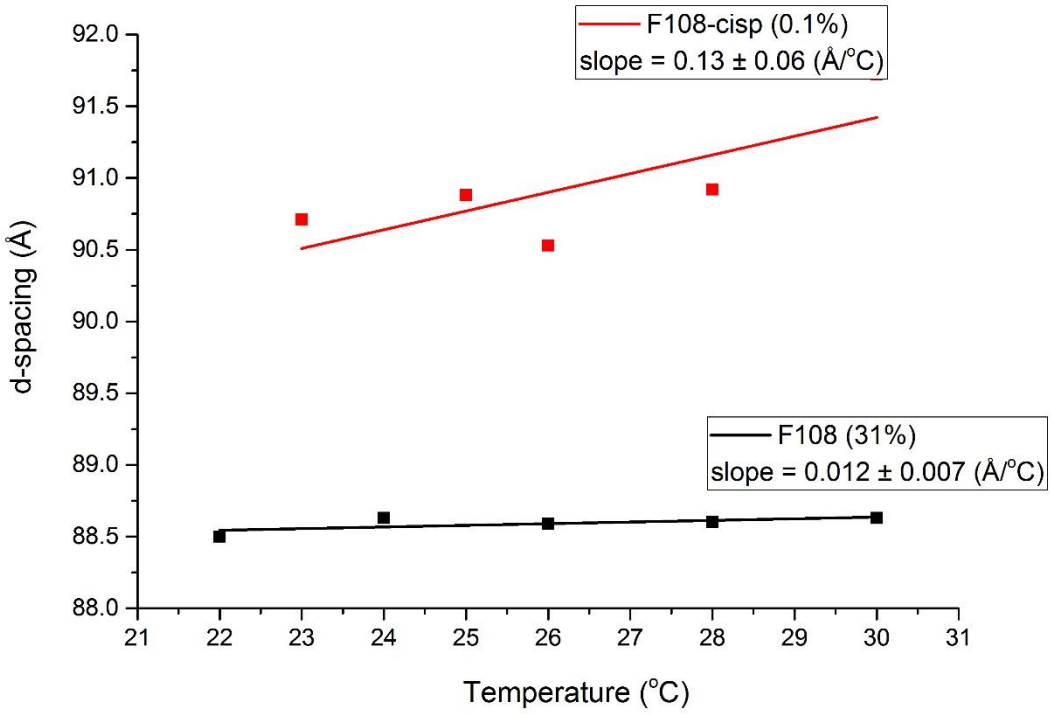

Figure 3.9: d-spacing (Å) of neat P105 (31% mass v^{-1}) and cisplatin (0.1% mass v^{-1}) mixed P105 with increasing temperature [157].

For F108, it seems cisplatin has a profound effect on the spacing between adjacent lattice planes in the bcc F108 crystal structure. As shown in Figure 3.9 [157], the spacing per unit temperature in neat F108 is 0.012 Å/°C, while with added cisplatin the length significantly increased to 0.13 Å/°C. This suggests that cisplatin has no swelling effect of the PEO block, but

the presence of cisplatin does cause the distance between adjacent lattice planes to increase. As shown in Figure 3.3 [157], cisplatin destabilizes the structural ordering of the bcc phase of micelle formation in F108. As the temperature is increased with added cisplatin, there are fewer ordered micelle structures in solution which causes the distance between the adjacent crystal lattice planes to increase.

Using the data in Figure 3.9 and Equation (3.6) [157], the linear thermal expansion coefficient, α_L, was calculated for neat F108 (31% mass v^{-1}) and cisplatin (0.1% mass v^{-1}) mixed F108. Results are shown in Table 3.2. As expected, the linear thermal expansion coefficient significantly increased with the addition of cisplatin from $1.8x10^{-4}\ ^oC^{-1}$ for neat F108, to $1.6x10^{-3}\ ^oC^{-1}$ for cisplatin mixed F108. This further indicates that cisplatin has no swelling effect of the PEO block, and the overall structure is greatly influenced by the addition of cisplatin and the change of temperature.

3.4 Conclusions

SAXS analysis of P104, P105, and F108 solutions also containing cisplatin has revealed several key changes in their phase behavior relative to neat systems. For P104 and P105, the presence of cisplatin facilitates or enhances the structural ordering with sharper peaks at the same temperatures compared to the neat samples. Unexpectedly, F108 showed the opposite effect as the intensity decreased with added cisplatin indicating a destabilization of the ordered phases. We have found little evidence to suggest that the presence of cisplatin helps coerce ordering of P104 and P105 as they evolve, but it apparently adds to the structural disorder in F108, a more hydrophilic colloidal crystal. The presence of cisplatin in the amphiphilic copolymers also produced a unique scattering behavior compared with the neat samples in that the fundamental scattering peak was suppressed for much of the tested temperature range.

The presence of cisplatin stabilized the quasicrystalline lattice in P104 and P105 gels, evidenced by the preservation of ordered phases and high scattering intensities at 30^{o}C for cisplatin mixed copolymers, but much lower scattering intensities at 30^{o}C for neat copolymers. For P104, adding cisplatin reduced the lattice plane spacing by a small amount, shown in Table 3.2 and Figure 3,7 [157], with increasing temperature suggesting crystal expansion. The linear thermal expansion coefficient for neat P104 was $9.7x10^{-3o}C^{-1}$. Adding cisplatin tended to lower the expansion coefficient in the range of 10-20% over the entire composition range of cisplatin, as resolved by SAXS. With F108, the expansion of the neat system was increased significantly, evidenced by the over 700% increase in linear thermal expansion coefficient from $1.8x10^{-4\ o}C^{-1}$ to $1.6x10^{-3\ o}C^{-1}$. The P105 crystal expanded slightly (16%) with added cisplatin.

Increasing cisplatin concentration was also found to have a weak decreasing trend in the unit cell dimensions of P104. Above 0.04% cisplatin, there was a pronounced 2-3% reduction in then unit cell size suggesting that there is larger shell overlap in the presence of cisplatin. Cisplatin had no effect on the size of P105 unit cell and F108, cisplatin increased the unit cell size as neat F108 217 Å, while 0.1% cisplatin mixed F108 increased to 223 Å. This indicates that cisplatin is influencing the overlap of the hydrophilic segments in the unit cell from where its situated in the micelle

These experiments show how using SAXS coupled with a dynamic heating protocol, structural changes in P104, P105, and F108 amphiphilic copolymer solutions (31% mass v^{-1}) can be characterized when formulated with the ternary additive cisplatin (0.02% to 0.1% mass v^{-1}). We have shown here that the evolution of the fcc or bcc phase in PEO-PPO-PEO solutions follow a nucleation and growth mechanism over a range of temperatures (10^{o}C to 35^{o}C). We have observed that adding cisplatin as a ternary additive alters the evolution mechanism from a

homogenous to a heterogeneous nucleation. Understanding where chemotherapeutic molecules as ternary additives are partitioned within micelles and how they influence the evolving structure is important to optimize controlled release systems utilizing amphiphilic copolymers as a drug delivery system.

3.5 Acknowledgments

This work was performed at the Advanced Photon Source (APS) at Argonne National Lab. We acknowledge the Rackham Graduate School at UM for support and the National Physical Science Consortium (NPSC) fellowship funded through the National Institute of Standards and Technology (NIST) for their financial support. We thank Sungsik Lee at Argonne National Lab for training on the SAXS beamline 12-BM-B.

CHAPTER IV

Diffusion and Controlled Release of Colloidal Gels

4.1 Introduction

Our group has previously studied the effects a third component has on the driving force to form polyethylene oxide-polypropylene oxide-polyethylene oxide, PEO-PPO-PEO, micelles linked with thermodynamics [72, 104], structural evolution [15], and its gelation [16]. We have observed that the third species helps as a chaperone to coerce the formation of micelles and colloidal crystals, at lower temperature than what forms normally in the neat stage [72, 104, 15, 16]. It is clear that the driving force to form a gel is influenced by the third component and as phase separation arises, the amphiphilic qualities of the additive likely have an effect on where within the forming micelles the ternary constituent is found [72, 104]. The location of the drugs within the micelle can also affect the permeability and bioavailability of drug elements sequestered within a forming colloidal gel [72, 104].

Our goal is to package cold chemotherapeutic drugs in these dispersions below their critical micelle temperatures, and inject them via syringe-intratumoral delivery therefore bypassing an IV drip. Latent body temperature equilibration will trigger the micelle and gelation of the copolymer and drug within, causing the drug to be sequestered and alter the release characteristics over time rather than from solution. In this chapter, we ran a series of diffusion experiments using dialysis tubing cellulose membrane on aqueous polymeric micelles (Pluronic F127) mixed with ternary additives at two temperatures over time to study the release

characteristics of micelles using Ultraviolet-Visible spectroscopy (UV-Vis) to monitor the release rate. The ternary additives studied here are cisplatin, malachite green chloride (green dye), and erythrosin B (red dye).

The experiments, results, and discussion covered in this chapter were submitted and published in the *Journal of Surfactants and Detergents* [165].

4.2 Materials and Methods

4.2.1 Materials

Polyethylene oxide-polypropylene oxide-polyethylene oxide, PEO-PPO-PEO, Pluronic F127 (12,600 g/mol molecular mass), malachite green chloride ($C_{23}H_{25}ClN_2$, 364.91 g/mol molecular mass), erythrosin B dye ($C_{20}H_8I_4O_5$, 835.89 g/mol molecular weight) and cisplatin ($[Pt(NH_3)_2Cl_2]$, 300.05 g/mol molecular mass) were all obtained from Sigma-Aldrich (Milwaukee, WI) and were used as received. The structures of each are shown in Figure 4.1 [165]. The dialysis tubing cellulose membrane, also obtained from Sigma-Aldrich (21 mm average diameter, 33 mm average flat width, 110 ml/ft capacity, 14,000 g/mol molecular mass cut-off), was soaked in room temperature deionized water for 5 minutes prior to use.

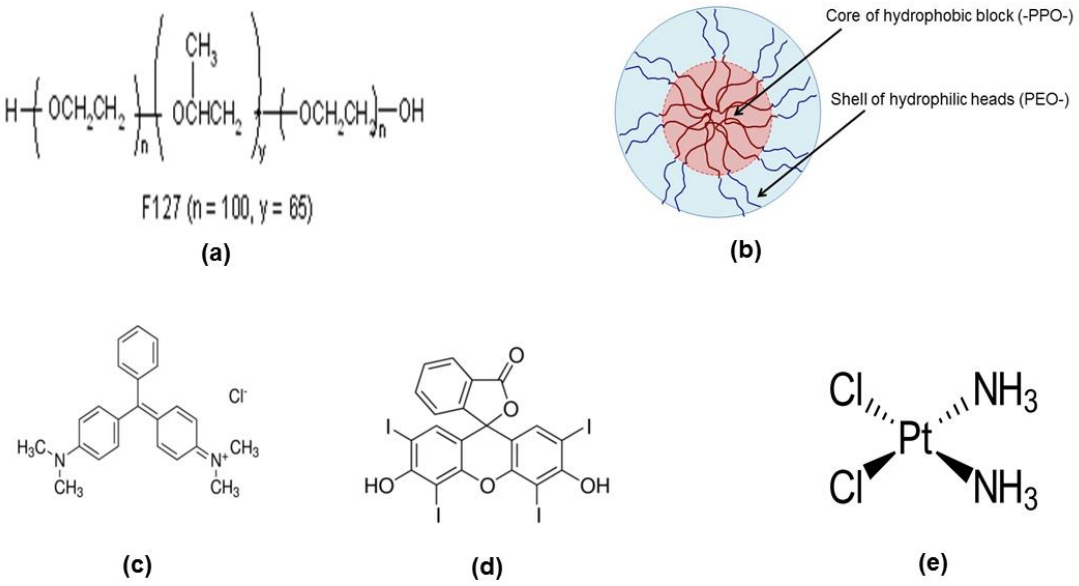

Figure 4.1: (a) Pluronic® F127 (b) Example of PEO-PPO-PEO micelle structure (c) Malachite green chloride (d) Erythrosin B dye (e) Cis-dichlorodiammineplatinum(II) (Cisplatin) [165].

4.2.2 Kinetics of Ternary Additives Release from Pluronic F127

Approximately 15cm of dialysis tubing cellulose membrane was measured and placed into 500ml of room temperature deionized water for several minutes until the tube opened. Then, one end of the tube was sealed with a rubber band seal, while the other end remained open to receive the solution. 20ml of each solution was added to each tube by pipette, and then the other end of the tube was sealed with a rubber band (leaving space for a small air bubble between the liquid and the tied knot). The outside of the tube was rinsed with deionized water. The tube and a magnetic stirrer were placed into a 1000ml beaker of 500ml of water (either at room temperature or at 40C) on a hot plate. Aliquots of the receiving solution inside the beaker were measured at various times using UV-Vis to track the release rate for each ternary additive. A schematic of this setup is provided in Figure 4.2 [166].

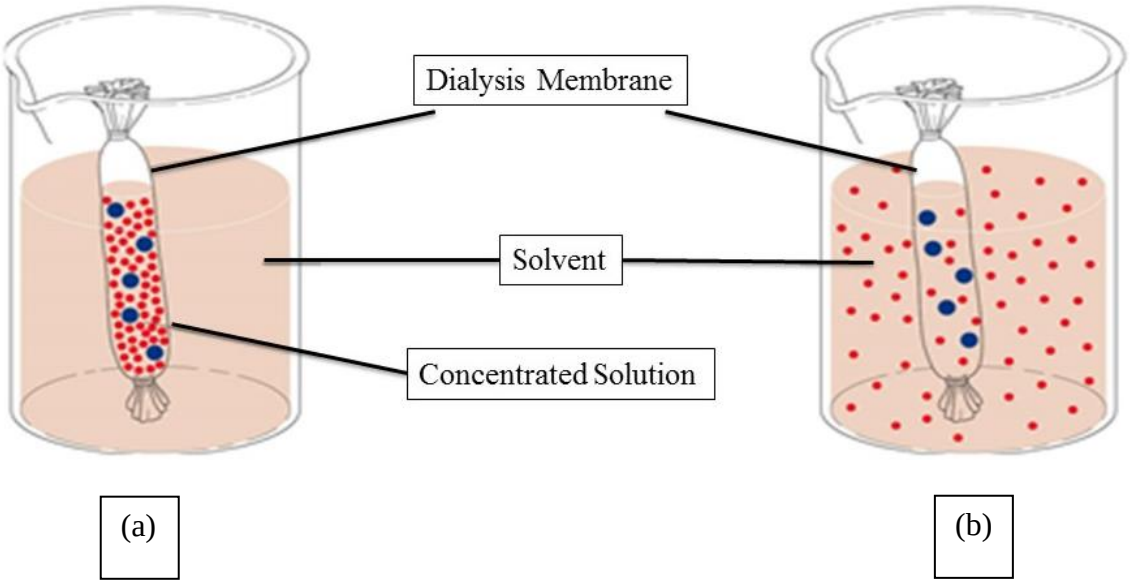

Figure 4.2: Setup of dialysis tubing experiment (a) at start of dialysis (b) at equilibrium [165].

Neat solutions of malachite green (10mg), erythrosin (20mg), and cisplatin (20mg) were each mixed into 20ml room temperature water then aliquoted into the dialysis tubing. Aqueous solutions of F127 (4g) were each prepared according to the "cold" processing methods of Schmolka [29]. The ternary additives were then mixed into each solution containing F127 and aliquoted into the dialysis tubing. Total volume of deionized water was maintained by adding the same volume of fresh deionized water. Each cumulative release profile (in the form of increasing UV intensity vs time) of the ternary additives was calculated from the absorption vs concentration plots (calibration curves) for each neat ternary additive. Our cisplatin release values are compared to Cheng et al. [64] whom used porous hollow Fe_3O_4 nanoparticles for controlled release of cisplatin. Their cumulative release profile of cisplatin was obtained via the concentration correction (the amount of cisplatin in each aliquot calculated to correct the overall cumulative releasing of cisplatin) of released cisplatin based on the following equation [64]:

$$C_t' = C_t + \frac{v}{V}\sum_{0}^{t-1} C_t$$

Where C_t' is the corrected concentration at time t, C_t is the apparent concentration at time t, v is the volume of the aliquots taken and V is the total volume of the solution. In this study, four separate conditions were tested for each ternary additive: neat additive at room temperature (20°C-25°C), neat additive at ~40°C (approx. body temperature), F127 mixed additive at room temperature (20°C-25°C), and F127 mixed additive at ~40°C (approx. body temperature). Since each ternary additive has a different diffusion release rate, UV-Vis measurements were taken between 200nm and 850nm at varying times per each condition for more accurate calculations, using a Varian Cary 50 Bio UV-Visible Spectrophotometer (Varian Inc. (Agilent Tech.), Palo Alto, CA, USA). All UV-Vis measurements for malachite green were analyzed every 10 minutes up to 1 hour for each condition. All UV-Vis measurements with erythrosin were analyzed every 30 minutes up to 3 hours for each condition. UV-Vis measurements involving cisplatin were analyzed for several hours throughout several days for each condition.

4.3 Results and Discussion

4.3.1 Calibration Curves of Ternary Additives

To study the release kinetics of the encapsulated ternary additives in F127, we dialyzed solutions of malachite green, erythrosine, and cisplatin in 500ml deionized water at room temperature and 40°C and compared those results to dialysis of dispersions containing the same small molecules with F127 in 500ml deionized water at room temperature and 40°C. The amount of ternary additive released from the micelle gels was measured by UV-Vis. Calibration curves for all three of the neat ternary additives: malachite green, erythrosin, and cisplatin, were calculated. Figure 4.3 [165] shows a graphical example of the calibration curve of neat malachite

green. In Table 4.1 [165] , we show a summary of our values of each ternary additives' wavelength ranges, concentration ranges (mg/ml), slopes, y-intercepts, and correlation values (R^2), and compare our results to the cisplatin complex by Basotra et al [167].

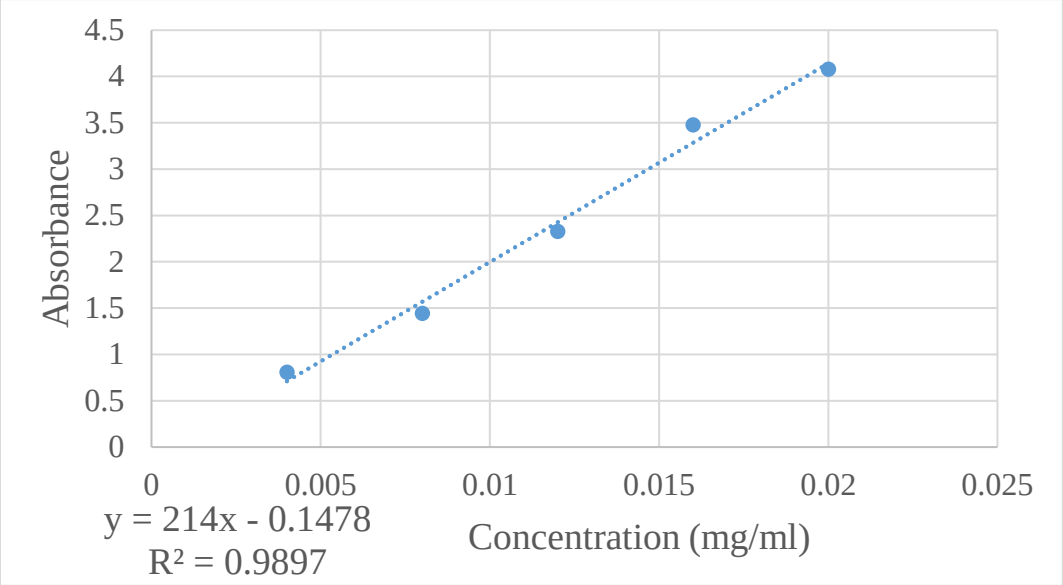

Figure 4.3: Neat malachite green absorption vs concentration calibration curve. Absorption analysis were measured in 500ml deionized water using UV-Vis at wavelengths 610-620nm [165]. Each measurement was analyzed at 60nm/min for most accurate results. Varian, Inc. (Agilent Technologies) reports standard deviation for 10 Abs measurements < 0.00030.

Table 4.1: Wavelength ranges, concentration ranges, slopes, y-intercepts, and correlation values of malachite green, erythrosin, neat cisplatin, dark colored cisplatin, and cisplatin complex [165].

Ternary Additive	**Wavelength range (nm)**	**Concentration Ranges (mg/mL)**	**Slope (Abs/conc.)**	**Y-intercept (Abs)**	**R^2**
Malachite Green	610-620	0.004 to 0.02	215	0.1	0.9897
Erythrosin	520-530	0.008 to 0.04	113	0.5	0.9356
Neat Cisplatin	270-300	0.02 to 0.22	0.3	0.008	0.9877
Dark Colored Cisplatin	250-270	0.02 to 0.22	17	1.1	0.9011
Cisplatin Complex [167]	700-710 [167]	0.0004 to 0.0014 [167]	0.00022 [167]	8.0×10^{-7} [167]	0.9999 [167]

As shown in Figure 4.3 [165], as the concentration of malachite green increases, the solution progressed from light green to a darker green tint that absorbed in 610-620nm range. This linear relationship was true for erythrosin and cisplatin as well at other wavelengths. For erythrosin, as the concentration increases, the solution progressed from light pink to a darker pink tint that absorbed in 520-530nm range. Basotra et al. [167] mixed o-Phenylenediamine with cisplatin to form a green colored complex with wavelength ranges 700-710nm. For neat cisplatin, since the dissociation of the yellow solid colored cisplatin is a clear liquid, direct visual observation is not possible hence the importance of UV-Vis to measure absorbance in the UV (270-300nm range).

The dynamic rise in absorption in the receiver solution was used to calculate the concentration of the diffused molecules in solution at a given time. During dialysis, aliquots of the solution were measured by UV-Vis to resolve a receiving solution concentration. The cumulative release of neat ternary additives and ternary additve-F127 at room temperatures and

40°C is shown in Figures 4.4, 4.5, and 4.6 [165]. For cisplatin, unexpectedly during our experimentation, observable dark black particles formed both inside the dialysis tubing and outside the tubing floating around in the receiver solution. This indicates a reaction is occurring and forming dark colored precipitates that eventually settled at the bottom of the beaker. Both the neat cisplatin trials and the cisplatin-F127 experiments resulted in precipitation occurring faster and more obviously in the dispersion than in the neat solution. These observations suggest cisplatin is unstable in solution. The instability is more pronounced at elevated temperatures and encapsulating cisplatin in a polymeric micelle might be ineffective in somehow stabilizing cisplatin from its transformation potential. We previously opened an old, stored sample of unused cisplatin and noticed similar discoloration. Upon reviewing the literature, Cubells et al. [168] concluded cisplatin is unstable in aqueous solutions and the primary mode of decomposition involves displacement of the chloride ligand so increasing the chloride ion concentration would likely improve the stability of the drug in aqueous solution [168-171]. We performed a calibration curve for the dark colored cisplatin and the results are in Table 4.1 [165]. Interestingly, the absorbance was much higher at the same concentrations for the dark colored cisplatin compared to the normal yellow colored cisplatin at slightly different wavelength ranges (250-270 dark colored compared to 270-300 neat cisplatin) which is indicated in Table 4.1 by their different slopes (0.3 neat cisplatin compared to 17.1 dark colored cisplatin). Since the dark colored particles were observed throughout the experiment for every condition, the calibration curve for dark colored cisplatin was used in Figure 4.6 [165] instead of the calibration curve results for neat cisplatin to calculate the concentration of diffused cisplatin in solution at a given time.

4.3.2 Kinetics of Malachite Green

To study the release kinetics of the encapsulated malachite green in F127, we dialyzed neat malachite green in deionized water at room temperature and 40°C and compared those results to the dialyzed malachite green-F127 in deionized water at room temperature and 40°C. The amount of malachite green released from the micelle gels was measured by UV-Vis at wavelengths 610-620 shown in Figure 4.4 [165].

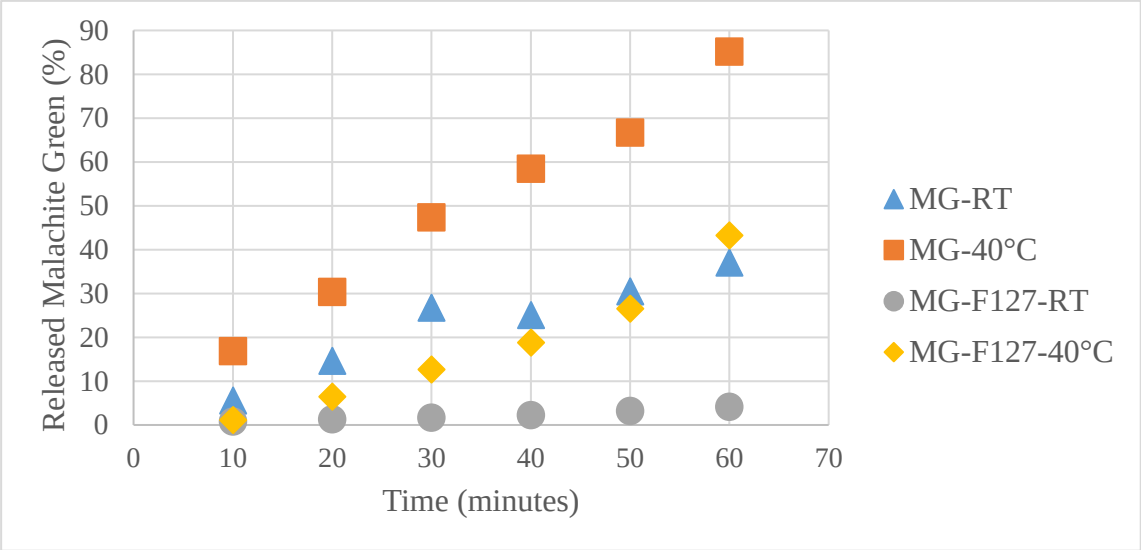

Figure 4.4: Release of neat malachite green, MG, and malachite green-F127, MG-F127, at room temperature, RT, and 40°C over time. Each condition the malachite green released was measured in 500ml deionized water by UV-Vis at wavelengths 610-620nm [165].

Probably what is most valuable from this type of analysis is the ability to extract a mass diffusion coefficient measurement for each condition, the determinations of which is shown in Table 4.2 [165]. The thickness of the membrane and the surface area of the dialysis tube are needed to perform the calculation. Clearly mass transfer is easiest (highest diffusion coefficient) for the MG-40^{o}C without the amphiphile. Adding the amphiphile, MG-F127-40^{o}C, cuts the flux in half but as time went on later in this experiment, there was a noted rise in the permeation rate. Similar release characteristics were observed in the neat MG-RT sample. The most sluggish

diffusion occurred when the amphiphiles were added and diffusion commenced at room temperature.

One observable was that none of these experiments achieved a saturation dose over the time scale evaluated. Clearly, the driving force for continued permeation existed for all experiments and we cannot comment on whether there was a difference in total release.

The rationale for why elevated temperature led to higher permeation is clear. There is higher Brownian motion in the solution when the temperature is raised from room temperature to 40^{o}C, and it is possible that the pore dimensions grow making the membrane more permeable with higher temperature as well. The increased activity of the higher temperature solution explains why the neat solutions show higher flux and a higher apparent diffusion coefficient at higher temperature.

The presence of the amphiphile has two likely physical outcomes. At elevated temperature, there is clearly enough energy to trigger the formation of the colloidal crystals and the more the amphiphiles are organized into bulk structures in solution, the lower the probability that the surfactants are bound on the wall of the membrane blocking MG transport. If the amphiphiles organize into hydrophobic cores, those regions are effectively excluded volume for aqueous soluble MG which will raise the concentration in the water phase and increase the mass flux across the boundary. Of course, if MG was strongly bound to regions of the amphiphiles because micelles have larger micellar hydrodynamic radii at elevated temperatures, there might be a lower driving force for allowing MG to permeate out of the dispersion. Clearly, lower transport was not observed.

Lower temperature lowers the driving force for forming micelles and gels. Our group has pointed out that the typical micelle formation temperatures dropped with higher concentrations

of F127 and with some ternary additives that interact with the micelle regulating the energetics of micelle formation [72, 104, 15, 16]. If the driving force to form micelles is small, it is quite possible that more adsorbed surfactant is blocking pores in the membrane. Clearly, the lower temperature is also reducing the Brownian motion as well, but here comparing MG-RT and MG-F127-RT, the presence of the surfactant is a strong impediment to permeation. Considering F127 reduced the release rate of malachite green at room temperature and 40^{o}C, this suggests it would offer a desired platform for drug delivery and release.

4.3.3 Kinetics of Erythrosin Release

To study the release kinetics of the encapsulated erythrosin in F127, we dialyzed neat erythrosin in deionized water at room temperature and 40°C and compared those results to the dialyzed erythrosin-F127 in deionized water at room temperature and 40°C. The amount of erythrosin released from the micelle gels was measured by UV-Vis at wavelengths 520-530nm shown in Figure 4.5 [165].

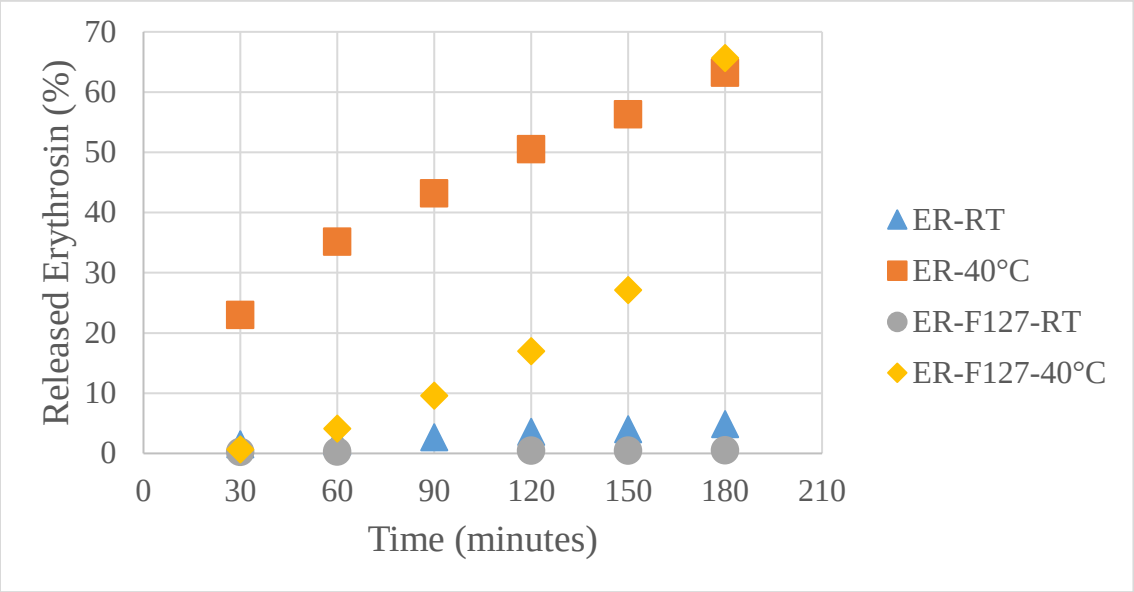

Figure 4.5: Release of neat erythrosin, ER, and erythrosin-F127, ER-F127, at room temperature, RT, and 40°C over time. Each condition of the erythrosin released was measured in 500ml deionized water by UV-Vis at wavelengths 520-530nm [165].

The diffusion coefficient measurements for each erythrosin condition is provided in Table 2 [165].. Similar to malachite green, the highest flux for erythrosin is ER-40^{o}C without the amphiphile. Adding the amphiphile, ER-F127-40^{o}C, cut the flux in half but as time went on in the experiment, there was a noted burst in the permeation rate. There was no observable change in release characteristics between the neat ER-RT and ER-F127-RT samples as both showed very low release (below 10%).

Similar to malachite green, none of these experiments achieved a saturation dose over the time scale evaluated. The driving force for continued permeation existed for all experiments, but we cannot comment on whether there was a difference in total release. At 40^{o}C, once again the Brownian motion is higher and that explains why the diffusion coefficient for ER-40^{o}C is the highest in the neat conditions for the first 150 minutes.

The presence of the amphiphile at elevated temperature cut the mass transfer rate in half for the first 150 minutes. There was enough energy to form colloidal crystals lowering the probability that the surfactants were bound on the wall of the membrane blocking the ER

transport. If ER was strongly bound to regions of the amphiphiles, there might be a lower driving force for allowing ER to permeate out of the dispersion. This was not observed as a diffusion coefficient of $1.0 \pm 0.01 \times 10^{-6}$ cm^2sec^{-1} was found in this condition. After 150 minutes, we observed a rising release of ER that was not observed with MG making the overall dynamic release curve more non-linear. The molecular mass of ER is larger than that of MG, so it takes longer for ER molecules to percolate through the gel and the membrane. This is an indication that while F127 does have a diffusion rate limiting effect on ternary additives, the rate at which the diffusion is limited varies for each ternary additive due to the molecular mass of the ternary additives. According to Mandal [172], translational and rotational motion diffusion coefficients can occur in solution simultaneously either in series or parallel. In congested polymeric micellar conditions, there is a possibility of self-diffusion (slow process) and mutual or collective diffusion (fast process). These conditions are indistinguishable when the small amount of supporting electrolytes and buffer solutions are present in the systems [173-177]. With the method used here, a diffusion coefficient can be determined, but the non-linearity of the ER release suggests its non-Fickian and a different model is more appropriate.

Lowering the temperature lowers the driving force for forming micelles and gels. If the driving force to form micelles is small, it is possible that more adsorbed surfactant is blocking the pores in the membrane. The lower temperature also reduces the Brownian motion. In this case, for ER-RT and ER-F127-RT, the driving force for diffusing ER is so low at room temperature, that similar results were observed with and without the amphiphile. Considering F127 still reduced the release rate of ER in both conditions, this is another indication that suggests it would offer a desired platform for drug delivery and release.

Conceptually, erythrosin permeation through the dialysis membranes has a similar profile to MG. The hydrophilic erythrosin is concentrated in the aqueous regions and excluded from the hydrophobic cores of the micelles which increases the concentration gradient across the dialysis membrane once micelles form. And at elevated temperature, the pores in the membrane are larger.

4.3.4 Kinetics of Cisplatin Release

The same protocol was used for dialyzed neat cisplatin in deionized water at room temperature and 40°C and compared to that of dialyzed cisplatin-F127 in deionized water at room temperature and 40°C. The amount of cisplatin released from the micelle gels was measured by UV-Vis at wavelengths 250-270nm shown in Figure 4.6 [165]. The cumulative release results in general compares well to previous cisplatin encapsulated drug delivery systems [64, 30, 178-180]. Guven et al. [30] reported less than 25% total released cisplatin from their Pluronic-F108-wrapped, W-CDDP@US-tubes after 200 hours. Cheng et al. [64] reported less than 10% total cisplatin release from their Fe-cisplatin loaded nanoparticles, Pt-PHNPs, at pH 7.4, 6, and 5 after 70 hours. Reardon et al. [178] reported less than 20% cumulative release of cisplatin after 10 hours from their core-shell poly(lactic-co-glycolic acid) (PLGA) nanoparticles. Fang et al. [179] reported less than 25% total cisplatin release from their chitosan hydrogels after 5 hours. Czarnobaj and Lukasiak [180] reported less than 50% cisplatin release after 20 hours from their silica (SiO_2) xerogels at room temperature and 120^{o}C.

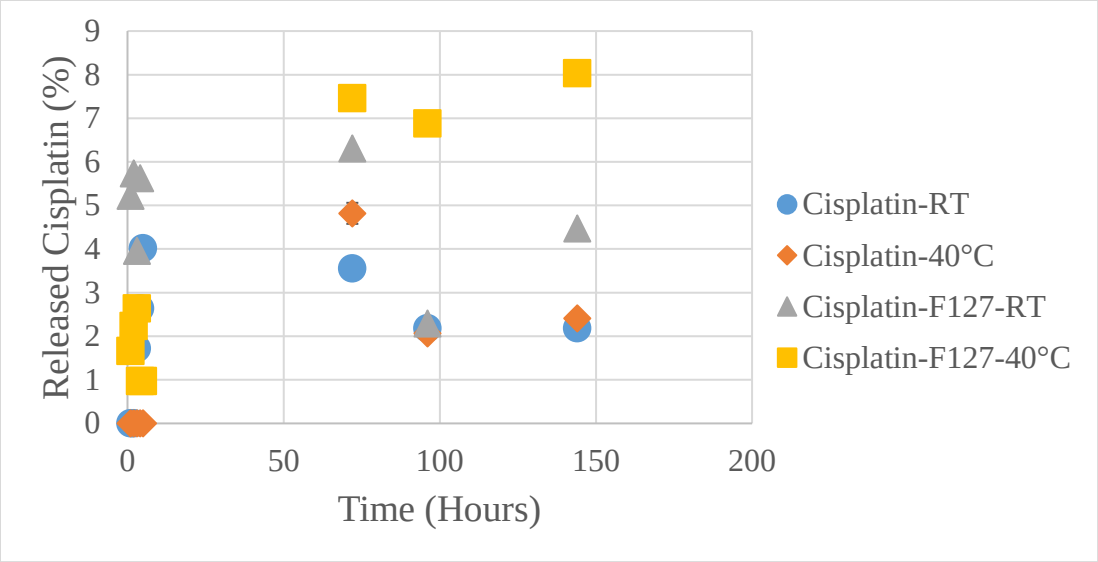

Figure 4.6: Release of neat cisplatin and cisplatin-F127 at room temperature, RT, and 40°C over time. Each condition of the cisplatin released was measured in 500ml deionized water by UV-Vis at wavelengths 250-270nm [165].

The diffusion results were unlike a normal diffusion profile. We observe a burst condition for three of the solution conditions including cisplatin neat (cisplatin-RT) in water at 25^{o}C, and for both dispersions (cisplatin-F127-RT and cisplatin-F127-40^{o}C)) at ambient temperature and at 40^{o}C. Reardon et al. [178] and Fang et al. [179] both also observed an initial burst release of cisplatin from their core-shell PLGA nanoparticles and chitosan hydrogels. It is worth noting that the size of the initial burst release is on the order of 8-9% while the neat MG and erythrosin release substantially more over the 150 hours of experimentation. We calculated a diffusion coefficient for the short, initial burst phase, but it is clear that three of the four conditions, there is burst followed by a much smaller release, compared with the systematic release of other dye molecules. The diffusion coefficient measurements for each cisplatin condition is provided in Table 4.2 [165]. From the analysis, the highest flux observed for cisplatin was cisplatin-F127-RT. The cisplatin-F127-RT release was slightly higher than cisplatin-RT.

There was no observable diffusion for neat cisplatin-40^{o}C in the first 5 hours. However, cisplatin was observed at much longer times finally permeating through after 50 hours. More Brownian motion should occur in the higher temperature neat systems but maybe there is a larger driving force to also transform and precipitate neat cisplatin as opposed to driving it across the dialysis membrane.

The presence of the amphiphile at elevated temperature increased the permeation for the first 5 hours relative to the neat system. This is possibly due to F127 interacts with cisplatin as we observed the formation of dark colored particles floating around in solution. If cisplatin was strongly bound to hydrophilic or hydrophobic regions of the amphiphiles, there might be a lower driving force to allow cisplatin to permeate out of the dispersion. This was not observed as a diffusion coefficient of $1.2 \pm 0.1 \times 10^{-6}$ cm^2s^{-1} was found in this condition. Continued release past the burst period is observed and there are indications of a plateau concentration is evident at ~8% drug release at longer times. So a little less than half the release comes in the first 5 hours and the rest with longer exposure.

Lowering the temperature lowers the driving force for forming micelles and gels. The lower temperature also reduces the Brownian motion. We observed a slightly higher initial burst at room temperature for the dispersion (F127-cisplatin RT) relative to the neat solution (cisplatin-RT). Since continued release of cisplatin occurred over time even after the initial burst, (3% release after 5 hours compared to 8% release after 144 hours), the presence of the amphiphile may aid in transporting cisplatin across a membrane.

Only with the dispersion at elevated temperature (cisplatin-F127-40^{o}C) is a plateau in permeation observed. There is a noted decrease in UV-Vis absorption for the other three conditions. Clearly, with black particles forming while conducting the diffusion experiments, one

rational for the lower absorption later might be due to the sedimentation of converted cisplatin particles that are not suspended in solution. If particles are denser than the fluid medium of the receiver solution, it's possible that the particles drift to the bottom of the receiver solution and are not sensed as part of the absorption at later time. If there was a nucleation and growth mechanism regulating particle formation, if the particles grew in size with time, they might be separated in the two-phase dispersion of particles in the receiver reservoir. We observed significant particle accumulation at the bottom of the reservoir as well. If the particle formation is linked with the inactivation of cisplatin, perhaps doing the experiments in saline solution might preserve the activity of the cisplatin and keep it in solution as opposed to directing its formation of a second particle phase as a dispersion.

Comparing the molecular structures of cisplatin with MG and ER, the two dyes are both stable and hydrophilic, while cisplatin is clearly unstable and perhaps more ambiguous in terms of its overall hydrophilicity. If the same mechanism of liberating the pores occurs with the amphiphile coalescence and formation of hydrophobic cores, if cisplatin was more drawn to the interface between the core and shell, that would reduce the amount available at the membrane boundary. With a time dependent stability issue, even if cisplatin was labile outside of the cores within the dialysis membrane, the fact that there is a nucleation and growth of the dark particulates which quickly grew larger than the pore dimensions of the membrane.

4.3.5 Comparison to Other Permeation Experiments

Table 4.2 [165] presents our results and includes a comparison of cisplatin diffusion coefficient values in a variety of delivery systems. The table includes references for cisplatin released from PLGA nanoparticles [178], PLGA microspheres, solid fibers, and hollow fibers [181], and chitosan-alginate nanoparticles [182].

Table 4.2: Diffusion coefficient of each experimental condition: neat malachite green, MG, erythrosin, ER, and cisplatin (first 5 hours) and mixed F127 at room temperature, RT, and 40°C [165]. Our results are compared to the in vitro release of cisplatin from core-shell poly(lactide-co-glycolide) (PLGA) nanoparticles [178], PLGA microspheres, solid fibers, and hollow fibers [181], and electrostatically cross-linked chitosan-alginate nanoparticles [182].

Experimental Condition	**Diffusion Coefficient (cm^2s^{-1})**
MG-RT	$2.6 \pm 0.01 \times 10^{-7}$
MG-F127-RT	$2.6 \pm 0.01 \times 10^{-8}$
MG-40°C	$7.9 \pm 0.1 \times 10^{-7}$
MG-F127-40°C	$5.2 \pm 0.01 \times 10^{-7}$
ER-RT	$4.7 \pm 0.01 \times 10^{-8}$
ER-F127-RT	$3.7 \pm 0.1 \times 10^{-9}$
ER-40°C	$5.2 \pm 0.01 \times 10^{-7}$
ER-F127-40°C	$1.0 \pm 0.01 \times 10^{-6}$
Cisplatin-RT (5 hours)	$6.7 \pm 0.01 \times 10^{-6}$
Cisplatin-F127-RT (5 hours)	$3.0 \pm 0.1 \times 10^{-7}$
Cisplatin-40°C (5 hours)	0
Cisplatin-F127-40°C (5 hours)	$1.2 \pm 0.1 \times 10^{-6}$
Cisplatin-PLGA nanoparticles (150 hours)	4.1×10^{-17} [178]
Cisplatin-PLGA microspheres (500 hours)	4.8×10^{-13} [181]
Cisplatin-PLGA solid fibers (200 hours)	6.1×10^{-10} [181]
Cisplatin-PLGA hollow fibers (400 hours)	3.3×10^{-10} [181]
Cisplatin-chitosan-alginate nanoparticles (t < 2 hours)	8.2×10^{-1} (average) [182]

Our diffusion results are higher than Campbell et al. [181] who observed much slower cisplatin diffusivity from PLGA microspheres. Campbell's lower diffusivity of cisplatin was caused by the low molecular mobility of the matrices where cisplatin is encapsulated. Campbell et al. [181] reported some microspheres engulfed other microspheres with shell-like pores surrounding some regions of a microsphere causing droplets of oil phase to disperse in the aqueous phase. The low porosity of these microspheres suggests more sluggish drug

permeability as there are few aqueous channels to allow paths for drug escape [181]. Campbell also observed a cumulative drug release over 500 hours, while our reported diffusion coefficient numbers are within the first 5 hours of release.

Our diffusion results are also higher than Campbell et al. [181] for diffused cisplatin from PLGA solid and hollow fibers. Campbell reported during fiber drying, as more solvent is extracted during the phase inversion, the oil phase becomes a poorer solvent to the polymer chains, and the chains retract and interact more with each other causing the glass transition temperature, Tg, to increase [181]. Since the polymer chains are less mobile, the diffusivity of the solvent in the oil phase decreases thus reduces the volume of the core, causing lower drug release [181]. Campbell also observed a cumulative drug release over 200 hours for solid fibers, and 400 hours for hollow fibers [181].

Our diffusion coefficients appear quite low, relative to Maan et al. [182] for in vitro release of cisplatin from electrostatically cross-linked chitosan-alginate nanoparticles. This discrepancy could be due to the differences in our controlled drug release methods. Our polymeric micelles form gels at elevated temperatures, which encapsulates cisplatin, thus significantly reduces its permeation. Maan et al's [182] release of the cisplatin complex from the nanoparticles involves the absorption of water into the nanoparticles matrix and simultaneous release of the drug via diffusion. When Maan's drug encapsulated nanoparticles are exposed to water, the polymer swells causing the T_g of the polymer to drop relative to the experimental temperature [182]. The release of the drug is regulated by the process of relaxation of macromolecular chains and the diffusion of the entrapped drug molecules into the exterior medium [182]. The Maan effort was tied to diffusion on a molecular level and our membrane dimensions are on the order of 100 microns, much larger overall. Man et al. [182] also observed

a cumulative drug release within 2 hours, while our reported diffusion coefficient numbers are within the first 5 hours of release.

Our diffusion results are also very low compared to Reardon et al. [178] for cisplatin release from core-shell PLGA nanoparticles. This discrepancy could be due to Reardon et al. [178] observed their cumulative release over 150 hours compared to our calculations after 5 hours. The Reardon effort also fabricated a drug delivery system on the Nano scale while our system is on the micro scale. Reardon et al. [178] also observed their diffusion study in Phosphate-buffered saline (PBS) while our study was observed in deionized water.

4.4 Conclusions

In summary, we demonstrated an approach using amphiphilic polymeric micelles (F127) to regulate controlled release of two indicator dyes (malachite green and erythrosin) and one chemotherapeutic drug (cisplatin). We tested the release at temperatures that would alter the driving force for forming colloidal gels in vivo (room temperature and 40^{o}C). We show the process tracking dye or drug collection in a receiver solution through a dialysis membrane from the absorbance measurements, via UV-Vis, to the determination of an apparent diffusion coefficient where applicable. Our cisplatin results were compared to a number of other studies in which permeation in a sequestered nanostructure was evaluated for its fluence [181, 182]. Adding the amphiphile lowered the permeability of dye molecules ($2.6 \pm 0.01 \times 10^{-7}$ cm^2s^{-1} MG-RT compared to $2.6 \pm 0.01 \times 10^{-8}$ cm^2s^{-1} MG-F127-RT), but tended to result in a burst delivery with cisplatin (6% total release with cisplatin-F127-RT compared to 4% total release cisplatin-RT). We noted instability with cisplatin in aqueous solution [168-171].

4.5 Acknowledgments

We acknowledge the Rackham Graduate School at UM for support. We would also like to thanl the GEM Fellowship funded through DuPont and the National Physical Science Consortium (NPSC) fellowship funded through the National Institute of Standards and Technology (NIST) for their financial support. Thanks to Tim Chambers for training on the UV-Vis at UM Van Vlack Labs.

CHAPTER V

Micelle Gels as Fire Retardants

5.1 Introduction

While Chapters II, III, and IV focused on PEO-PPO-PEO micelles for drug delivery applications, this chapter explores a novel concept of using micelle gels for fire retardant applications.

Fire is a useful tool throughout human history, but it can bring disasters if not carefully controlled [183]. By inhibiting a voluminous fire, there is a better chance for fire-fighters to extinguish it or for people to escape uncontrolled fires before they cause significant damage. Cotton is a very important natural textile fiber used to produce clothing, furniture, and industrial products, but it has a low limiting oxygen index (18%) [184] and thermal decomposition temperature (360 °C to 425 °C) that makes it very flammable [185]. When cotton fabrics are ignited, the flame spreads rapidly potentially causing fatal burns within 15 seconds of ignition [186]. Various methods have been used to impart flame retardancy to cotton fabrics [187-192]. Boron and halogenated containing additives have been widely used that function by liberating large volumes of non-flammable gases to starve the flames and forming a glass coating, respectively, during thermal decomposition [186, 193]. Boron-based flame retardants are quite water soluble and might impart only fleeting flame retardancy on fabrics that undergo numerous washing cycles [185]. The effectiveness of the most common halogenated flame retardants in general has been compromised by their latent toxicity concerns linked with bioaccumulation and

exposure issues to both humans and aquatic species in the environment [194]. While there are certainly new halogenated chemistries that might prove somehow better than those compounds with documented concerns, our focus here is phosphorus-based flame retardants that have also been successful in imparting flame retardancy to cellulosic fabrics [195, 196]. Some Phosphorous-based coatings can withstand repeated wash cycles [185], reduce volatile fuel, lower pyrolysis temperature, increase carbonaceous char, and decrease afterglow [195]. Leistner et al. [196] studied the use of chitosan/melamine polyphosphate as a water-insoluble coating on cotton fabric via layer-by-layer assembly.

Layer-by-layer (LbL) deposition [197-201] is a common technique for fabricating thinner, multifunctional flame-retardant films/coatings. These coatings are formed by repeatedly depositing alternating layers of oppositely charged materials. The multilayer assembly of the coating is self-regulated by electrostatic repulsion within the individual layers and is enabled by attractive forces; electrostatic [202], van der Waals [203, 204], and H bonding [205, 206]. LbL coatings/films can be applied by either dip coating [207, 208] or spray coating [209, 210]. They have range of functionalities that can produce conducting films [211-213], antireflection films [214, 215], and oxygen barriers [216, 217]. More recently, researchers have pivoted from layer-by-layer assembly and are aiming for one-step processes for fabricating a flame retardant coating on fabrics [218] and polyurethane foams [219]. Each additional monolayer requires an additional depositing and washing step; therefore, these 20 or more monolayer coatings required a total of 30 or more steps in the fabrication process, considerably more than required for the conventional and preferred single bath coatings. In this study we propose using melamine, sodium hexametaphosphate (SHMP), and polyethylene oxide-polypropylene oxide-polyethylene oxide,

PEO-PPO-PEO, triblock copolymer to form a water-insoluble flame retardant gel that can be applied onto cotton fabrics.

Sodium hexametaphosphate (SHMP) [220], melamine [221], and PEO-PPO-PEO triblock copolymers are all relatively non-toxic chemicals in small doses. SHMP is used as a sequestrant and as a food additive [222]. Melamine is the starting material for resins used in the production of a wide variety of thermosetting plastics [223]. When melamine is mixed with SHMP in aqueous solution, they form the water-insoluble flame retardant melamine polyphosphate (MPP) [196]. The amphiphilic PEO-PPO-PEO triblock copolymer F127 has surfactant properties that make it useful in industrial applications including drug delivery [224, 225].

Researchers have studied the mechanism for the gel formation of aqueous dispersions of PEO-PPO-PEO triblock copolymers and have attributed the gel formation to the close packing and ordering of micelles [6, 8, 226]. The PEO-PPO-PEO triblock copolymer F127 (70% PEO content) has been studied extensively as it has the most pronounced gel forming abilities of the commercially available polymer surfactants [29]. As the temperature of these solutions is increased, the decreasing aqueous solubility of the PPO causes micelle formation with the hydrophobic (PPO) cores and hydrophilic (PEO) shells [15]. Lam et al [17] suggested that the micelles grow via Ostwald ripening and Barba et al [18] suggested that the volume fraction occupied by the micelles in solution rises with increasing temperature. The micelles experience repulsive interactions and order into quasicrystalline cubic lattices [15]. The observed lattice structure for F127 gels are typically face centered cubic or body centered cubic [227, 228]. This lattice structure is believed to give these materials their gel-like properties [15].

This chapter describes chemical formulations and one-step procedures to yield relatively non-toxic, flame retardant coatings for cotton fabrics. The coatings were made with the

amphiphilic PEO-PPO-PEO triblock copolymer F127, melamine, and SHMP. The impact of the formulations on flammability was determined by measuring ignition resistance combustion heat released rate, and decomposition behavior using vertical flame testing (VFT), micro-scale combustion calorimetry (MCC), and thermogravimetric analysis (TGA). Scanning electron microscopy (SEM) was used to observe surface quality assessments of the coatings on the cotton fabrics.

The experiments, results, and discussion covered in this chapter were conducted at the National Institute of Standards and Technology (NIST) as a part of the National Physical Science Consortium (NPSC) fellowship. This work was submitted to *Advanced Materials Interfaces* for review [23].

5.2 Materials and Methods

5.2.1 Materials

Polyethylene oxide-polypropylene oxide-polyethylene oxide, PEO-PPO-PEO F127 (12,600 g/mol molecular mass), SHMP ($Na_6P_6O_{18}$, 611.77 g/mol molecular mass), and melamine ($C_3H_6N_6$, 126.12 g/mol molecular mass) were all obtained from Sigma-Aldrich (Milwaukee, WI) and were used as received. The structures of each are shown in Figure 5.1 [23]. The cotton fabric (James Thompson & Co. Inc., 228.6 cm Quilter's Flannel, double-napped 100% cotton) with area density of 102g/m^2 was used as received. All solutions were prepared using deionized water from a PURELAB Flex (18.2 MΩ·cm, ELGA).

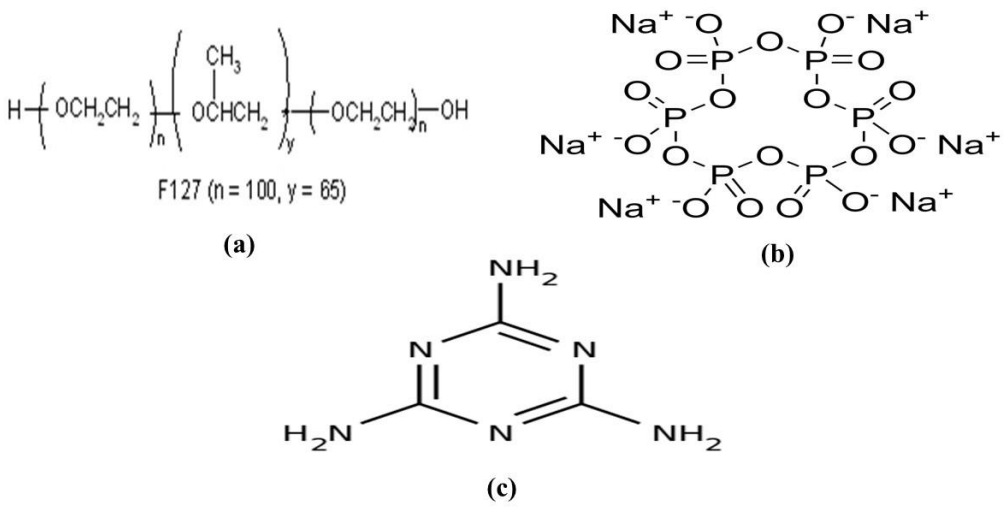

Figure 5.1: (a) Pluronic F127 (b) sodium hexametaphosphate (c) melamine [23].

5.2.2 Coating Procedure

Aqueous solutions of F127 were each prepared according to "cold" processing methods [29] and formulated in varying concentrations (10% to 20%) to probe its flame retardant properties. Concentrations of melamine (5% to 15%) were mixed in aqueous solutions of F127. Lastly, varying concentrations of SHMP (5% to15%) were added. The total volume of the mixtures during treatment was held constant as an attempt to control the thickness of the coatings. After several hours of mixing at room temperature, the coating gel formed. The white gel was coated onto the cotton fabric (10 cm by 10 cm) using a stainless steel laboratory spatula. Both sides of the cotton fabrics were coated to ensure a thorough coating. The coated cotton fabric was placed in an oven for at least 12 hours at 70^{o}C. If the fabric still felt damp to the touch after 12 hours, it was placed back in the oven until moisture was no longer present. Two types of coating protocols were followed, one with melamine, SHMP, and F127, and the other without F127. The protocol without F127 used aqueous solutions of melamine (5%) and SHMP (5%) all

mixed into a single bath. The cotton fabric was manually dipped into the solution and soaked for 10 minutes to allow complete wetting and good adhesion of the coating to the substrate. The coated cotton fabric was then placed in an oven at 70°C for a minimum of 12 hours. The resulting color of the cotton fabric turned white due to the melamine polyphosphate. The overall hand of the fabric after coating felt stiffer and heavier compared to the soft and stretchy feel prior to coating.

5.2.3 Flammability Testing

Ignition resistance assessments were done on the coated fabric using vertical flame testing (VFT) to identify promising formulations. These formulations were reproduced and their combustion behavior was measured using micro-scale combustion calorimetry (MCC) from 100°C to 750 °C under an environment of 20% oxygen and 80% nitrogen with a heating rate of 1°C s^{-1} and a sample mass of 5mg; using a ASTM D7309 (Concept Equipment). This test revealed the influence of the coating on the fabric's heat release. Thermogravimetric analysis (TGA) was also performed on coated fabrics tested from 90°C to 850°C under nitrogen with a constant heating rate of 20°C min^{-1} and a sample mass of 10 mg, using a NETZSCH STA 449 F1 (Germany). TGA tests revealed the mass loss of the coated sample due to non-oxidative thermal decomposition. A Ziess Ultra 60 Field Emission-Scanning Electron Microscope (FE-SEM, Carl Zeiss Inc., Thornwood, NY) was used to acquire surface images of the coatings on the cotton fabrics under a 5 kV accelerating voltage. All SEM images were sputter-coated with 8 nm of gold/platinum (60%/40% by mass) prior to imaging.

The cotton fabrics were used as received. No conditioning was performed prior to testing. The vertical flame test was setup as shown in Figure 5.2 [23]. The ignition source was applied to

the middle, bottom edge of the sample for 5 seconds. If the sample failed to ignite or it self-extinguished, the torch was applied again at the same place on the fabric for another 5 seconds. This ignition process was repeated no more than three times on the same specimen. The test was complete when there were no visible flames or when the specimen was completely consumed during combustion. The 100% cotton fabric was used as a control to qualitatively rank the formulations. The type of behavior used for ranking included the following: number of applications of the torch before ignition, time until flames extinguished, and extent of flame propagation across the cotton surface. The results of this test is shown in Table 5.1 [23].

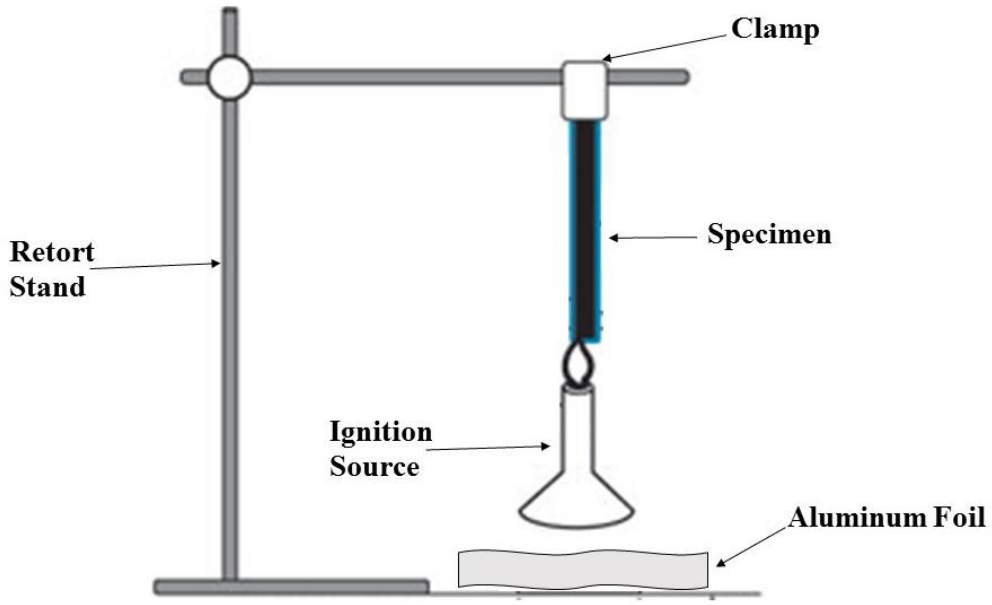

Figure 5.2: Example of vertical flame test (VFT) setup [23].

5.3 Results and Discussion

5.3.1 Fabrication and Flammability Screening

In a single step coating process, PEO-PPO-PEO F127 (F127), co-formulated with melamine, and sodium hexametaphosphate (SHMP) flame retardant were deposited as gel coatings on cotton fabrics. The coatings were characterized to determine coating morphology (SEM) and ignition resistance (vertical flame testing). Only the coatings that did not ignite were evaluated through MCC, TGA, and SEM.

10 flame retardant-coated cotton fabric were made by applying gel coatings containing F127 (0%, 15%, and 20%), melamine (0%, 5%, 10%, and 15%), and SHMP (0%, 5%, 10%, 15%). The coating composition, mass gain percent (percentage of mass increase after coating is applied), and flammability results are provided below in Table 5.1 [23]. The data in Table 5.1 [23] reflect the averages of at least three specimens for each formulation.

Table 5.1: Coating composition, mass gain %, and open flame screening for flame retardant-coated cotton fabrics. Mass gain is reported with a 2σ uncertainty [23].

Coating Composition (%)			**Mass Gain (%)**	**Flammability observations**
F127	**Melamine**	**SHMP**		
25	10	10	143 ± 10	Ignition, slow flame spread
20	15	15	238 ± 10	No ignition
20	15	-	143 ± 10	Ignition, slow flame spread
20	-	15	137 ± 10	Ignition, charred
20	-	-	105 ± 10	Complete combustion
15	15	15	220 ± 10	No ignition
-	5	5	54 ± 10	No ignition
-	5	-	30 ± 10	Extensive combustion
-	-	5	10 ± 10	Ignition, charred
-	-	-	-	Complete combustion

Flammability of a material is defined by a number of factors, including its ignition resistance and by the size of the exotherm formed during combustion. Typically for fabrics, ignition resistance is the more important of the two, at least for screening fabrics for a specific use. Therefore, in this study, ignition resistance tests were used as initial screens of fabric flammability.

Based on the ignition resistance test results from Table 5.1 [23], all the flame retardant formulations for cotton raised its flame resistance. The control and 20% F127 gel coated cotton fabrics ignited as soon as the ignition flame source was applied. Within 60 seconds the fabrics were completely engulfed in flames. The best performing coatings (no ignition, Table 5.1 [23]) were the 5% melamine/5% SHMP, 20% F127/15% melamine/15% SHMP, and 15% F127/15% melamine/15% SHMP formulations. Depending on the coating on the cotton fabrics, the overall mass gain is dramatically affected. Even though the 20% F127/15% melamine/ 15% SHMP coating also did not ignite according to Table 5.1 [23], only the 15% F127/15% melamine/ 15% SHMP coating was further explored for testing because of its lower coating weight and higher ignition resistance. The lower overall mass gain also attributed to a more flexible and softer fabric compared to the higher mass gains. A 10% F127/15% melamine/15% SHMP coating was also tried, but a gel did not form a coating because it was below the critical gel formation concentration [29]. In this case, adding melamine and SHMP was not a strong enough driving force to form a gel at 10% F127. In order to compare the combustion behavior and decomposition of the paste itself before applying it onto cotton fabrics to the coated fabrics, a 20% F127/15% melamine/15% SHMP paste was also analyzed using MCC and TGA.

5.3.2 Instrumentation: TGA, MCC, and SEM

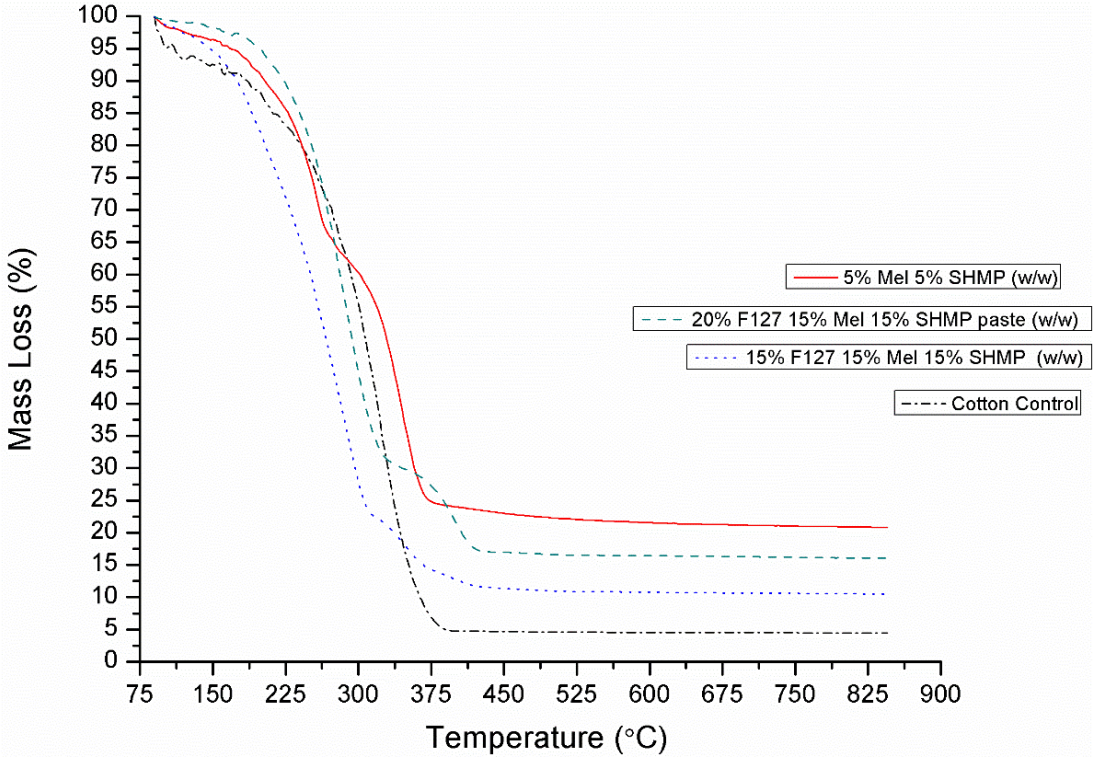

Figure 5.3: TGA data for F127/melamine/SHMP gel coating on cotton fabric (blue dots), melamine/SHMP (red solid line), uncoated cotton fabric (black dash-dots), and coating paste itself without cotton fabric (green dashes) [23].

Table 5.2: TGA properties of uncoated cotton fabric, melamine/SHMP on cotton, F127/melamine/SHMP gel coating on cotton, and F127/melamine/SHMP coating paste itself. Data is reported with a 2σ uncertainty. The slopes correspond to the dehydration of the coated fabric (1) followed by the active combustion of the dehydrated composite (2) [23].

Sample ID	1st Slope (%/°C) (R^2)	2nd Slope (%/°C) (R^2)	Intermediate Plateau Temperature Range (°C)	Residue (%)
Cotton Control	-0.07 (0.86)	-0.5 (0.95)	-	5 ± 1
5% Melamine 5% SHMP	-0.05 (0.97)	-0.3 (0.94)	275-375	20 ± 2
15% F127 15% Melamine 15% SHMP	-0.08 (0.99)	-0.5 (0.97)	300-375	10 ± 2
20% F127 15% Melamine 15% SHMP paste	-0.04 (0.93)	-0.6 (0.97)	325-425	15 ± 2

As shown in Figure 5.3 and Table 5.2 [23], TGA results on untreated cotton show some level of mass loss below 225^{o}C, but there is a rapid decline in residual mass with rising temperature above 225^{o}C. The lower and higher temperature decompositions can be interpreted as a two-stage decomposition process with slopes of percent mass loss/^{o}C summarized in Table 5.2 [23]. Coating cotton with the SHMP/melamine mixtures led to TGA results that show some intermediate plateau of mass stability with increasing temperature that makes coated cotton degradation more complicated than simply interpreting the two-step degradation model. The mass loss at lower temperatures for the coated fabrics is due to the decomposition of melamine and SHMP. Both the coating and the cotton contribute to the mass loss of the coated fabrics. Despite the 15% F127/15% melamine/15% SHMP coating losing mass at lower temperatures than the cotton control, the mass above 400^{o}C for cotton is less than 5% while that for the coated cotton is about 15% or less.

The 5% melamine/5% SHMP, 15% F127/15% melamine/15% SHMP coated cotton**,** and the 20% F127/15% melamine/15% SHMP coating exhibited similar TGA profiles, except the coatings had higher mass residues at the end of the test compared to cotton. For neat cotton decomposition ended at ~375 °C with 5% ±1% of the original mass as char residue.

Significant mass changes in the TGA residue occurred when the cotton fabric was coated with 15% F127/15% melamine/15% SHMP and 5% melamine/5% SHMP. The temperature of the onset of degradation occurred at 150^{o}C and 185^{o}C respectively for 15% F127/15% melamine/15% SHMP and 5% melamine/5% SHMP, compared to 75^{o}C for cotton control. In addition, the char yield increased from 5% ± 1% for cotton control at 375°C to 10% ± 2% (~100% increase) at 450°C for 15% F127/15% melamine/15% SHMP coating. Since the percent mass loss for 20% F127/15% melamine/15% SHMP paste is lower than the percent mass loss for

cotton control, the coating is more thermally stable than cotton. Since the 15% F127/15% melamine/15% SHMP coating on cotton fabric has a lower percent mass loss than the cotton control, this coating on cotton lowers decomposition behavior. The mass loss behavior for 15% F127/15% melamine/15% SHMP is similar to that for flame-retardant agent CFR-201 (an organophosphorus nitrogen containing compound) reported by Zhu et al [229].

MCC probed the combustion behavior of the same formulations analyzed by TGA. Figure 5.4 [23] shows the heat release rate (HRR) of coated and uncoated cotton with temperature (°C). The MCC results are shown in Figure 5.4 and Table 5.3 [23].

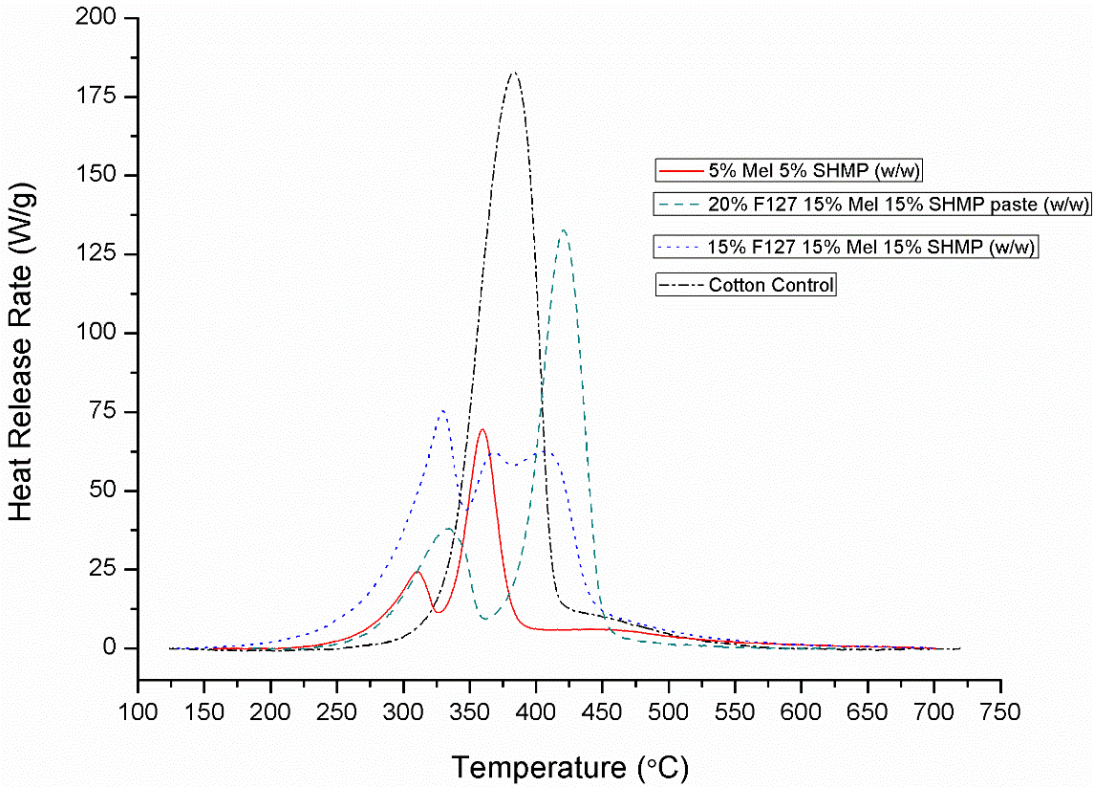

Figure 5.4: MCC results of F127/melamine/SHMP gel coating on cotton fabric (blue dots), melamine/SHMP (red solid line), uncoated cotton fabric (black dash-dots), and coating paste itself without cotton fabric (green dashes) [23].

Table 5.3: Heat release properties of uncoated cotton fabric, melamine/SHMP on cotton, F127/melamine/SHMP gel coating on cotton, and F127/melamine/SHMP coating paste itself. Data is reported with a 2σ uncertainty [23].

Sample ID	**Residue (%) (% increased)**	**THR (kJ/g) (% reduction)**	**PHRR (W/g) (% reduction)**
Cotton Control	12 ± 1	11 ± 3	183 ± 3
5% Melamine 5% SHMP	39 ± 1 (218 ± 1)	4 ± 2 (62 ± 2)	70 ± 2 (62 ± 2)
15% F127 15% Melamine 15% SHMP	30 ± 1 (144 ± 1)	8 ± 12 (21 ± 12)	74 ± 12 (60 ± 12)
20% F127 15% Melamine 15% SHMP paste	24 ± 1	8 ± 4	133 ± 4

As shown in Figure 5.4 and Table 5.3 [23], 5% melamine/5% SHMP, 15% F127/15% melamine/15% SHMP, and 20% F127/15% melamine/15% SHMP paste all show lower heat release rates, THR, and PHRR and higher residue mass values than the cotton control. For cotton, thermal decomposition initiated at ~ 300°C. The decomposition, as indicated by rising HRR, intensified as the temperature rose. The maximum HRR at ~400oC was 183 ± 3 W/g which was identified as the peak heat release rate (PHRR). The decomposition was complete at 550°C with 12% ± 1 of the original mass as char residue.

As a percentage basis, the drop-off in PHRR is more dramatic by coating (reductions as much as 2/3 of PHRR cotton) whereas the total heat release was only 20-50% lower overall with the same coating conditions. The released energy measurements compare favorably with other MCC type measurements on other cotton coatings shown in Figure 5.6 [218, 192].

As shown in Figure 5.4 [23], the HRR curve for cotton control has one peak, but cotton-coated fabrics have two peaks. The additional peaks appear at the early stages (lower

temperatures) of cotton's decomposition as shown in Figure 5.4 [23], are due to the decomposition of melamine and SHMP. Such premature decomposition of a flame retardant would reduce its effectiveness on the coated cotton fabric, therefore identifying ever more effective flame retardants packaged within a gel deserves to be probed more.

SEM images observed the coating quality (surface morphology) of the coated samples. SEM images for 15% F127/15% melamine/15% SHMP**,** 5% melamine/5% SHMP, and cotton control are provided in Figure 5.5 [23].

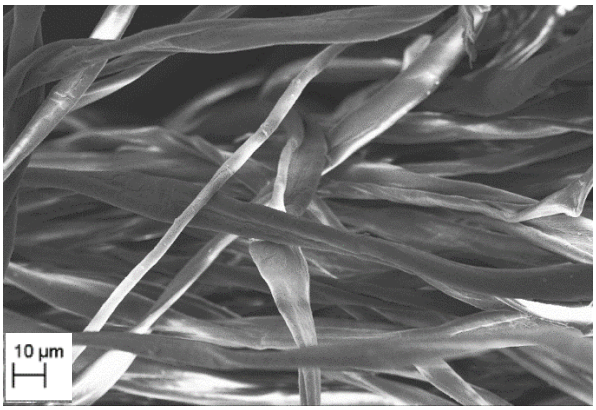

(a)

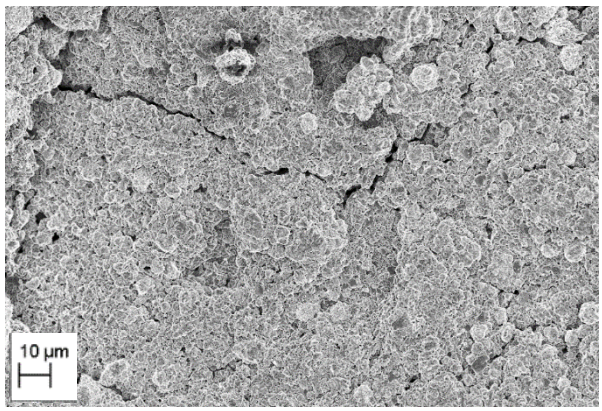

(b)

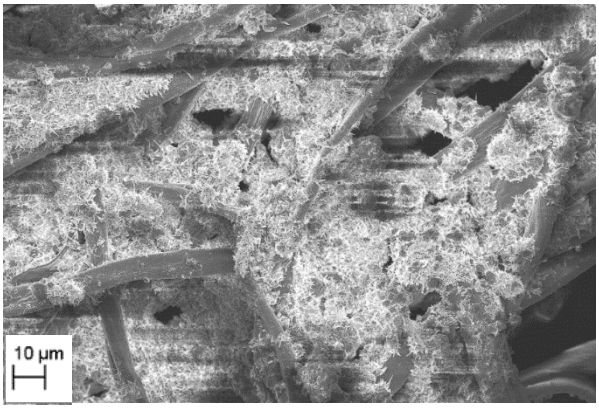

(c)

Figure 5.5: SEM images (a) cotton control (b) 15% F127/15% melamine/15% SHMP on cotton fabric (c) 5% melamine/5% SHMP on cotton fabric. The 5% melamine/5% SHMP coating is not very uniform on the cotton fibers and is randomly dispersed. The 15% F127/15% melamine/15%

SHMP coating shows a more uniform coating on the cotton fibers but there are noticeable cracks which indicates insufficient adhesion of the paste onto the cotton fabric [23].

Some coating was observed on the 5% melamine/5% SHMP, but the coating is randomly dispersed as some fibers have more coating on them than others. For the 15% F127/15% melamine/15% SHMP coating on cotton fabric, it shows a more uniform mixture of coating paste all over the cotton fibers. All of the fibers are coated and completely covered. There are some noticeable cracks that appear in the image that indicate insufficient adhesion of the paste onto the cotton fabric and varying thickness. A more uniform and thinner coating is required to ensure the flame does not touch the fabric directly without dramatically adding to the cotton mass. If the flame was more effectively isolated from the flame, the coating will contact the flame, causing no ignition. This was a proof in concept and more work is needed to explore a more uniform coating thickness, as well as a more stable coating after washing.

5.3.3 Comparison to Other Technologies

Figure 5.6 [23] presents other flame retardant strategies, incorporated in or applied onto cotton fabrics [192, 196, 218]. These flame retardants were deposited using single bath and LbL assembly protocol and constructed using N-methylol dimethylphosphonopropionamide (MDPA) and trimethylol melamine (TMM) [192], soaked in a polyethylenimine (PEI)/poly(phosphate sodium salt) (PSP) complex [218], polyallylamine/poly(phosphate sodium salt) (PAAm/PSP) [218], and PA/CH at PH 4 [218]. The LbL coatings ranged from 10 monolayers to 64 monolayers and resulted in a mass increase of 2% to 18%. These deposited coatings gave heat release reductions of 42% to 61% (PHRR) and 54% to 76% (THR).

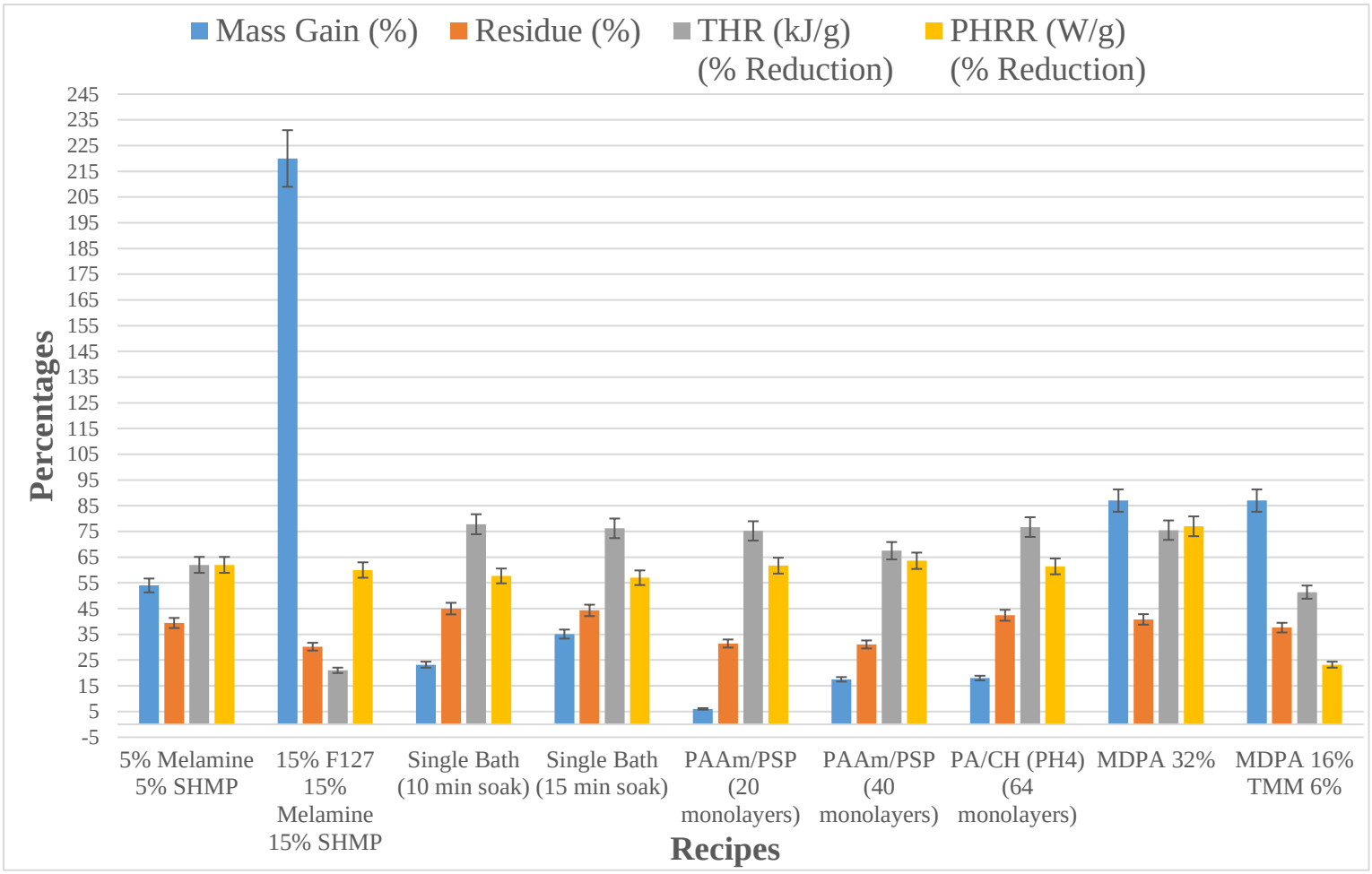

Figure 5.6: Comparison of MCC data for F127, melamine, and SHMP coatings to the previously reported single bath [218], LbL [218], and MDPA/TMM [192] coatings on or deposits within cotton fabrics. Mass gain % (blue), residue % (orange), THR (kJ/g) % reduction (grey), and PHRR (W/g) % reduction (yellow) for each recipe is compared. Data is reported with a 2σ uncertainty [23].

All coatings reduce the cotton flammability by MCC. In terms of total energy of combustion, the gel-coating has statistically lower energy released relative to any of the other coatings. That enhancement comes at the cost of a huge increase in coating thickness, primarily consisting of amphiphilic copolymer. The amphiphile is still hydrophilic even after the drying process before combustion and its presence probably absorbs energy from the combustion that can explain why the THR for the gel coating is so much lower. Of course, if one could optimize the coating thickness to not triple the mass of the fabric, the effectiveness of the coating might be diminished. That same effect could have occurred if the amphiphiles were extracted from the gel

coating with subsequent washings. In terms of a peak combustion rate, there is little difference between the coatings and the coating with the lowest PHR is the MDPA/TMM co-mixture which is statistically lower than the rest. It is also interesting to note that the presence of more LbL layers adds to the mass but doesn't improve the residue or the energy of combustion suggesting that the thinnest LbL coatings are more retardant.

5.4 Conclusions

Aqueous-based amphiphile solutions have been co-formulated with potentially alternative flame retardants in a one-step process to make flame retardant gel coatings for cotton fabrics. Coatings containing an amphiphilic block copolymer in aqueous solution and formulated with melamine and SHMP on cotton fabrics are self-extinguishing as found by vertical flame testing. Coatings with higher compositions of the amphiphile led to lower ignition resistance hence the 15% F127 composition was used throughout for the subsequent analyses. Coating effectiveness was probed with micro-scale combustion calorimetry (MCC) and thermogravimetric analysis (TGA). The most successful performing gel formulation was 15% F127/15% melamine/15% SHMP which produced 74 W/g ±12 W/g in PHRR (a 60% reduction), and 8.0 kJ/g ±12 kJ/g in THR (a 21% reduction). The gel coatings are too thick to be commercially viable. The coated fabric also turned white due to the melamine polyphosphate. The overall hand of the fabric after coating felt stiffer and heavier compared to the soft and stretchy feel prior to coating. SEM imaging showed a more uniform coating over all of the cotton fibers for the 15% F127/15% melamine/15% SHMP coating compared to less concentrated coatings. The thicker gel coating showed evidence of cracks but that alone could have been a function of the large coating film thickness. Overall, the scheme for using precursors that result in the formation of a solid phase,

insoluble flame retardant in a coating seems valid, although larger amounts of qualification testing and better tools to provide for a thinner and more controlled thickness are appropriate.

5.5 Acknowledgments

We acknowledge the National Physical Science Consortium (NPSC) fellowship funded through the National Institute of Standards and Technology (NIST) for their financial support. We also acknowledge the Rackham Graduate School at UM for their support. We thank Yeon Seok Kim (NIST) for conducting the TGA and MCC experiments.

CHAPTER VI

Summary and Future Work

6.1 Summary

The aim of this dissertation work was to better understand how ternary additives perturb the micelle formation energetics and where within the micelle ternary additives are portioned to resolve how formulated micelles perform as drug delivery vehicles. We attempted to better understand the linkage between forming structures of amphiphiles housing other molecules and the effect on availability and performance. Chapter II was dedicated to showing how the presence of methylparaben and cisplatin affect the thermodynamics of micelle formation, and resolving where within amphiphilic copolymer micelles various drugs of a certain hydrophilicity are situated. Chapter III studied how temperature and the presence of cisplatin affects the structural evolution of phase formation in PEO-PPO-PEO solutions. Chapter IV showed how temperature and different ternary additives affect the diffusion for controlled release and driving force for forming colloidal gels. Finally, Chapter V was a unique study that analyzed how to form micelle gels mixed with fire retardants to study flame resistant properties when applied onto cotton fabrics.

In Chapter II, Differential Scanning Calorimetry was performed on a series of aqueous solutions of polyethylene oxide-polypropylene oxide-polyethylene oxide, PEO-PPO-PEO, (L101, P104, P105, and F108) amphiphiles in the low concentration regime (0-2/% mass v^{-1}) to resolve the critical micelle concentrations (cmc) of the neat polymers. We confirmed the cmc for

P105 to be ~0.4%w/v at 26.3ºC, which is close to but slightly larger than 0.3%w/v at 25ºC of Alexandridis et al. [119, 120]. Increasing Pluronic P105 from 4% to 10% reduced $T_{micelle}$ and raised the endotherm. Work was done from 2% mass v^{-1} to 10% mass v^{-1} (in 2% mass v^{-1} increments) amphiphilic copolymer concentrations and co-formulated with cisplatin and methylparaben concentrations (0% mass v^{-1} - 0.1/% mass v^{-1} in 0.02/% mass v^{-1} increments) to resolve any deviation in the enthalpy of micelle formation. Enthalpy-entropy compensation plots for each neat copolymer and each amphiphile solution mixed with drug were obtained. The compensation temperature, $T_{compensation}$, was determined from the analyses for neat P105 as 293.9 K; adding MP raises this to 328.43K. This change was compared to Bouchemal's $T_{compensation}$ of 293.3K for neat F127 and 316.5K when loaded with 1,2-propanediol [121]. For added cisplatin, two types of behaviors were observed; a drug influenced compensation temperature profile (P104), and a drug invariant behavior (L101, P105 and F108) where the change in compensation temperature was less than 1 K. Only neat P104 was found to be profoundly influenced by the presence of cisplatin that must reorganize the core/shell interface between the hydrophobic and hydrophilic regions of the micelle. Adding cisplatin lowered $T_{compensation}$ from 302.1 to 288.8 K for Pluronic P104. Our findings present a rationale for explaining how the presence of a ternary additive, like MP and cisplatin, interacts thermodynamically with forming micelles, and the potency of the interaction between drug and micelle might regulate drug bioavailability.

In Chapter III, the arrangement into cubic lattices of aqueous solutions of PEO-PPO-PEO triblock copolymers as their temperature is raised was analyzed. This structural evolution is seen macroscopically as a gelation, and the presence of these ordered phases can be controlled through both polymer concentration and temperature. The presence of added solutes within the dispersions can also affect the onset and kinetics of structure formation. In Chapter III, we

investigated the structures formed in the amphiphiles P104, P105, and F108 solutions at 31% mass v^{-1} both neat and co-formulated with the chemotherapeutic drug cisplatin (0.02% to 0.1% mass v^{-1}) using small-angle X-ray scattering (SAXS). We observed both the progressive evolution and breakdown of these structures as the temperature is increased from 10ºC to 35ºC. The size of the unit cell as well as the thermal expansion coefficients for each system was also calculated. As the samples were being heated, added cisplatin changes the nucleation behavior of fcc or bcc phases within the sample from a homogeneous process to a more heterogeneous distribution of nucleated species. For P104 and P105, added cisplatin enhanced the structural ordering with sharper peaks. Unexpectedly for F108, added cisplatin showed the opposite effect as the intensity decreased indicating a destabilization of the ordered phases. The presence of cisplatin also caused the primary peaks of the F108 structure factor to be suppressed, while preserving the higher order peaks. Understanding where chemotherapeutic molecules as ternary additives are partitioned within micelles and how they influence the evolving structure is important to optimize controlled release systems utilizing amphiphilic copolymers as a drug delivery system.

In Chapter IV, dynamic diffusion experiments were performed on aqueous polymeric micelles mixed with the ternary additives: malachite green (0.05% mass v^{-1}), erythrosin (0.1% mass v^{-1}), and cisplatin (0.1% mass v^{-1}) to gauge their release from sequestered structures using Ultraviolet-Visible spectroscopy. The additives were formulated with 20% mass v^{-1} aqueous solutions of PEO-PPO-PEO (F127). Each additive was tested neat at room temperature, neat at 40°C, and formulated with F127 at room temperature, and 40ºC. After making calibration curves, the dynamic release for each ternary additive and corresponding diffusion coefficients were calculated. Results showed F127 retarded permeation at room temperature. In general, the

neat additives at 40°C showed the highest permeability for both malachite green and erythrosin. Malachite green released almost 90% of the dye by 60 minutes of permeation. When formulated with F127 at 40°C, sizeable release was still noted, but with an induction period of 10-30 minutes to register release. The behavior with cisplatin was more complicated as the first 5 hours of permeation resulted in a burst delivery with cisplatin (6% total release with cisplatin-F127-RT compared to 4% total release cisplatin-RT) but with overall lower release. The higher fluence at elevated temperature is attributed to reducing the blocking effect of the amphiphiles on the walls of the dialysis tubing as they are directed to form colloidal gels. There is also likely a correlation between higher temperature and higher overall permeability if the membrane pores also expand with temperature. Our cisplatin results were compared to a number of other studies in which permeation in a sequestered nanostructure was evaluated for its fluence [181, 182]. Adding the amphiphile lowered the permeability of dye molecules ($2.6 \pm 0.01 \times 10^{-7}$ cm^2s^{-1} MG-RT compared to $2.6 \pm 0.01 \times 10^{-8}$ cm^2s^{-1} MG-F127-RT), but tended to result in a burst delivery with cisplatin (6% total release with cisplatin-F127-RT compared to 4% total release cisplatin-RT). We also noted instability with cisplatin in aqueous solution [168-171].

In Chapter V, cotton fabrics with flame retardancy were made from gel coatings applied from a single bath solution formulated with polymeric micelles and flame retardant amphiphiles. The flame retardant coatings were made from aqueous formulations of PEO-PPO-PEO (F127), in the low concentration regime (15% w/w), mixed with melamine (5%-15% w/w) and sodium hexametaphosphate (SHMP) (5%-15% w/w). After coating, the cotton fabrics were more difficult to ignite and, if ignition occurred, the coatings would self-extinguish. Vertical flame testing (VFT), micro-scale combustion calorimetry (MCC), thermogravimetric analysis (TGA), and scanning electron microscopy (SEM) were used to evaluate the coating quality of the flame

retardancy. Coated cotton decomposed at higher temperatures, as shown by MCC and TGA. While there is a need to optimize the coating conditions to yield an appropriate thickness compared to those reported in Chapter V, the combination of SHMP and melamine packaged in an amphiphilic matrix raises cotton flame retardancy. Overall, the scheme for using precursors that result in the formation of a solid phase, insoluble flame retardant in a coating seems valid, although larger amounts of qualification testing and better tools to provide for a thinner and more controlled thickness are appropriate.

6.2 Future Work

The data presented in this dissertation presents a more complete picture of the specific interactions of ternary additives and PEO-PPO-PEO micelle structures. In certain situations, other additives produced different behavior in the resulting micelle gels. Added hydrophobic methylparaben changed the thermodynamics of micelle formation in P105 gels for compensation temperature, but added hydrophilic cisplatin showed an invariant behavior where the change in compensation temperature was less than 1 K. Only neat P104 was found to be profoundly influenced by the presence of cisplatin that must reorganize the core/shell interface between the hydrophobic and hydrophilic regions of the micelle. This suggests that differences in the molecular interactions between micelles and hydrophilic/hydrophobic ternary additives can lead to a different resulting behavior. DSC experiments of solutions containing P104 and methylparaben may help interpret how dissolved methylparaben affects the energetics of micellization of Pluronic P104. Overall, a more detailed investigation into the specific interactions that take place between ternary additives of a certain hydrophobicity is needed to offer a molecular explanation for the observed changes. Nuclear magnetic resonance (NMR)

may prove useful in determining the types of intermolecular interactions that are being formed between molecules of amphiphilic micelles and ternary additives.

Although the scattering studies presented here analyze the structural changes in the micelle lattice, other techniques are also available. Most notably, Small-Angle Neutron Scattering (SANS) as opposed to SAXS may optimize the scattering contrast between the micelle core and the micelle shell, which would help better determine if changes in the micelle lattice were a result of changing core size, or if the micelle shell was similarly being affected by added cisplatin. SANS would be especially useful with added cisplatin because of its high neutron scattering capabilities. The platinum, chlorine, and nitrogen atoms each produce high neutron scattering data which is shown in Figure 6.1. Similar methods have been carried out previously by Sharma et al. [13] using F127 and methylparaben, dibucaine, lidocaine, tetracaine, paclitaxel, baccatin III, sulindac, ethyl paraben, and propyl paraben. In addition to SANS, Dynamic Light Scattering (DLS) could also be used to see how adding ternary additives affect micelle size. Our group previously used DLS to analyze the affect methlyparaben has on the micelle size of F127 [16].

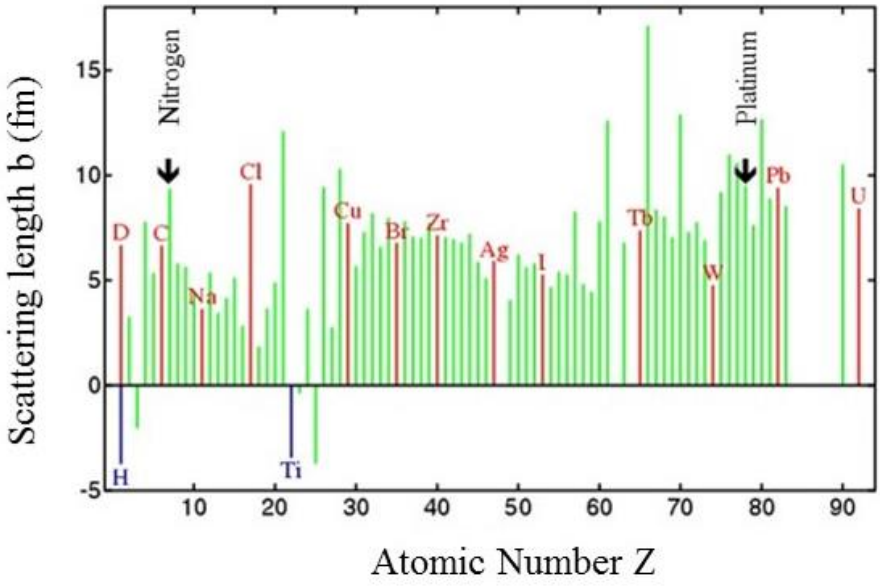

Figure 6.1: The variation of neutron scattering lengths as a function of atomic number.

Efforts to apply these characterization techniques to more hydrophilic or hydrophobic additives are also worth further study. Results for more hydrophilic/hydrophobic or high molecular weight/low molecular weight additives can be used to generalize observed trends and create models for a particular additive and a corresponding amphiphilic micelle. These models can be used to help explain the result of a particular ternary additive interacting with a particular amphiphilic triblock copolymer. This would allow predictions that are more accurate in the micellization and aggregation behavior of amphiphilic copolymers in complex formulations. Studying other ternary additives like carboplatin in PBS solution instead of aqueous solutions may also help to understand the stability issue as well as the linkage between forming structures of amphiphiles housing other molecules and the effect on availability and performance in real world applications.

To further study the kinetics of gel formation in amphiphilic copolymer solutions, Rheology could be used to measure its thermophysical properties at different heating rates. Our

group previous used Rheology to study the thermophysical properties of F127 with added methylparaben using ramp rates of 0.1-10^{o}C min^{-1} [16]. An expanded set of Rheology studies targeting the kinetics of the gel transition at different heating rates would produce useful information on the process of gel formation itself.

For the fire retardant work in Chapter V, commercialization of this new technology will require extensive testing and characterization to ensure the technology complies with environmental, health, and safety requirements. This will require a better understanding of how the technology deteriorates the routes of exposure and the toxicity of the deterioration products and the probability of the deterioration and exposure. Though the risk of exposure at levels that can cause harmful effects is quite low, which is why these compounds are still used in a variety of commercial products. Additional research is needed to improve the wash durability of these coatings and reducing the mass gain and stiffness (hand) of the fabric upon coating.

REFERENCES

1. Mortensen K, Batsberg W, Hvidt S. Effects of PEO-PPO diblock impurities on the cubic strucutre of aqueous PEO-PPO-PEO pluronics micelles: fcc and bcc ordered structures in F127. Macromolecules. 2008;41:1720-7.

2. Kabanov AV, Lemieux P, Vinogradov S, Alakhov V. Pluronic® block copolymers: novel functional molecules for gene therapy. Advanced Drug Delivery Reviews. 2002;54(2):223-33.

3. Yu G-E, Deng Y, Dalton S, Wang Q-G, Attwood D, Price C et al. Micellisation and gelation of triblock copoly(oxyethylene/oxypropylene/oxyethlene), F127. Journal of the Chemical Society, Faraday Transactions. 1992(17).

4. Meznarich NAK. Effect of ternary solutes on the evolution of structure and gel formation in amphiphilic copolymer solutions: University of Michigan; 2012.

5. Mortensen K, Pedersen JS. Structural study on the micelle formation of poly(ethylene oxide)-poly(propylene oxide)-poly(ethylene oxide) triblock copolymer in aqueous solution. Macromolecules. 1993;26:805-12.

6. Lau BK, Wang Q, Sun W, Li L. Micellization to gelation of a triblock copolymer in water: thermoreversibility and scaling. Journal of Polymer Science B: Polymer Physics. 2004;42(10):2014-25.

7. Vadnere M, Amidon G, Lindenbaum S, Haslam JL. Thermodynamic studies on the gel-sol transition of some pluronic polyols. International Journal of Pharmaceutics. 1984;22(2-3):207-18.

8. Wanka G, Hoffmann H, Ulbricht W. Phase diagrams and aggregation behavior of poly(oxyethylene)-poly(oxypropylene)-poly(oxyethlene) triblock copolymers in aqueous solutions. Macromolecules. 1994;27:4145-59.

9. Alexandridis P, Navaggioli T, Hatton TA. Temperature effects on structural properties of pluronic P104 and F108 PEO-PPO-PEO block copolymer solutions. Langmuir. 1995;11:1468-76.

10. Alexandridis P, Holzwarth JF, Hatton TA. Micellization of poly (ethylene oxide)-poly (propylene oxide)-poly (ethylene oxide) triblock copolymers in aqueous solutions: thermodynamics of copolymer association. Macromolecules. 1994;27(9):2414-25.

11. Sharma PK, Bhatia SR. Effect of anti-inflammatories on Pluronic® F127: micellar assembly, gelation and partitioning. International Journal of Pharmaceutics. 2004;278(2):361-77. doi:10.1016/j.ijpharm.2004.03.029.

12. Sharma PK, Reilly MJ, Bhatia SK, Sakhitab N, Archambault JD, Bhatia SR. Effect of pharmaceuticals on thermoreversible gelation of PEO–PPO–PEO copolymers. Colloids and Surfaces B: Biointerfaces. 2008;63(2):229-35. doi:10.1016/j.colsurfb.2007.12.009.

13. Sharma PK, Reilly MJ, Jones DN, Robinson PM, Bhatia SR. The effect of pharmaceuticals on the nanoscale structure of PEO–PPO–PEO micelles. Colloids and Surfaces B: Biointerfaces. 2008;61(1):53-60.

14. Bouchemal K, Agnely F, Koffi A, Ponchel G. A concise analysis of the effect of temperature and propanediol-1, 2 on Pluronic F127 micellization using isothermal titration microcalorimetry. Journal of Colloid And Interface Science. 2009;338(1):169-76. doi:10.1016/j.jcis.2009.05.075.

15. Meznarich NAK, Juggernauth KA, Batzli KM, Love BJ. Structural changes in PEO–PPO–PEO gels induced by methylparaben and dexamethasone observed using time-resolved SAXS. Macromolecules. 2011;44(19):7792-8. doi:10.1021/ma2015358.

16. Meznarich NAK, Love BJ. The kinetics of gel formation for PEO−PPO−PEO triblock copolymer solutions and the effects of added methylparaben. Macromolecules. 2011;44(9):3548-55. doi:10.1021/ma200302s.

17. Lam Y-M, Goldbeck-Wood G. Mesoscale simulation of block copolymers in aqueous solution: parameterisation, micelle growth kinetics and the effect of temperature and concentration morphology. Polymer. 2003;44:3593-605.

18. Barba AA, d'Amore M, Grassi M, Chirico S, Lamberti G, Titomanlio G. Invenstigation of pluronic F127-water solutions phase transitions by DSC and dielectric spectroscopy. Journal of Applied Polymer Science. 2009;114:688-95.

19. Callister S, Keller A, Hikmet RM. On thermoreversible gels: their classification, relation to phase transitions and vitrification, their morphology and properties. Macromolecular Symposia. 1990;39(1):19-54.

20. Hamley W, Pople JA, Fairclough JPA, Terrill NJ, Ryan AJ. Effect of shear on cubic phases in gels of a diblock copolymer. The Journal of Chemical Physics. 1998;108(6929).

21. Alexandridis P, Hatton TA. Poly(ethylene oxide) poly(propylene oxide) poly(ethylene oxide) block copolymer surfactants in aqueous solutions and at interfaces: thermodynamics, structure, dynamics, and modeling. Colloids and Surfaces A: Physicochemical and Engineering Aspects. 1995;96(1-2):1-46.

22. Schmolka IR. A review of block polymer surfactants. Journal of the American Oil Chemists' Society. 1977;54(3):110-6.

23. Thompson AL, Love BJ, Davis RD. Water-based PEO-PPO-PEO micelles, melamine, and sodium hexametaphosphate used as gel coatings to reduce flammability of cotton fabrics. Advanced Materials Interfaces (submitted). 2017.

24. Nalbandian RM, Henry RL, Balko KW, Adams DV, Neuman NR. Pluronic F-127 gel preparation as an artificial skin in the treatment of third-degree burns in pigs. Journal of Biomedical Materials Research. 1987;21:1135-48.

25. Hsu S-H, Leu Y-L, Hu J-W, Fang J-Y. Physiochemical characterization and drug release of thermosensitive hydrogels composed of a hyaluronic acid/pluronic F127 graft. Chemical and Pharmaceutical Bulletin. 2009;57(5):453-8.

26. Kabanov A, Zhu J, Alakhov V. Pluronic block copolymers for gene delivery. Advances in Genetics. 2005;53:231-61.

27. Ohta S, Nitta N, Takahashi M, Sonoda A, Tanaka T, Yamasaki M et al. Pluronic F127: Application in arterial embolization. Journal of Vascular and Interventional Radiology. 2006;17:533-9.

28. Escobar-Chavez JJ, Lopez-Cervantes M, Naik A, Kalia YN, Quintanar-Guerrero D, Ganem-Quintanar A. Applications of thermo-reversible pluronic F-127 gels in pharmaceutical formulations. Journal of Pharmacy & Pharmaceutical Sciences. 2006;9(3):339-58.

29. Schmolka IR. Artificial skin I. preparation and properties of pluronic F-127 gels for treatment of burns. Journal of Biomedical Materials Research. 1972;6:571-82.

30. Guven A, Rusakova IA, Lewis MT, Wilson LJ. Cisplatin@US-tube carbon nanoparticles for enchanced chemotherapeutic delivery. Biomaterials. 2012;5(33):1455-61.

31. Cepeda V, Fuertes MA, Castilla J, Alonso C, Quevedo C, Perez JM. Biochemical mechanisms of cisplatin cytotoxicity. Anti-Cancer Agents in Medicinal Chemistry. 2007;7:3-18.

32. Lebwohl D, Canetta R. Clinical development of platinum complexes in cancer therapy: an historical perspective and an update. European Journal of Cancer. 1998;34(10):1522-34.

33. Siddik ZH. Cisplatin: mode of cytotoxic action and molecular basis of resistance. Oncogene. 2003;22:7265-79.

34. Wang D, Lippard SJ. Cellular processing of platinum anticancer drugs. Nature Reviews Drug Discovery. 2005;4:307-20.

35. Kataoka K, Harada A, Nagasaki Y. Block copolymer micelles for drug delivery: design, characterization and biological significance. Advanced Drug Delivery Reviews. 2001;47:113-31.

36. Nasongkla N, Bey E, Ren J, Ai H, Khemtong C, Guthi JS et al. Multifunctional polymeric micelles as cancer-targeted, MRI-Ultrasensitive drug delivery systems. Nano Letters. 2006;6(11):2427-30.

37. Nishiyama N, Okazaki S, Cabral H, Miyamoto M, Kato Y, Yuichi S et al. Novel cisplatin-incorporated polymeric micelles can eradicate solid tumors in mice. Cancer Research. 2003;63:8977-83.

38. Moffitt M, Khougaz K, Eisenberg A. Micellization of ionic block copolymers. Accounts of Chemical Research 1996;29:95-102.

39. Tuzar Z, Kratochvil P. Block and graft copolymer micelles in solution. Advances in Colloid and Interface Science. 1976;6:201-32.

40. Munk P, Prochazka K, Tuzar Z, Webber SE. Exploiting polymer micelle technology. CHEMTECH. 1998;28(10):20-8.

41. Talingting MR, Munk P, Webber SE. Onion-type micelles from polystyrene-block-poly(2-vinylpyridine) and poly(2-vinylpyridine)-block-poly(ethylene oxide). Macromolecules. 1999;32:1593-601.

42. Kwon GS, Kataoka K. Block copolymer micelles as long-circulating drug vehicles. Advanced Drug Delivery Reviews. 1995;16:295-309.

43. Kreuter J, Attwood D, Bouwstra JA, Crommelin DJA, Hofland HEJ, Junginer HE et al. Colloidal drug delivery systems. Drugs and the Pharmaceutical Sciences. New York: Marcel Dekker, Inc.; 1994.

44. Scholes PD, Coombes AGA, Davis MC, Illum L, Davis SS. Particle engineering of biodegradable colloids for site-specific drug delivery. Controlled Drug Delivery Challenges and Strategies, American Chemical Society. 1997:73-106.

45. Cammas S, Kataoka K. Site specific drug-carriers: polymeric micelles as high potential vehicles for biologically active molecules. Solvents and Self-Organizations of Polymers. NATO ASI Series E: Applied Sciences, Kluwer, Dordrecht; 1996.

46. Kwon GS, Okano T. Polymeric micelles as new drug carriers. Advanced Drug Delivery Reviews. 1996;21:107-16.

47. Verma SK, Ghosh KK. Micellar and surface properties of some monomeric surfactants and a gemini cationic surfactant. Journal of Surfactants and Detergents. 2011;14:347-52.

48. James J, Ramalechume C, Mandal AB. Two-dimentional surface properties of PEO-PPO-PEO triblock copolymer film at the air/water interface in the absence and presence of Tyr-Phe dipeptide, Val-Tyr-Val tripeptide, SDS and stearic acid. Colloids and Surfaces B: Biointerfaces. 2011;82:345-53.

49. James J, Mandal AB. Micelle formation of Tyr-Phe dipeptide and Val-Tyr-Val tripeptide in aqueous solution and their influence on the aggregation of SDS and PEO-PPO-PEO copolymer micelles. Colloids and Surfaces B: Biointerfaces. 2011;84:172-80.

50. Prameela GKS, Kumar BVNP, Aswal VK, Mandal AB. Influence of water-insoluble nonionic copolymer $E_6P_{39}E_6$ on the microstructure and self-aggregation dynamic of aqueous SDS solution - NMR and SANS investigations. Physical Chemistry Chemical Physics. 2013;15:17577-86.

51. Naskar B, Ghosh S, Moulik SP. Solution behavior of normal and reverse triblock copolymers (Pluronic L44 and 10R5) individually and in binary mixture. Langmuir. 2012;28:7134-46.

52. Matsumoto A, Matsukawa Y, Suzuki T, Yoshino H, Kobayashi M. The polymeralloys method as a new preparation method of biodegradable microspheres: principle and application to cisplatin-loaded microspheres. Journal of Controlled Release. 1997;48:19-27.

53. Mathiowitz E, Jacob JS, Jong YS, Carino GP, Chickering DE, Chaturvedi P et al. Biologically erodable microspheres as potential oral drug delivery systems. Nature. 1997;386:410-4.

54. Gillies ER, Frechet JMJ. Dendrimers and dendritic polymers in drug delivery. Drug Discovery Today. 2005;10(1):35-43.

55. Samad A, Sultana Y, Aqil M. Liposomal drug delivery systems: an update review. Current Drug Delivery. 2007;4:297-305.

56. Yatvin MB, Weinstein JN, Dennis WH, Blumenthal R. Design of liposomes for enhanced local release of drugs by hyperthermia. American Association for the Advancement of Science. 1978;202(4374):1290-3.

57. Allen TM. Liposomal drug formulations: rational for development and what we can expect for the future. Drugs. 1998;56(5):747-56.

58. Ramachandran S, Quist AP, Kumar S, Lal R. Cisplatin nanoliposomes for cancer therapy: AFM and fluorescence imaging of cisplatin encapsulation, stability, cellular uptake, and toxicity. Langmuir. 2006;22:8156-62.

59. Ajima K, Yudasaka M, Murakami T, Maigne A, Shiba K, Iijima S. Carbon Nanohorns as anticancer drug carriers. Molecular Pharmaceutics. 2005;2(6):475-80.

60. Ajima K, Murakmi T, Mizoguchi Y, Tsuchida K, Ichihashi T, Iijima S et al. Enhancement of in vivo anticancer effects of cisplatin by incorporation inside single-wall carbon nanohorns. ACS Nano. 2008;2(10):2057-64.

61. Murakami T, Ajima K, Miyawaki J, Yudasaka M, Iijima S, Shiba K. Drug-loaded carbon nanohorns: adsorption and release of dexamethasone in vitro. Molecular Pharmaceutics. 2004;1(6):399-405.

62. Mohanty RK, Thennarasu S, Mandal AB. Resveratrol stabilized gold nanoparticles enable surface loading of doxorubicin and anticancer activity. Colloids and Surfaces B: Biointerfaces. 2014;114:138-43.

63. Mandal A, Sekar S, Chandrasekaran N, Mukherjee A, Sastry T. Poly(ethylene) glycol-capped silver and magnetic nanoparticles: synthesis, characterization, and comparison of bactericidal and cytotoxic effects. Journal of Engineering in Medicine. 2013;227(11):1224-36.

64. Cheng K, Peng S, Xu C, Sun S. Porous hollow Fe_3O_4 nanoparticles for target delivery and controlled release of cisplatin. Journal of the American Chemical Society. 2009;131(30):10637-44.

65. Mandal A, Sekar S, Kanagavel M, Chandrasekaran N, Mukherjee A, Sastry TP. Collagen based magnetic nanobiocomposite as MRI contrast agent and for targeted delivery in cancer therapy. Biochmica et Biophysica Acta. 2013;1830:4628-33.

66. Xu P, Kirk EAV, Murdoch WJ, Zhan Y, Isaak DD, Radosz M et al. Anticancer efficacies of cisplatin-releasing pH-responsive nanoparticles. Biomacromolecules. 2006;7:829-35.

67. Oishi M, Hayashi H, Iijima M, Nagasaki Y. Endosomal release and intracellular delivery of anticancer drugs using pH-sensitive PEGylated nanogels. Journal of Materials Chemistry. 2007;17:3720-5.

68. Barbe C, Bartlett J, Kong L, Finnie K, Lin HQ, Larkin M et al. Silica particles: a novel drug-delivery system. Advanced Materials. 2004;16(21):1959-66.

69. Slowing II, Trewyn BG, Giri S, Lin VS-Y. Mesoporous silica nanoparticles for drug delivery and biosensing applications. Advanced Functional Materials. 2007;17:1225-36.

70. Chaibundit C, Ricardo NMPS, Muryn CA, Madec MB, Yeates SG, Booth C. Effect of ethanol on the gelation of aqueous solutions of Pluronic F127. Journal of Colloid and Interface Science. 2010;351(1):190-6.

71. Tsui H-W, Wang J-H, Hsu Y-H, Chen L-J. Study of heat of micellization and phase separation for Pluronic aqueous solutions by using a high sensitivity differential scanning calorimetry. Colloid and Polymer Science. 2010;288(18):1687-96. doi:10.1007/s00396-010-2308-5.

72. Thompson AL, Love BJ. Thermodynamic properties of aqueous PEO-PPO-PEO micelles with added methylparaben determined by differential scanning calorimetry. Journal of Colloid And Interface Science. 2013;398:270-2. doi:10.1016/j.jcis.2013.01.064.

73. Foster B, Cosgrove T, Hammouda B. Pluronic triblock copolymer systems and their interactions with ibuprofen. Langmuir. 2009;25(12):6760-6. doi:10.1021/la900298m.

74. Nagant C, Savage PB, Dehaye JP. Effect of pluronic acid F-127 on the toxicity towards eukaryotic cells of CSA-13, a cationic steroid analogue of antimicrobial peptides. Journal of Applied Microbiology. 2012;112(6):1173-83. doi:10.1111/j.1365-2672.2012.05297.x.

75. Malmsten M, Lindman B. Self-Assembly in aqueous block copolymer solutions. Macromolecules. 1992;25:5440-5.

76. Veyries ML, Couarraze G, Geiger S, Agnely F, Massias L, Kunzli B et al. Controlled release of vancomycin from Poloxamer 407 gels. International Journal of Pharmaceutics. 1999;192:183-93.

77. Bentley MVLB, Marchetti JM, Ricardo N, Ali-Abi Z, Collett JH. Influence of lecithin on some physical chemical properties of poloxamer gels: rheological, microscopic and in vitro permeation studies. International Journal of Pharmaceutics. 1999;193:49-55.

78. Pepić I, Jalšenjak N, Jalšenjak I. Micellar solutions of triblock copolymer surfactants with pilocarpine. International Journal of Pharmaceutics. 2004;272(1-2):57-64. doi:10.1016/j.ijpharm.2003.11.032.

79. Pluta J, Karolewicz B. In vitro studies of the properties of thermosensitive systems prepared on Pluronic F-127 as vehicles for methotrexate for delivery to solid tumors. Polymers in Medicine. 2006;36(3):37.

80. Scherlund M, Brodin A, Malmsten M. Micellization and gelation in block copolymer systems containing local anesthetics. International Journal of Pharmaceutics. 2000;211:37-49.

81. Lumry R, Rajender S. Enthalpy–entropy compensation phenomena in water solutions of proteins and small molecules: a ubiquitous properly of water. Biopolymers. 1970;9(10):1125-227.

82. Armstrong J, Chowdhry B, O'Brien R, Beezer A, Mitchell J, Leharne S. Scanning microcalorimetric investigations of phase transitions in dilute aqueous solutions of Poly (oxypropylene). The Journal of Physical Chemistry. 1995;99(13):4590-8.

83. Sikorska E, Wyrzykowski D, Szutkowski K, Greber K, Lubecka EA, Zhukov I. Thermodynamics, size, and dynamics of zwitterionic dodecylphosphocholine and anionic sodium dodecyl sulfate mixed micelles. Journal of Thermal Analysis and Calorimetry. 2016;123:511-23.

84. Cornish-Bowden A. Enthalpy-entropy compensation: a phantom phenomenon. Journal of Biosciences. 2002;27:121-6.

85. Lee DJ, Huang WH. Enthalpy-entropy compensation in micellization of sodium dodecyl sulphate in water/methanol, water/ethylene glycol and water/glycerol binary mixtures. Colloid and Polymer Science. 1996;274:160-5.

86. Sugihara G, Hisatomi M. Enthalpy-entropy compensation phenomenon observed for different surfactants in aqueous solution. Journal of Colloid And Interface Science. 1999;219:31-6.

87. Lee DJ. Enthalpy-entropy compensation in ionic micelle formation. Colloid and Polymer Science. 1995;273:539-43.

88. Friedman HL, Krishnan CV. Studies of hydrophobic bonding in aqueous alcohols: enthalpy measurements and model calculations. Journal of Solution Chemistry. 1973;2(2/3):119-40.

89. Bedö Z, Berecz E, Lakatos I. Enthalpy-entropy compensation of micellization of ethoxylated nonyl-phenols. Colloid and Polymer Science. 1992;270:799-805.

90. Jolicoeur C, Philip PR. Enthalpy-entropy compensation for micellization and other hydrophobic interactions in aqueous solutions. Canadian Journal of Chemistry. 1974;52(10):1834-9.

91. Paterson I, Armstrong J, Chowdhry B, Leharne S. Thermodynamic model fitting of the calorimetric output obtained for aqueous solutions of oxyethylene-oxypropylene-oxyethylene triblock copolymers. Langmuir. 1997;13:2219-26.

92. Tsui H-W, Hsu Y-H, Wang J-H, Chen L-J. Novel behavior of heat of micellization of pluronics F68 and F88 in aqueous solutions. Langmuir. 2008;24:13858-62. doi:10.1021/la803272y.

93. Kadam Y, Singh K, Marangoni DG, Ma JH, Aswal VK, Bahadur P. Thermodynamic of micelle formation of nonlinear block co-polymer Tetronic® T904 in aqueous salt solution. Colloids and Surfaces A: Physicochemical and Engineering Aspects. 2010;369(1-3):121-7. doi:10.1016/j.colsurfa.2010.08.010.

94. Moulik SP, Mitra D. Amphiphile self-aggregation: an attempt to reconcile the agreement–disagreement between the enthalpies of micellization determined by the van't Hoff and Calorimetry methods. Journal of Colloid And Interface Science. 2009;337(2):569-78. doi:10.1016/j.jcis.2009.05.064.

95. Chen L-J, Lin S-Y, Huang C-C, Chen E-M. Temperature dependence of critical micelle concentration of polyoxyethylenated non-ionic surfactants Colloids and Surfaces A: Physicochemical and Engineering Aspects. 1998;135:175-81.

96. Krishnan CV, Friedman HL. Model calculations for setchenow coefficients. Journal of Solution Chemistry. 1974;3(9):727-44.

97. Naskar B, Ghosh S, Moulik SP. Solution behavior of normal and reverse triblock copolymers (pluronic L44 and 10R5) individually and in binary mixture. Langmuir. 2012;28(18):7134-46. doi:10.1021/la3000729.

98. Liu G, Gu D, Liu H, Ding W, Li Z. Enthalpy-entropy compensation of ionic liquid-type Gemini imidazolium surfactants in aqueous solutions: A free energy perturbation study. Journal of Colloid And Interface Science. 2011;358(2):521-6. doi:10.1016/j.jcis.2011.03.064.

99. Kauzmann W. Some factors in the interpretation of protein denaturation. Advances in Protein Chemistry. 1959;14:1-63.

100. Poland DC, Scheraga HA. Hydrophobic bonding and micelle stability. The Journal of Physical Chemistry. 1965;69(7):2431-42.

101. Chen L-J, Lin S-Y, Huang C-C. Effect of hydrophobic chain length of surfactants on enthalpy-entropy compensation of micellization. Journal of Physical Chemistry. 1998;102:4350-6.

102. Goldstein RE. Model for phase equilibria in micellar solutions of nonionic surfactants. Journal of Chemical Physics. 1986;84:3367-78.

103. Ranatunga R, Vitha MF, Carr PW. Mechanistic implications of the equality of compensation temperatures in chromatography. Journal of Chromatography A. 2002;946:47-9.

104. Thompson AL, Love BJ. Thermodynamic properties of aqueous PEO-PPO-PEO micelles of varying hydrophilicity with added cisplatin determined by differential scanning calorimetry. Journal of Thermal Analysis and Calorimetry. 2016;127(2):1583-92.

105. Desoize B, Madoulet C. Particular aspects of platinum compounds used at present in cancer treatment. Critical Reviews in Oncology/Hematology. 2002;42:317-25.

106. Duffull SB, Robinson BA. Clinical pharmacokinetics and dose optimisation of carboplatin. Clinical pharmacokinetics. 1997;33(3):161-83.

107. Exner AA, Krupka TM, Scherrer K, Teets JM. Enhancement of carboplatin toxicity by pluronic block copolymers. Journal of Controlled Release. 2005;106(1-2):188-97. doi:10.1016/j.jconrel.2005.04.015.

108. Sonoda A, Nitta N, Ohta S, Nitta-Seko A, Morikawa S, Tabata Y et al. Controlled release and antitumor effect of pluronic F127 mixed with cisplatin in a rabbit model. CardioVascular and Interventional Radiology. 2009;33(1):135-42. doi:10.1007/s00270-009-9741-1.

109. Kwon GS, Forrest ML. Amphiphilic block copolymer micelles for nanoscale drug delivery. Drug Development Research. 2006;67(1):15-22. doi:10.1002/ddr.20063.

110. Nishiyama N, Kataoka K. Current state, achievements, and future prospects of polymeric micelles as nanocarriers for drug and gene delivery. Pharmacology and Therapeutics. 2006;112(3):630-48.

111. Nishiyama N, Koizumi F, Okazaki S, Matsumura Y, Nishio K, Kataoka K. Differential gene expression profile between PC-14 Cells treated with free cisplatin and cisplatin-incorporated polymeric micelles. Bioconjugate Chemistry. 2003;14(2):449-57. doi:10.1021/bc025555t.

112. Aliabadi HM, Shahin M, Brocks DR, Lavasanifar A. Disposition of drugs in block copolymer micelle delivery systems. Clinical pharmacokinetics. 2008;47(10):619-34.

113. Alakhov VY, Moskaleva EY, Batrakova EV, Kabanov AV. Hypersensitization of multidrug resistant human ovarian carcinoma cells by pluronic P85 block copolymer. Bioconjugate Chemistry. 1996;7:209-16.

114. Le Garrec D, Ranger M, Leroux J-C. Micelles in anticancer drug delivery. American Journal of Drug Delivery. 2004;2(1):15-42.

115. Kwon GS. Polymeric micelles for delivery of poorly water-soluble compounds. Critical Reviews in Therapeutic Drug Carrier Systems. 2003;20(5):357-403.

116. Oerlemans C, Bult W, Bos M, Storm G, Nijsen JFW, Hennink WE. Polymeric micelles in anticancer therapy: targeting, imaging and triggered release. Pharmaceutical Research. 2010;27(12):2569-89. doi:10.1007/s11095-010-0233-4.

117. Nishiyama N, Kataoka K. Preparation and characterization of size-controlled polymeric micelle containing cis-dichlorodiammineplatinum(II) in the core. Journal of Controlled Release. 2001;74:83-94.

118. Zhu W, Li Y, Liu L, Chen Y, Wang C, Xi F. Supramolecular hydrogels from cisplatin-loaded block copolymer nanoparticles and α-cyclodextrins with a stepwise delivery property. Biomacromolecules. 2010;11(11):3086-92. doi:10.1021/bm100889j.

119. Alexandridis P, Holzworth JF, Hatton TA. MIcellization of poly(ethylene oxide)-poly(propylene oxide)-poly(ethylene oxide) triblock copolymers in aqueous-solutions-thermodynamics of copolymer association. Macromolecules. 1994;27(9):2414-25.

120. Alexandridis P, Hatton TA. Polyethylene oxide-polypropylene oxide-polyethylene oxide block-copolymer surfactants in aqueous-solutions at interfaces-thermodynamics, structure, dynamics and modeling. Colloids and Surfaces A: Physicochemical and Engineering Aspects. 1995;96:1-46.

121. Bouchemal K, Agnely F, Koffi A, Ponchel G. A concise analysis of the effect of temperature and propanediol 1,2 on Pluronic F-127 micellization using isothermal titration microcalorimetry. Journal of Colloid and Interface Science. 2009;338:169-76.

122. Kelarakis A, Havredaki V, Rekatas C, Booth C. Thermodynamics of micellisation of a diblock copolymer of ethylene oxide and styrene oxide in water. Physical Chemistry Chemical Physics. 2001;3(24):5550-2.

123. Kelarakis A, Havredaki V, YU G, Derici L, Booth C. Temperature dependences of the critical micelle concentrations of diblock oxyethylene/oxybutylene copolymers. A case of athermal micellization. Macromolecules. 1998;31(3):944-6.

124. Tsui HW, Wang JH, Hsu YH, Chen LJ. Study of heat of micellization and phase separation for Pluronic aqueous solutions by using a high sensitivity differential scanning calorimetry. Colloid & Polymer Science. 2010;288:1687-96.

125. Ng XW, Mundargi RC, Venkatraman SS. Nanomedicine: size-related drug delivery applications, including periodontics and endodontics. In: Kishen A, editor. Nanotechnology in Endodontics: Current and Potential Clinical Applications. Springer; 2015.

126. Desale SS, Cohen SM, Zhao Y, Kabanov AV, Bronich TK. Biodegradable hybrid polymer micelles for combination drug therapy in ovarian cancer. Journal of Controlled Release. 2013;171(3):339-48.

127. Wolff M, Magerl A, Zabel H. NS-SANS for the investigation of micellar systems. Thin Solid Films. 2007;515:5724-7.

128. Prud'homme RK, Wu G, Schneider DK. Structure and rheology studies of poly(oxyethylene-oxypropylene-oxyethylene) aqueous solution. Langmuir. 1996;12:4651-9.

129. Svensson B, Olsson U, Alexandridis P, Mortensen K. A SANS investigation of reverse (water-in-oil) micelles of amphiphilic block copolymers. Macromolecules. 1999;32:6725-33.

130. Lazzara G, Milioto S, Gradzielski M. The solubilisation behavior of some dichloroalkanes in aqueous solutions of PEO-PPO-PEO triblock copolymers: a dynamic light scattering, fluorescence spectroscopy, and SANS study. Physical Chemistry Chemical Physics. 2006;8:2299-312.

131. Khimani M, Ganguly R, Aswal VK, Nath S, Bahadur P. Solubilization of parabens in aqueous pluronic solutions: investigating the micellar growth and interaction as a function of paraben composition. The Journal of Physical Chemistry B. 2012;116:14943-50.

132. Khimani M, Verma G, Kumar S, Hassan PA, Aswal VK, Bahadur P. pH induced tuning of size, charge and viscoelastic behavior of aqueous micellar solution of Pluronic® P104-anthranilic acid mixtures: a scattering, rheology, and NMR study. Colloids and Surfaces A: Physicochemical and Engineering Aspects. 2015;470:202-10.

133. Chen S-H, Liao C, Fratini E, Baglioni P, Mallamace F. Interaction, critical, percolation and kinetic glass transitions in pluronic L-64 micellar solutions. Colloids and Surfaces A: Physicochemical and Engineering Aspects. 2001;183-185:95-111.

134. Liu Y, Chen S-H, Huang JS. Small-angle neutron scattering analysis of the structure and interaction of triblock copolymer micelles in aqueous solution. Macromolecules. 1998;31:2236-44.

135. Svensson B, Alexandridis P, Olsson U. Self-assembly of a poly(ethylene oxide)/poly(propylene oxide) block copolymer (pluronic P104, $(EO)_{27}(PO)_{61}(EO)_{27}$) in the presence of water and xylene. The Journal of Physical Chemistry B. 1998;102:7541-8.

136. Kayali I, Khan A, Lindman B. Solubilization and location of phenethylalcohol, benzaldehyde, and limonene in lamellar liquid crystal formed with block copolymer and water. Journal of Colloid And Interface Science. 2006;297:792-6.

137. Hamley IW, Castelletto V, Ricardo NM, Pinho ME, Booth C, Attwood D et al. A SAXS study of the structure of gels formed by mixtures of polyoxyalkylene triblock copolymers. Polymer International. 2007;56:88-92.

138. Zhang J, Han B, Zhao Y, Li J, Yang G. Switching micellization of pluronics in water by CO_2. Chemistry a European Journal. 2011;17:4266-72.

139. Zhang R, Liu J, He J, Han B, Liu Z, Jiang T et al. Compressed ethylene-assisted formation of the reverse micelle of PEO-PPO-PEO copolymer. Macromolecules. 2003;36:1289-94.

140. Santos Sd, Luigjes B, Piculell L. Associative phase behavior and disintegration of copolymer aggregates on adding poly(acrylic acid) to aqueous solutions of a PEO-PPO-PEO triblock copolymer. Soft Matter. 2010;6:4756-67.

141. Cui X, Moon S-W, Zin W-C. High-yield synthesis of monodispersed SBA-15 equilateral hexagonal platelet with thick wall. Materials Letters. 2006;60:3857-60.

142. Zhou D, Alexandridis P, Khan A. Self-assembly in a mixture of two poly(ethylene oxide)-b-poly(propylene oxide)-b-poly (ethylene oxide) copolymers in water. Journal of Colloid And Interface Science. 1996;183:339-50.

143. Baldrian J, Steinhart M, Amenitsch H, Bernstorff S. Disorder-order-crystalline state transitions of PEO-b-PPO-b-PEO copolymers and their blends: SAXS/WAXS/DSC study. Journal of Macromolecular Science®, Part B: Physics. 2009;48:174-84.

144. Aramaki K, Hossain MK, Rodriguez C, Uddin MH, Kunieda H. Miscibility of block copolymers and surfactants in lamellar liquid crystals. Macromolecules. 2003;36:9443-50.

145. Hossain MK, Hinata S, Lopez-Quintela A, Kunieda H. Phase behavior of poly(oxyethylene)-poly(oxypropylene)-poly(oxyethylene) block copolymer in water and water-$C_{12}EO_5$ Systems. Journal of Dispersion Science and Technology. 2003;24(3):411-22.

146. Alexandridis P, Zhou D, Khan A. Lyotropic liquid crystallinity in amphiphilic block copolymers: temperature effects on phase behavior and structure for poly(ethylene oxide)-b-poly(propylene oxide)-b-poly(ethylene oxide) copolymers of different composition. Langmuir. 1996;12:2690-700.

147. Alexandridis P. Structural polymorphism of poly(ethylene oxide)-poly(propylene oxide) block copolymers in nonaqueous polar solvents. Macromolecules. 1998;31:6935-42.

148. Li J, Tang H, Chen L, Chen R, Pan M, Jiang SP. Highly ordered and periodic mesoporous nafion membranes via colloidal silica mediated self-assembly for fuel cells. Chemical Communications - Royal Society of Chemistry. 2013;49:6537-9.

149. Lu J, Tang H, Xu C, Jiang SP. Nafion membranes with ordered mesoporous structre and high water retention properties for fuel cell applications. Journal of Materials Chemistry. 2012;22:5810-9.

150. Nambam JS, Philip J. Thermogelling properties of triblock copolymers in the presence of hydrophilic Fe_3O_4 nanoparticles and surfactants. Langmuir. 2012;28:12044-53.

151. Shih K-C, Li C-Y, Li W-H, Lai H-M. Fine structures of self-assembled beta-cyclodextrin/Pluronic in dilute and dense systems: a small angle X-ray scattering study. Soft Matter. 2014;10:7606-14.

152. Quinn MDJ, Du J, Boyd BJ, Hawley A, Notley SM. Lipid liquid-crystal phase change induced through a near-infrared irradiation of entrained graphene particles. Langmuir. 2015;31:6605-9.

153. Hartnett TE, Ladewig K, O'Connor AJ, Hartley PG, McLean KM. Physicochemical and cytotoxicity analysis of glycerol monoolein-based nanoparticles. RSC Advances. 2015;5:26543-9.

154. Tirumala VR, Romang A, Agarwal S, Lin EK, Watkins JJ. Well ordered polymer melts from blends of disordered triblock copolymer surfactants and functional homopolymers**. Advanced Materials. 2008;20:1603-8.

155. Li Y, Keilbach A, Mizoshita N, Inagaki S, Bein T. Formation of hexagonal and cubic fluorescent periodic mesoporous organosilicas in the channels of anodic alumina membranes. Journal of materials Chemistry C. 2014;2:50-5.

156. Lin Y, Daga VK, Anderson ER, Gido SP, Watkins JJ. Nanoparticle-driven assembly of block copolymers: a simple route to ordered hybrid materials. Journal of the American Chemical Society. 2011;133:6513-6.

157. Thompson AL, Mensah LM, Love BJ. The effect of cisplatin on the nanoscale structure of aqueous PEO-PPO-PEO micelles of varying hydrophilicity observed using SAXS. (To Be Submitted). 2018.

158. Olsen BD, Li X, Wang J, Segalman RA. Near-surface and internal lamellar structure and orientation in thin films of rod-coil block copolymers. Soft Matter. 2009;5:182-92.

159. Nagarajan R. Solubilzation of hydrocarbons and resulting aggregate shape transitions in aqueous solutions of Pluronic® (PEO-PPO-PEO) block copolymers. Colloids and Surfaces B: Biointerfaces. 1999;16:55-72.

160. Nagarajan R. Solubilization of "guest" molecules into polymeric aggregates. Polymers for Advanced Technologies. 2001;12:23-43.

161. Steinbeck CA, Hedin N, Chmelka BF. Interactions of Charged Porphyrins with Nonionic Triblock Copolymer Hosts in Aqueous Solutions. Langmuir. 2004;20:10399-412.

162. Jia L, Guo C, Yang L, Xiang J, Tang Y, Liu H. Interaction between reduced glutathione and PEO-PPO-PEO copolymers in aqueous solutions: studied by ^{1}H NMR and spin-lattice relaxation. The Journal of Physical Chemistry. 2011;115:2228-33.

163. Ruthstein S, Raitsimring AM, Bitton R, Frydman V. Distribution of guest molecules in pluronic micelles studied by double electron electron spin resonance and small angle X-ray scattering. Physical Chemistry Chemical Physics. 2009;11:148-60.

164. Desale SS, Cohen SM, Zhao Y, Kabanov AV, Bronich TK. Biodegradable hybrid polymer micelles for combination drug therapy in ovarian cancer. Journal of Controlled Release. 2013;171:339-48.

165. Thompson AL, Ball AN, Love BJ. Controlled release characteristics of aqueous PEO-PPO-PEO micelles with added malachite green, erythrosin, and cisplatin determined by UV-Visible Spectroscopy. Journal of Surfactants and Detergents (accepted). 2017.

166. Team SE. Selective permeability of dialysis tubing lab: explained. Creative Commons 4.0. 2010-2017. https://schoolworkhelper.net. 2017.

167. Basotra M, Singh SK, Gulati M. Development and validation of a simple and sensitive spectrometric method for estimation of cisplatin hydrochloride in tablet dosage forms: application to dissolution studies. ISRN Analytical Chemistry. 2013;2013:1-8.

168. Cubells MP, Aixela JP, Brumos VG, Pou SD, Flaque MV. Stability of cisplatin in sodium chloride 0.9% intravenous solution related to the container's material. Pharmacy World & Science. 1993;15(1):34-6.

169. Banerjea D, Basolo F, Pearson RG. Mechanism of substitution reactions of complex ions. XII. Reactions of some platinum(II) complexes with various reactants. Reactions of Platinum Complexes with Various Reactants. 1957;79:4055-62.

170. Reishus JW, Don S. Martin J. cis-Dichlorodiammineplatinum(II). Acid hydrolysis and isotopic exchange of the chloride ligands. Acid Hydrolysis of cis-dichlorodiammineplatinum(II). 1961;83:2457-62.

171. Lee KW, D. S. Martin J. Cis-dichlorodiammineplatinum(II). Aquation equilibria and isotopic exchange of chloride ligans with free chloride and tetrachloroplatinate(II)*. Inorganica Chimica Acta. 1976;17:105-10.

172. Mandal AB. Shape, size, hydration and flow behavior of nitrocellulose lacquer emulsion in absence and presence of urea. Journal of the American Oil Chemists' Society. 1987;64(8):1202-7.

173. Mandal AB, Nair BU. Cyclic voltammetric technique for the determination of the critical micelle concentration of surfactants, self-diffusion coefficient of micelles, and partition coefficient of an electrochemical probe. Journal of Physical Chemistry. 1991;95:9008-13.

174. Mandal AB. Self-diffusion studies on various micelles using ferrocene as electrochemical probe. Langmuir. 1993;9:1932-3.

175. Geetha B, Mandal AB. Self-diffusion studies on ω-methoxy polyethylene glycol macromonomer micelles by using cyclic voltammetric and fourier transform pulsed gradient spin-echo nuclear magnetic resonance techniques. Langmuir. 1995;11:1464-7.

176. Geetha B, Mandal AB. Determination of the critical micelle concentration of the methoxy polyethylene glycol based macromonomer and partition coefficient of a new electrochemical probe using a cyclic voltammetric technique. Langmuir. 1997;13:2410-3.

177. James J, Ramalechume C, Mandal AB. Self-diffusion studies on PEO-PPO-PEO triblock copolymer micelles in SDS micelles and vice versa using cyclic voltammetry. Chemical Physics Letters. 2005;405:84-9.

178. Reardon PJ, Parhizkar M, Harker AH, Browning RJ, Vassileva V, Stride E et al. Electrohydrodynamic fabrication of core-shell PLGA nanoparticles with controlled release of cisplatin for enhanced cancer treatment. International Journal of Nanomedicine. 2017;12:3913-26.

179. Fang J-Y, Chen J-P, Leu Y-L, Hu J-W. The delivery of platinum drugs from thermosensitive hydrogels containing different ratios of chitosan. Drug Delivery. 2008;15:235-43.

180. Czarnobaj K, Lukasiak J. In vitro release of cisplatin from sol-gel processed organically modified silica xerogels. Journal of Materials Science: Materials in Medicine. 2007;18:2041-4.

181. Campbell CS, Delgado-Charro MB, Camus O, Perera S. Comparison of drug release from PLGA microsperes and novel fibre formulations. Journal of Biomaterials Applications. 2016;30(8):1142-53.

182. Maan GK, Bajpai J, Bajpai AK. Investigation of in vitro release of cisplatin from electrostatically crosslinked chitosan-alginate nanoparticles. Synthesis and Reactivity in Inorganic, Metal-Organic, and Nano-Metal Chemistry. 2016;46:1532-40.

183. Ahrens M. Home structure fires. National Fire Protection Association; 2015.

184. Wu W, Yang CQ. Comparison of different reactive organophosphorus flame retardant agents for cotton. Part II: Fabric flame resistance performance and physical properties. Polymer Degradation and Stability. 2007;92:363-9.

185. Wakelyn PJ, Bertoniere NR, French AD, Thibodeaux DP, Triplett BA, Rousselle M-A et al. Cotton Fiber Chemistry and Technology. Boca-Raton, Florida: CRC Press (Taylor and Francis Group); 2007.

186. Carr CM. Chemistry of the Textiles Industry. Springer-Science+Business Media, B.V.; 1995.

187. Li Y-C, Schulz J, Mannen S, Delhom C, Condon B, Chang S et al. Flame retardant behavior of polyelectrolyte-clay thin film assemblies on cotton fabric. ACS Nano. 2010;4(6):3325-37.

188. Lessan F, Montazer M, Moghadam MB. A novel durable flame-retardant cotton fabric using sodium hypophosphite, nano TiO2 and maleic acid. Thermochimica Acta. 2011;520:48-54.

189. Mostashari SM, Zanjanchi MA. Burning of a cotton fabric impregnated by synthetic zinc carbonate hydroxide as a flame retardant. Combustion, Explosion, and Shock Waves. 2005;41(4):426-9.

190. Reddy PRS, Agathian G, Kumar A. Ionizing radiation graft polymerized and modified flame retardant cotton fabric. Radiation Physics and Chemistry. 2005;72:511-6.

191. Wu W, Yang CQ. Correlation between limiting oxygen index and phosphorus/nitrogen content of cotton fabrics treated with a hydroxy-functional organophosphorus flame-retarding agent and dimethyloldihydroxyethyleneurea. Journal of Applied Polymer Science. 2003;90:1885-90.

192. Yang CQ, He Q. Applications of micro-scale combustion calorimetry to the studies of cotton and nylon fabrics treated with organophosphorus flame retardants. Journal of Analytical and Applied Pyrolysis. 2011;91:125-33.

193. Martin C, Ronda JC, Cadiz V. Boron-containing novolac resins as flame retardant materials. Polymer Degradation and Stability. 2006;91:747-54.

194. Alaee M, Arias P, Sjodin A, Bergman A. An overview of commercially used brominated flame retardants, their applications, their use patterns in different countries/regions and possible modes of release. Environment International. 2003;29:683-9.

195. Sather JM, Richards HR. Efficiency of phosphorus-containing compounds for inhibiting afterglow in cellulose fabrics. American Dyestuff Reporter. 1970;59:21-6.

196. Leistner M, Abu-Odeh AA, Rohmer SC, Grunlan JC. Water-based chitosan/melamine polyphosphate multilayer nanocoating that extinguishes fire on polyester-cotton fabric. Carbohydrate Polymers. 2015;130:227-32.

197. Decher G, Schlenoff JB. Multilayer thin films. Wiley-VCH Verlag Cmbh & Co. KGaA; 2003.

198. Hammond PT. Form and function in multilayer assembly: new applications at the nanoscale. Advanced Materials. 2004;16(15):1271-93.

199. Bertrand P, Jonas A, Laschewsky A, Legras R. Ultrathin polymer coatings by complexation of polyelectrolytes at interfaces: suitable materials, structure and properties. Macromolecular Rapid Communications. 2000;21:319-48.

200. Alongi J, Carosio F. All-inorganic intumescent nanocoating containing montmorillonite nanoplatelets in ammonium polyphosphate matrix capable of preventing cotton ignition. Polymers. 2016;8(430).

201. Alongi J, Carosio F, Kiekens P. Recent advances in the design of water based-flame retardant coatings for polyester and polyester-cotton blends. Polymers. 2016;8(357).

202. Lvov Y, Ariga K, Ichinose I, Kunitake T. Assembly of multicomponent protein films by means of electrostatic layer-by-layer adsorption. Journal of American Chemical Society. 1995;117:6117-23.

203. Sato M, Sano M. Van der waals layer-by-layer construction of a carbon nanotube 2D network. Langmuir. 2005;21:11490-4.

204. Podsiadlo P, Kaushik aK, Shim BS, Agarwal A, Tang Z, Waas AM et al. Can nature's design be improved upon? High strength, transparent nacre-like nanocomposites with double network of sacrificial cross links. Journal of Physical Chemistry B. 2008;112:14359-63.

205. Zhang H, Wang Z, Zhang Y, Zhang X. Hydrogen-bonding-directed layer-by-layer assembly of poly(4-vinylpyridine) and Poly(4-vinylphenol): effect of solvent composition on multilayer buildup. Langmuir. 2004;20:9366-70.

206. Bai S, Wang Z, Zhang X. Hydrogen-bonding-directed layer-by-layer films: effect of electrostatic interaction on the microporous morphology variation. Langmuir. 2004;20:11828-32.

207. Jang W-S, Grunlan JC. Robotic dipping system for layer-by-layer assembly of multifunctional thin films. Review of Scientific Intruments. 2005;76.

208. Gamboa D, Priolo MA, Ham A, Grunlan JC. Note: Influence of rinsing and drying routines on growth of multilayer thin films using automated deposition system. Review of Scientific Intruments. 2010;036103.

209. Porcel CH, Izquierdo A, Ball V, Decher G, Voegel JC, Schaaf P. Ultrathin coatings and (poly(glutamic acid)/polyallylamine) films deposited by continuous and simultaneous spraying. Langmuir. 2005;21:800-2.

210. Krogman KC, Lowery JL, Zacharia NS, Rutledge GC, Hammond PT. Spraying asymmetry into functional membranes layer-by-layer. Nature Materials. 2009;8.

211. Walton MD, Kim YS, Jan CJ, McConnel EP, Everett WN, Grunlan JC. Deposition and patterning of conductive carbon black thin films. Synthetic Metals. 2007;157:632-9.

212. Everett WN, Jan CJ, Sue HJ, Grunlan JC. Micropatterning and impedance characterization of an electrically percolating layer-by-layer assembly. Electroanalysis. 2007;19:964-72.

213. DeLongchamp DM, Hammond PT. Highly ion conductive poly(ethlene oxide)-based solid polymer electrolytes from hydrogen bonding layer-by-layer assembly. Langmuir. 2004;20:5403-11.

214. Hiller JA, Mendelsohn JD, Rubner MF. Reversibly erasable nanoporous anti-reflection coatings from polyelectrolyte multilayers. Nature Materials. 2002;1.

215. Wu Z, Nolte A, Walish J, Zhai L, Rubner M, Cohen R. Layer-by-layer assembled nanoparticles on flexible substrates: toward deformable anti-reflection coatings. Polymeric Materials Science. 2005.

216. Priolo MA, Gamboa D, Holder KM, Grunlan JC. Super gas barrier of transparent polymer-clay multilayer ultrathin films. Nano Letters. 2010;10:4970-4.

217. Yang Y-H, Haile M, Park YT, Malek FA, Grunlan JC. Super gas barrier of all-polymer multilayer thin films. Macromolecules. 2011;44:1450-9.

218. Cain AA, Murray S, Holder KM, Nolen CR, Grunlan JC. Intumescent nanocoating extinguishes flame on fabric using aqueous polyelectrolyte complex deposited in single step. Macromolecular Materials and Engineering. 2014;299:1180-7.

219. Davis R, Li Y-C, Gervasio M, Luu J, Kim YS. One-pot, bioinspired coactings to reduce the flammability of flexible polyurethane foams. ACS Applied Materials Interfaces. 2015;7:6082-92.

220. Panel CIRE. Final report on the safety assessment of sodium metaphosphate, sodium trimetaphosphate, and sodium hexametaphosphate. International Journal of Toxicology. 2001;20(3):75-89.

221. Skinner CG, Thomas JD, Osterloh JD. Melamine Toxicity. Journal of Medical Toxicology. 2010;6:50-5.

222. Tompkin RB. Indirect antimicrobial effects in foods: phosphates. Journal of Food Safety. 1983;6:13-27.

223. Mast RW, Jeffcoat AR, Sadler BM, Kraska RC, Friedman MA. Metabolism, disposition and excretion of [^{14}C] melamine in male fischer 344 rats. Food and Chemical Toxicology. 1983;21(6):807-10.

224. Desai SD, Blanchard J. In vitro evaluation of pluronic F127-based controlled-release ocular delivery systems for pilocarpine. Journal of Pharmaceutical Sciences. 1998;87(2).

225. Miyazaki S, Tobiyama T, Takada M, Attwood D. Percutaneous absorption of indomethacin from pluronic F127 gels in rats. Journal of Pharmacy and Pharmacology. 1995;47:455-7.

226. Wanka G, Hoffmann H, Ulbricht W. The aggregation behavior of poly-(oxyethylene)-poly-(oxypropylene)-poly-(oxyethylene)-block-copolymers in aqueous solution. Colloid Polymer Science. 1990;268:101-17.

227. Mortensen K, Batsberg W, Hvidt S. Effects of PEO-PPO diblock impurities on the cubic structure of aqueous PEO-PPO-PEO micelles: fcc and bcc ordered structures in F127 Macromolecules. 2008;41:1720-7.

228. Jian J, Burger C, Li C, Li J, Lin MY, Colby RH. Shear-induced layered structure of polymeric micelles by SANS. Macromolecules. 2007;40:4016-22.

229. Zhu P, Sui S, Wang B, Sun K, Sun G. A study of pyrolysis and pyrolysis products of flame-retardant cotton fabrics by DSC, TGA, and PY-GC-MS. Journal of Analytical and Applied Pyrolysis. 2004;71:645-55.